Aus der

Klinik und Poliklinik für Strahlentherapie und Radioonkologie
des Klinikums der Universität München

Ludwig-Maximilians-Universität München

Ärztlicher Direktor: Professor Dr. med. Claus Belka

Optimierte Planung und bildgestützte Applikation der intensitätsmodulierten Strahlentherapie

Habilitationsschrift

zur Erlangung der Venia legendi

im Fach

STRAHLENTHERAPIE

vorgelegt von

Dr.med. Dr.rer.nat. Christian Thieke

München 2017

Der kumulativen Habilitationsschrift liegen im Wesentlichen folgende Arbeiten zugrunde:

1. **Thieke C**, Küfer KH, Monz M, Scherrer A, Alonso F, Oelfke U, Huber PE, Debus J, Bortfeld T:
   A new concept for interactive radiotherapy planning with multicriteria optimization: first clinical evaluation.
   Radiother Oncol 2007; 85:292-8

2. Süss P, Bortz M, Küfer KH, **Thieke C**:
   The critical spot eraser-a method to interactively control the correction of local hot and cold spots in IMRT planning.
   Phys Med Biol. 2013;58(6):1855-67

3. Askoxylakis V, Dinkel J, Eichinger M, Stieltjes B, Sommer G, Strauss LG, Dimitrakopoulou-Strauss A, Kopp-Schneider A, Haberkorn U, Huber PE, Bischof M, Debus J, **Thieke C**:
   Multimodal hypoxia imaging and intensity modulated radiation therapy for unresectable non-small-cell lung cancer: the HIL trial.
   Radiat Oncol. 2012 14;7:157

4. **Thieke C**, Malsch U, Schlegel W, Debus J, Huber P, Bendl R, Thilmann C:
   Kilovoltage CT using a linac-CT scanner combination.
   Br J Radiol 2006 Sep;79 Spec No 1:79-86

5. Stoiber EM, Lechsel G, Giske K, Muenter MW, Hoess A, Bendl R, Debus J, Huber PE, **Thieke C**:
   Quantitative assessment of image-guided radiotherapy for paraspinal tumors.
   Int J Radiat Oncol Biol Phys 2009; 75:933-40

6. **Thieke C**, Nicolay NH, Sterzing F, Hoffmann H, Roeder F, Safi S, Debus J, Huber PE:
   Long-term results in malignant pleural mesothelioma treated with neoadjuvant chemotherapy, extrapleural pneumonectomy and intensity-modulated radiotherapy.
   Radiat Oncol. 2015; 10:267

Inhaltsverzeichnis

1. Einführung und Übersicht 5
1.1. Strahlentherapieplanung auf Basis multikriterieller Optimierung (MCO) 5
1.2. Funktionelle und molekulare Bildgebung für die Strahlentherapie 8
1.3. Bildführung im Bestrahlungsraum 9
1.4. Quantitative Analyse des Therapieansprechens 9
2. Eigene Arbeiten 11
2.1. Strahlentherapieplanung auf Basis multikriterieller Optimierung (MCO) 11
2.1.1. A new concept for interactive radiotherapy planning with multicriteria optimization: first clinical evaluation 11
2.1.2. The critical spot eraser-a method to interactively control the correction of local hot and cold spots in IMRT planning. 12
2.1.3. Weitere, thematisch verbundene eigene Arbeiten 14
2.2. Funktionelle und molekulare Bildgebung für die Strahlentherapie 15
2.2.1. Multimodal hypoxia imaging and intensity modulated radiation therapy for unresectable non-small-cell lung cancer: the HIL trial. 15
2.2.2. Weitere, thematisch verbundene eigene Arbeiten 16
2.3. Bildführung im Bestrahlungsraum 16
2.3.1. Kilovoltage CT using a linac-CT scanner combination. 16
2.3.2. Quantitative assessment of image-guided radiotherapy for paraspinal tumors. 18
2.3.3. Weitere, thematisch verbundene eigene Arbeiten 18
2.4. Quantitative Analyse des Therapieansprechens 19
2.4.1. Long-term results in malignant pleural mesothelioma treated with neoadjuvant chemotherapy, extrapleural pneumonectomy and intensity-modulated radiotherapy. 19
2.4.2. Weitere, thematisch verbundene eigene Arbeiten 19
3. Zusammenfassung und Ausblick 21
4. Abkürzungsverzeichnis 22
5. Literaturverzeichnis 23
6. Lebenslauf 24
7. Eigene wissenschaftliche Publikationen 28
Übersicht 28
7.1. Originalarbeiten als Erst- oder Letztautor 28
7.2. Originalarbeiten als Koautor 30
7.3. Kasuistiken / Case Reports 33
7.4. Übersichtsartikel / Reviews 34
7.5. Buchkapitel / Book Chapters 34
7.6. Sonstige Veröffentlichungen 34

8. Danksagung 35
9. Eidesstattliche Erklärung 36
10. Faksimile der themenrelevanten Arbeiten.....37

1. Einführung und Übersicht

Die technische Entwicklung der Strahlentherapie ist geprägt von dem Bestreben, eine möglichst hohe Dosis im Zielvolumen zu deponieren bei gleichzeitig bestmöglicher Schonung des umliegenden Normalgewebes. Dies betrifft sowohl die Strahlerzeugung und -formung als auch die Planoptimierung und die sichere Deposition im Patienten während der meist mehrwöchigen fraktionierten Therapieserie. Eine der bedeutendsten technischen Innovationen in der Geschichte der Strahlentherapie in diesem Kontext ist die intensitätsmodulierte Radiotherapie (IMRT) [2, 4-6]. Sie beruht auf dem Prinzip, jeden einzelnen der aus verschiedenen Richtungen auf den Patienten einfallenden Therapiestrahlen nicht nur in seiner äußeren Begrenzung auf die Form des Tumors anzupassen, sondern auch die Fluenz über die gesamte Strahlapertur so zu modulieren, dass die Überlagerung aller Therapiestrahlen das Zielvolumen möglichst konformal abdeckt. Erst mit der IMRT ist es möglich, konkave Dosisverteilungen zu erzeugen, d.h. Dosisverteilungen, deren Hochdosisbereich Aussparungen besitzt, wie es zum Beispiel zur Schonung des Rückenmarks bei um das Rückenmark herumwachsenden Tumoren erforderlich ist. Die Intensitätsverteilungen werden im Rahmen der Bestrahlungsplanung vom Computer mit Hilfe von Optimierungsverfahren berechnet; die Verbesserung dieses Prozesses und die Anpassungen an neue Bestrahlungstechniken sind Gegenstand aktueller Forschung und Entwicklung.

Parallel dazu werden die biologischen Eigenschaften von Tumoren erforscht, um die Dosisverschreibung der individuellen Strahlensensibilität anzupassen. Dabei könnte das Zielvolumen entweder homogen mit einer niedrigeren oder höheren Dosis bestrahlt werden, oder die Dosisverteilung sogar angepasst werden an einzelne Tumor-Subareale, die durch ortsauflösende tomographische Bildgebungsverfahren im Rahmen der Bestrahlungsplanungsuntersuchungen identifiziert werden.

Bildgebung spielt auch während der Applikation, d.h. unmittelbar vor oder während der Behandlung im Bestrahlungsraum, eine zentrale Rolle. Gerade bei hochkonformalen Dosisverteilungen mit steilen Gradienten am Rand des Zielvolumens könnte es bei Abweichungen der aktuellen Behandlungssituation von der Planungssituation zu Unterdosierungen im Zielvolumen oder Überdosierungen im Normalgewebe kommen. Bildgeführte Strahlentherapie stellt die korrekte Lagerung des Patienten sicher. Bei komplexeren Veränderungen des Patienten während der meist mehrwöchigen Therapie, z.B. durch Tumoransprechen oder Gewichtsverlust, kann der Plan zudem adaptiert werden.

In der strahlentherapeutischen Nachsorge schließlich werden die Wirksamkeit der Therapie überprüft und strahlenbedingte Nebenwirkungen erfasst. Dies dient zum einen der Qualitätskontrolle, zum anderen sollen aus den Daten neue Hypothesen generiert werden können, die neue Entwicklungen und Methoden zur weiteren Verbesserung der Therapie ermöglichen.

Das hier vorliegende Habilitationsvorhaben soll auf diesen vier Feldern zur Verbesserung der intensitätsmodulierten Strahlentherapie beitragen. Im Folgenden sollen diese näher vorgestellt werden.

1.1 Strahlentherapieplanung auf Basis multikriterieller Optimierung (MCO)

Die Therapiestrahlen werden in der IMRT in der Regel in sogenannte „Bixel“ (Kurzform für Beam Elements) aufgeteilt. Die Größe eines Bixels hängt ab von der Lamellenbreite des verwendeten Multileaf-Kollimators und der Diskretisierung entlang der Leafrichtung, typisch sind z.B. 5x5mm^2. Für jedes Bixel, das sich auf das Tumor-Zielvolumen projiziert, muss ein individueller Intensitätswert gefunden werden (alle nicht auf das Tumor-Zielvolumen projizierenden

Bixel werden auf Null gesetzt). Je nach Zahl der Einstrahlrichtungen, Bixelgröße und Zielvolumengröße sind damit mehrere Hundert bis mehrere Tausend individuelle Bixel-Intensitäten zu bestimmen. Dies kann nicht mehr manuell erfolgen, sondern muss durch den Computer unterstützt werden. Mit der Einführung der IMRT einher ging damit auch ein neues Prinzip der Strahlentherapieplanung, die sog. „inverse Planung“: Statt wie zuvor Einstrahlrichtungen und Feldform manuell festzulegen (entweder direkt an einem Röntgensimulator oder computergestützt in der sog. „virtuellen Simulation“, mit nachfolgender Dosisberechnung auch „3D-Planung“ genannt), geht man nun von einer gewünschten Dosisverteilung aus und lässt den Computer „invers“ die erforderlichen Bestrahlungseinstellungen bestimmen. Dazu werden der Tumor sowie die Risikoorgane auf einer Bestrahlungsplanungs-Computertomographie (BPL-CT) segmentiert und den einzelnen Strukturen Dosisvorgaben der Art „mindestens 60 Gy und maximal 62 Gy im Tumor-Zielvolumen, maximal 40 Gy im Rückenmark“ verschrieben. Meist werden auch grundlegende Therapieparameter wie Strahlenergie und Zahl und Winkel der Einstrahlrichtungen manuell festgelegt. Anschließend berechnet der Computer die nötige Intensitätsmodulation. Erste analytische Ansätze nutzten die aus der CT-Rekonstruktion bekannten Prinzipien der Rückprojektion, waren allerdings nur für sehr einfache Geometrien einsetzbar. Universell verwendbar und bis heute im Einsatz sind stattdessen Optimierungsverfahren, die aus den Dosisvorgaben eine Zielfunktion $f(D)$ konstruieren (wobei D die aktuelle Dosisverteilung bezeichnet) und diese durch Veränderung der Bixelwerte bis zum Erreichen eines bestimmten Abbruchkriteriums minimiert [3, 16]. Aus Geschwindigkeitsgründen werden in der Praxis meist konvexe Zielfunktionen und Gradientenverfahren eingesetzt.

Die ursprüngliche Hoffnung bei der Entwicklung der inversen Planung war auch eine Vereinfachung des gesamten Planungsprozesses: Wenn der Computer den Bestrahlungsplan in einem Optimierungsprozess findet und dabei die vollen Möglichkeiten der Intensitätsmodulation nutzt, sollte man nach der Dosisverschreibung und einem einmaligen Optimierungslauf den für den Patienten besten Bestrahlungsplan erhalten und sofort mit der Behandlung beginnen können. Die Praxis hat jedoch gezeigt, dass dies nicht der Fall ist. Der Grund ist, dass trotz der drastisch besseren Konformalität von IMRT-Plänen oftmals Tumor-Zielvolumina und Risikoorgane so eng benachbart sind, dass allein aufgrund der physikalischen Eigenschaften der Photonenstrahlung (Tiefendosisverlauf, seitliche Streuung) die Idealvorstellungen des Planers nicht umgesetzt werden können. Für die obige Beispiel-Verschreibung heißt dies: Wenn der Tumor dem Rückenmark direkt anliegt, muss entweder ein gewisser Teil des Tumors unter 60 Gy oder ein gewisser Teil des Rückenmarks über 40 Gy erhalten, denn ein ansatzloser Sprung der Dosisverteilung von 40 auf 60 Gy entlang der Grenze ist physikalisch nicht möglich. Der Computer wird also einen Plan errechnen, der die Vorgaben in mindestens einem Kriterium verletzt. Wenn der Planer mit dem Ergebnis nicht einverstanden ist, wird er die Vorgaben ändern und einen erneuten Optimierungslauf starten. Neben den Dosisvorgaben können auch sog. Wichtungsfaktoren modifiziert werden, die die relative Bedeutung der einzelnen Kriterien festlegen. Die Zielfunktion hat dabei die Form $f(D)=w_1f_1(D)+w_2f_2(D)+\ldots+w_Nf_N(D)$, wobei f_i die einzelnen Zielfunktionen für Zielvolumina und Risikoorgane bezeichnet und w_i die dazugehörigen Wichtungsfaktoren. Die Modifikation der Parameter wiederholt sich solange, bis ein klinisch akzeptabler Plan gefunden ist. Die inverse Planung in dieser Form hat damit drei ungünstige Charakteristika: 1) Die Dosisvorgaben entsprechen nicht den klinisch etablierten und dokumentierten Tumorkontrolldosen bzw. Toleranzdosen, sondern müssen als abstraktes Steuerungsinstrument so gewählt werden, dass vielmehr das Optimierungsergebnis den gewünschten Dosen möglichst nahekommt. 2) Da die Auswirkung der Dosisvorgaben und dazugehörigen Wichtungsfaktoren auf das Optimierungsergebnis a priori nicht abgeschätzt werden

kann, ist der Planungsprozess geprägt von zeitaufwändigem Versuch und Irrtum. 3) Entscheidet sich der Planer für einen bestimmten Plan und beendet den Planungsprozess, so kann er nicht sicher sein, ob durch weiteres Probieren anderer Optimierungsvorgaben nicht ein klinisch noch besseres Ergebnis hätte erzielt werden können.

Um die oben beschriebene Situation der IMRT-Planung zu verbessern, wurde die sogenannte multikriterielle Optimierung (multicriterial optimization, MCO) vorgeschlagen. Ursprünglich in sozial- und wirtschaftswissenschaftlichen Zusammenhängen entwickelt, befasst sich die MCO mit Optimierungsproblemen, die mehrere Einzelziele umfassen, die nicht alle zugleich ihr individuelles Optimum erreichen können, da sie einander widersprechen. Genau dies ist die Situation in der Strahlentherapieplanung, bei der die Einzelziele aus der Dosismaximierung in den Zielvolumina und der dazu konträren Dosisminimierung in den Risikoorganen bestehen. Der „ultimativ optimale“ Bestrahlungsplan, bei dem die Zielvolumina mit exakt der gewünschten Dosis bestrahlt und alle umliegenden Risikoorgane perfekt geschont werden (also gar eine Dosis erhalten), existiert aus physikalischen Gründen nicht. Die MCO wird dieser Tatsache gerecht, indem sie einen dem Problem angepassten Optimalitätsbegriff verwendet: Die Lösung eines multikriteriellen Problems ist genau dann optimal („Pareto-optimal“, benannt nach Vilfredo Pareto, dem Begründer des multikriteriellen Optimierungsprinzips), wenn sie in keinem Einzelkriterium verbessert werden kann, ohne dafür mindestens ein anderes Einzelkriterium zu verschlechtern. Es handelt sich also um einen „optimalen Kompromiss“. Nun gibt es nicht einen einzelnen optimalen Kompromiss, sondern mathematisch beliebig viele, d.h. Pläne mit besonders guter Zielvolumenabdeckung und dafür hoher Risikoorganbelastung, Pläne mit sehr guter Risikoorganschonung und dafür schlechter Zielvolumenerfassung, und alle kontinuierlichen Übergänge. Die Menge aller Pareto-optimalen Lösungen bildet die sog. Pareto-Front (auch Lösungsraum genannt). Jeder einzelne Plan der Pareto-Front ist ein optimaler Kompromiss in dem Sinne, dass er physikalisch nicht weiter verbessert werden kann. Welcher dieser Pläne der beste für den individuellen Patienten ist, ist eine klinische Entscheidung des Bestrahlungsplaners. Nicht alle der Pläne der Pareto-Front sind dabei von Interesse: So ist keine Bestrahlung (Intensitätswerte aller Bixel gleich Null) sicher nicht zur Therapie geeignet, aber ebenfalls ein Pareto-optimaler Plan, denn jede Verbesserung im Zielvolumen wird immer eine, eventuell auch nur geringe, Verschlechterung der Risikoorgane zur Folge haben. Bei N Einzelzielen bildet die Paretofront eine Hyperebene im N-dimensionalen Raum und kann damit ab N>3 nicht mehr visualisiert und auf einen Blick erfasst werden. Stattdessen wird immer ein einzelner Plan gezeigt, und der Lösungsraum wird dann interaktiv navigiert, indem jedes Einzelziel durch einen Regler verstellbar ist. Zumindest der Planungshorizont, d.h. das Spektrum aller in den einzelnen Kriterien erreichbaren Werte, ist als Stellbereich des Reglers auf einen Blick erfassbar. Zur Unterscheidung, ob die Dosisverteilung einer Struktur eines bestimmten Plans besser oder schlechter als die eines anderen Plans ist, wird ein Modell benötigt, das die dreidimensionale, im Allgemeinen heterogene Dosisverteilung in einen skalaren Wert überführt, der mit dem klinischen Effekt korreliert ist. Idealerweise wären dies die Tumorkontrollwahrscheinlichkeit (tumor control probability, TCP) und die Normalgewebs-Komplikationswahrscheinlichkeit (normal tissue complication probability, NTCP). Allerdings sind diese Modelle noch nicht so ausgereift, dass sie für den klinischen Routineeinsatz geeignet wären. Stattdessen wird das Konzept der „equivalent uniform dose“ (EUD) verwendet. Die EUD ist definiert als diejenige homogene Dosis mit dem gleichen klinischen Effekt wie die vorliegende heterogene Dosisverteilung. Man verbleibt also in der Dosisdomäne und vermeidet den mit Unsicherheiten behafteten Modellierungsschritt in Wirkungswahrscheinlichkeiten. Zugleich ist die EUD geeignet zur Optimierung und den Vergleich von Dosisverteilungen, denn die TCP und NTCP sind monoton steigende Funktionen der EUD. Neben der EUD sind auch weitere

Zielfunktionen insbesondere für das Zielvolumen anwendbar, so z.B. Maßzahlen für die Homogenität der Dosisverteilung. Es sind auch mehrere Zielfunktionen für die gleiche Struktur verwendbar, die dann wie alle anderen Einzelkriterien gleichberechtigt nebeneinander stehen und navigiert werden können.

1.2 Funktionelle und molekulare Bildgebung für die Strahlentherapie

Die Grundlage der Bestrahlungsplanung ist ein Modell des Patienten, in dem in hoher Auflösung (typischerweise 2-3mm in jeder Raumrichtung) jedes einzelne Volumenelement (kurz Voxel genannt) einer bestimmten Struktur zugeordnet wird. Wichtige Strukturklassen sind dabei Zielvolumen, Risikoorgan (z.B. Lunge, Herz, Rückenmark, Niere) und Restgewebe. Für jedes Risikoorgan gelten dann in der Bestrahlungsplanung spezifische Toleranzdosen, während im Restgewebe (üblicherweise der Bereich zwischen einzelnen Organen, wie z.B. Muskeln und Bindegewebe) die Dosis generell möglichst gering gehalten werden soll.

Der Bereich der Zielvolumina soll noch etwas differenzierter betrachtet werden. Die Internationale Kommission für Strahlungseinheiten und Messungen (International Commission on Radiation Units & Measurements, ICRU) hat verschiedene Zielvolumenbegriffe definiert [11]: Den makroskopisch erkennbaren Tumor (gross tumor volume, GTV), das mikroskopisch mit hoher Wahrscheinlichkeit befallene Gewebe (clinical target volume, CTV), das von bewegten Tumoren (z.B. atembewegten Lungentumoren) überstrichene Gebiet (internal target volume, ITV), und das aufgrund von physikalischen Unsicherheiten in der Applikation wie z.B. Lagerungsvariationen zu erfassende Zielgebiet (planning target volume, PTV). Basierend auf der Erkenntnis, dass makroskopische Tumoren Subareale mit unterschiedlicher Strahlensensibilität besitzen können [10], wurde weiterhin die Einführung sog. biologischer Zielvolumina (biological target volume, BTV) vorgeschlagen [14].

Üblicherweise basiert die Strahlentherapieplanung auf einer CT-Untersuchung mit oder ohne Kontrastmittel. Die Vorteile der CT für diesen Zweck sind: Hohe Verfügbarkeit, kurze Untersuchungszeit, hohe geometrische Genauigkeit, und die Generierung von Elektronendichteverteilungen für akkurate Dosisberechnung. Allerdings bestehen auch Nachteile, insbesondere für die Erfassung der genannten Zielvolumina: Der geringe Weichteilkontrast der CT kann bereits die Erkennbarkeit des makroskopischen GTV erschweren oder gar unmöglich machen. Die 4D-CT zur Erfassung von Atembewegungen und anderen schnelle Bewegungen für das ITV umfasst nur wenige Atemzyklen, ist mit einer höheren Dosisbelastung verbunden, und ist wegen der retrospektiven Sortierung der Projektionen in einzelne Atemphasen durch Surrogatsignale (z.B. Bauchgurt, auf das Sternum gesetzter Marker) fehleranfällig. Biologische Parameter wie Stoffwechsel oder Tumormikromilieu für das BTV schließlich sind in der CT regelhaft nicht darstellbar.

Im Rahmen des Habilitationsvorhabens wurden daher Bildgebungsverfahren untersucht, die ergänzend zur CT eine verbesserte Zielvolumendefinition erlauben sollen. Dies ist zum einen die Magnetresonanztomographie (MRT), die durch unterschiedliche Untersuchungssequenzen eine Vielzahl unterschiedlicher Bildkontraste erzeugen kann, darunter auch solche, die neben der reinen Morphologie auch Hinweise auf funktionelle Charakteristika geben können. Zum anderen ist dies die Positron-Emissionstomographie (PET), die durch unterschiedliche Tracer verschiedene Strukturen und Stoffwechselvorgänge bildgebend darstellen kann.

1.3 Bildführung im Bestrahlungsraum

Nach Identifizierung von Zielvolumina und Risikoorganen und erfolgter Bestrahlungsplanung liegt ein Bestrahlungsplan vor, der üblicherweise fraktioniert über mehrere Wochen abgestrahlt wird. Insbesondere beim hochkonformalen Verfahren der IMRT, das steile Dosisgradienten zwischen Zielvolumina und Risikoorganen ermöglicht, ist es dabei von entscheidender Bedeutung, die Therapieserie genau zu überwachen. Abweichungen der aktuellen Geometrie von der Planungssituation könnten andernfalls zu einer Unterdosierung im Zielvolumen oder Überdosierung in Risikoorganen führen. Die Überwachung erfolgt meist durch bildgebende Verfahren (z.B. In-Room CT, MV-ConeBeam CT mit dem Therapiestrahl, kV-ConeBeam CT mittels an der Beschleunigergantry angebrachter Röntgenröhre, 3D/4D-Ultraschall, optische Kamerasysteme [13, 15]) oder auch durch andere Methoden (Tracking invasiv implantierter elektromagnetischer Transponder, Surrogatmarker-Systeme wie z.B. ein Bauchgurt zur Atemüberwachung) und dient folgenden Zwecken: i) Reproduktion der Lagerung des Patienten an derselben Stelle wie zur Zeit der Bestrahlungsplanungsuntersuchungen, vorzugsweise orientiert an den inneren Zielstrukturen und nicht nur an der Patientenoberfläche. ii) Verfolgung des Bestrahlungsgebietes auch während der Bestrahlung, z.B. bei Atembewegungen. iii) Erkennen größerer Abweichungen der Patientengeometrie von der Planungssituation, z.B. durch elastische Verformungen innerer Organe oder durch Massenzu- bzw. -abnahme. Je nach Art und Relevanz sind mehrere Korrekturmechanismen möglich: Verschiebung des Patiententisches zur Lagerungskorrektur vor Bestrahlung, Gating bzw. Tracking bei atembewegten Strukturen, Erstellung einer Planbibliothek für verschiedene Geometrien („Plan of the Day"-Konzepte), oder komplette Re-Planungen. Auch kann die Bildgebung verwendet werden zur genauen Rekonstruktion und Dokumentation der tatsächlich applizierten Dosis [9].

Die Etablierung einer hochpräzisen bildgestützten Applikation der Strahlung kombiniert mit ortsaufgelösten Detailinformationen über das Tumorvolumen bildet die Grundlage für fortgeschrittene strahlentherapeutische Konzepte wie verbesserte Risikoorganschonung [7], Dosiseskalation [8] und differenzierte Zielvolumenkonzepte [12].

Im Rahmen des Habilitationsvorhabens wurde mit den zwei bildgebenden Methoden „In-Room CT" und „kV-ConeBeam CT" gearbeitet.

1.4 Quantitative Analyse des Therapieansprechens

Nach Abschluss der Bestrahlungsserie werden die Patienten in regelmäßigen Nachsorgeuntersuchungen weiter betreut und beobachtet. Die dabei dokumentierten klinischen Verläufe können dazu genutzt werden, für bestimmte Tumorentitäten und/oder Patientengruppen das Behandlungsergebnis hinsichtlich der Tumorkontrolle und etwaiger strahlenbedingter Nebenwirkungen festzustellen. Dies dient der Qualitätssicherung ebenso wie der Generierung einer Datenbasis für Dosis-Wirkungsmodelle und für den Vergleich mit anderen Behandlungstechniken. Typische Parameter für klinische Analysen dieser Art sind die lokale Tumorkontrolle, das progressionsfreie Überleben und das Gesamtüberleben. Die Toxizität wird in der Regel nach dem in fünf Schweregraden eingeteilten „Common Toxicity Criteria (CTC)" Score des US-amerikanischen Krebsinstituts (National Cancer Institute, NCI) erfasst und dokumentiert.

In der Nachsorge bzw. nach Therapiebeginn werden funktionelle und molekulare Verfahren wie MRT und PET zunehmend eingesetzt, um möglichst frühzeitig das Ansprechen eines Tumors auf die Bestrahlung zu detektieren und die Patienten damit in Responder und Non-Responder zu stratifizieren. Dies soll eine frühzeitige Anpassung der Therapie, ggf. des gesamten

Therapieschemas, im Sinne einer individualisierten Krebstherapie ermöglichen. Dabei werden auch computergestützte automatisierte Verfahren eingesetzt (Radiomics), die wesentlich weitergehende Informationen aus der Bildgebung gewinnen können als dem menschlichen Auge direkt zugänglich ist [1].

Über die rein binären Auswertungen (z.B. Tumor kontrolliert ja/nein) hinaus wird auch an quantitativen Verfahren gearbeitet, die die genaue Zuordnung z.B. eines Lokalrezidivs mit der zuvor applizierten Dosis ermöglichen sollen, was eine Basis für weitergehende Therapieoptimierungen darstellen kann.

2. Eigene Arbeiten

In diesem Kapitel werden die sechs dieser kumulativen Habilitationsschrift im Wesentlichen zu Grunde liegenden Arbeiten vorgestellt. Darüber hinaus werden in den jeweiligen Unterabschnitten die weiteren eigenen wissenschaftlichen Publikationen aufgelistet, die thematisch mit diesen Arbeiten verbunden sind.

2.1. Strahlentherapieplanung auf Basis multikriterieller Optimierung (MCO)

***2.1.1. Thieke C**, Küfer KH, Monz M, Scherrer A, Alonso F, Oelfke U, Huber PE, Debus J, Bortfeld T: A new concept for interactive radiotherapy planning with multicriteria optimization: first clinical evaluation. Radiother Oncol 2007; 85:292-8*

Im Rahmen einer Kollaboration zwischen dem Deutschen Krebsforschungszentrum (DKFZ) und dem Universitätsklinikum in Heidelberg, dem Fraunhofer-Institut für Techno- und Wirtschaftsmathematik (ITWM) in Kaiserslautern und dem Massachusetts General Hospital und der Harvard Medical School in Boston, USA wurden grundlegende Methoden und ein experimentelles Planungssystem für die intensitätsmodulierte Radiotherapie auf Basis der multikriteriellen Optimierung (MCO) entwickelt und implementiert. Einzelne Aspekte dieses Systems wurden regelmäßig auf Konferenzen und in wissenschaftlichen Fachzeitschriften publiziert (siehe Abschnitt 2.1.3). In der hier vorgestellten Publikation werden erstmalig alle Einzelkomponenten zu einem kompletten, klinisch einsatzfähigen Workflow zusammengeführt, das neue System klinisch evaluiert, und ein Vergleich mit einem aktuellen, im klinischen Einsatz befindlichen inversen Planungssystem durchgeführt.

Der grundsätzlich neue Workflow im MCO-Setting teilt die inverse Planung in zwei Abschnitte: Zunächst berechnet der Computer ohne Nutzerinteraktion eine Datenbasis aller klinisch relevanten Pareto-optimalen Lösungen, und in einem zweiten Schritt wird die Datenbasis interaktiv vom Planer exploriert und der klinisch optimale Kompromiss ausgewählt. Für jede relevante Planstruktur, d.h. das Zielvolumen und die Risikoorgane, werden eine oder mehrere Zielfunktionen definiert, die die dreidimensionale Dosisverteilung innerhalb dieser Struktur auf eine skalare Größe F_i (mit i als Index der Planstruktur) reduzieren und damit auch inhomogene Dosisverteilungen vergleichbar machen.

Das hier entwickelte MCO-Planungssystem nutzt für die Risikoorgane das oben beschriebene Konzept EUD. Volumeneffekte (die sich z.B. in der Unterteilung in serielle und parallele Risikoorgane äußern) können durch organspezifische Parameter erfasst werden. Für die Berechnung der EUD wurden zwei Modelle implementiert, die p-Norm der Dosisverteilung und eine Konvexkombination aus mittlerer und maximaler Dosis. Für das Zielvolumen werden zwei Zielfunktionen definiert, da neben einem bestimmten Mindest-Dosislevel auch eine möglichst große Homogenität erreicht werden soll. Implementiert wurden zum einen die mittlere Dosis mit der Standardabweichung, und zum anderen die p-Norm aller Dosiswerte kleiner einer Unterschranke L und die q-Norm aller Dosiswerte oberhalb einer Oberschranke U.

Nach einer Vorgabe des klinisch relevanten Dosisbereichs generiert das System die Datenbasis von Pareto-optimalen Plänen. Die Vorgaben können dabei sehr großzügig gewählt werden und sind nicht mit den Dosisverschreibungen und Wichtungsfaktoren der klassischen inversen Planung vergleichbar. Sie sollen lediglich sicherstellen, dass das System keine Zeit und Speicherkapazität auf Pläne aufwendet, die zwar im mathematischen Sinne Pareto-optimal, aber klinisch nicht von Interesse sind. Sobald die Datenbasis berechnet wurde, kann sie vom Planer interaktiv navigiert werden. Dabei werden durch Echtzeitinterpolation fließende Übergänge der Dosisverteilung erzielt, auch wenn die Datenbasis aus nur wenigen Stützplänen besteht.

Das System wurde auf zwei klinische Fälle, einen paraspinalen Tumor und einen Prostatatumor, angewendet. Beide Patienten wurden am DKFZ behandelt, wobei der tatsächlich verwendete IMRT-Bestrahlungsplan mit dem etablierten Planungsprogramm „KonRad“ erstellt wurde. Es zeigte sich, dass das MCO-System Pläne mit gleich hoher Qualität erzeugen konnte. Durch die Echtzeitnavigation konnte sehr schnell ein Plan gefunden, der dem Plan des KonRad-Systems physikalisch sehr ähnlich und klinisch gleichwertig war. Dabei konnten mehrere Vorteile des MCO-Systems demonstriert werden: 1) Es ist keine kritische und zugleich nicht-intuitive Definition von Wichtungsfaktoren und Dosisvorgaben mehr erforderlich, vielmehr reicht die grobe Angabe des relevanten Planungshorizonts (dies ließe sich durch Templates für die einzelnen Entitäten ganz automatisieren). 2) Die interaktive Navigation benötigt nur wenige Minuten und verringert damit den Zeitaufwand für die inverse IMRT-Planung erheblich. 3) Bisher wurde der Planungsprozess in der Regel beendet, sobald eine klinisch akzeptable Lösung gefunden wurde. Ob nicht noch weitere Verbesserungen des Planes möglich wären, konnte aus Zeitgründen oft nicht untersucht werden. Mit dem MCO-System erhält der Planer nicht nur Informationen über eine einzelne Lösung, sondern kann durch die interaktive Navigation sehr schnell und intuitiv feststellen, ob nicht noch eine starke Verbesserung in einer Struktur erreichbar ist ohne starke Verschlechterungen in anderen Bereichen.

Diese Publikation ist eine der ersten, die die Vorteile der inversen IMRT-Bestrahlungsplanung basierend auf multikriterieller Optimierung anhand konkreter klinischer Testfälle aufzeigt.

2.1.2. *Süss P, Bortz M, Küfer KH,* ***Thieke C****: The critical spot eraser-a method to interactively control the correction of local hot and cold spots in IMRT planning. Phys Med Biol. 2013;58(6):1855-67*

Vor der endgültigen Freigabe eines Bestrahlungsplans prüfen der Bestrahlungsplaner und der Strahlentherapeut die Dosisverteilung sorgfältig auf jeder einzelnen CT-Schicht. Dabei kann es vorkommen, dass zwar die globalen Parameter wie z.B. die jeweiligen Maximaldosen in den Risikoorganen eingehalten werden, dass aber kleine Areale der Dosisverteilung verbesserungsbedürftig sind. Häufig handelt es sich dabei um eng umschriebene Dosisüberhöhungen („Hot Spots“) im Restgewebe, da diese auf das skalare Qualitätsmaß in der Optimierung in der Regel keinen großen Einfluss haben. Es kann sich aber auch um Hot Spots in speziellen Risikoorganen oder um Cold Spots im Zielvolumen handeln. Das Auftreten dieser unerwünschten lokalen Dosiseffekte ist bereits bekannt von den klinisch etablierten inversen Bestrahlungsplanungssystemen, und sie wurden im Rahmen der klinischen Evaluierung auch beim experimentellen multikriteriellen Planungssystem beobachtet. Da sie prinzipiell an jeder Stelle des bestrahlten Volumens auftreten können, gibt es aktuell keine Möglichkeit, sie bereits im Vorfeld abzufangen oder während der ersten Optimierung zu verhindern. Im Setting der multikriteriellen Optimierung mit der Vorberechnung einer ganzen Datenbank von Plänen würden die praktischen Limits von Berechnungszeiten und Speicherkapazitäten gesprengt.

Ein in der Praxis häufig beschrittener Weg zur Beseitigung dieser lokalen Effekte nutzt sogenannte Hilfsvolumina. Sobald ein Bestrahlungsplan gefunden wurde, der im Wesentlichen klinisch zufriedenstellend ist und nur noch lokale Problemstellen aufweist, werden die Hilfsvolumina manuell um die lokalen Spots herumgezeichnet und ein erneuter Optimierungslauf mit spezifischen Vorgaben für diese Bereiche gestartet. In der klassischen inversen Planung kann dann allerdings das Problem auftreten, dass die neuen Vorgaben zu weit gingen und dadurch Bereiche um das Hilfsvolumen herum in unerwünschter Weise beeinflusst werden. Das Prinzip

der Hilfsvolumina ist prinzipiell auch im multikriteriellen Setting denkbar, wobei nach der Definition des Hilfsvolumens alle bereits vorhandenen Pläne für dieses Hilfsvolumen nachbewertet würden und ein neuer Plan mit speziellen Vorgaben für das Hilfsvolumen der Datenbank hinzugefügt würde. Allerdings bliebe dies in der Praxis recht aufwändig.

In der hier vorgestellten Arbeit wurde daher ein neuartiges Planungswerkzeug („Critical Spot Eraser“) für lokale Dosiskorrekturen entwickelt und getestet, das ohne Hilfsvolumina auskommt und die Möglichkeiten der interaktiven Plannavigation im multikriteriellen Setting noch besser nutzt. Es folgt folgendem Prinzip:

1. Wie im Abschnitt 2.1.1 vorgestellt, wird nach dem multikriteriellen Optimierungsprinzip und interaktiver Navigation ein Bestrahlungsplan identifiziert, der im Wesentlichen akzeptabel ist.
2. Wenn bei der Beurteilung der Dosisverteilung ein lokaler Hot- oder Cold-Spot auffällt, kann mit Hilfe des Tools „Critical Spot Eraser“ mit der Maus direkt auf den betroffenen Bereich geklickt werden.
3. Das Tool zeigt den aktuellen Dosiswert an dieser Stelle an und fragt ab, auf welche Zieldosis dieser Bereich vermindert oder erhöht werden soll. Zusätzlich lässt sich auch die Größe des Bereichs um das angeklickte Voxel herum definieren, auf den sich die Zieldosis beziehen soll.
4. Das System berechnet dann automatisch Lösungen, die die vorgegebene Zieldosis erreichen. Dies geschieht durch Lösung eines entsprechend formulierten Optimierungsproblems, das als Nebenbedingung eine größtmögliche Ähnlichkeit der neuen Dosisverteilung zur ursprünglichen Dosisverteilung hat. Ein weiterer Parameter des Optimierungsproblems ist der Radius um Bereich herum, auf den sich die Veränderungen der Dosisverteilung konzentrieren sollen. Dieser Radius wird vom Tool automatisch variiert und somit werden mehrere Lösungen erzeugt, die alle die gewünschte Zieldosis erreichen, bei denen sich aber die Auswirkungen auf die restliche Dosisverteilung um den Bereich herum auf unterschiedlich große Areale verteilen. Diese Lösungen werden dann der Datenbank hinzugefügt.
5. Anschließend kann der Planer interaktiv alle Pläne explorieren, die zwischen den neu hinzugekommen und den bereits vorhandenen liegen. Damit ist volle Kontrolle darüber gegeben, wie stark die lokale Dosiskorrektur ausfallen soll und wie sich die Änderungen auf die benachbarte Umgebung auswirken sollen.

Es sollte erwähnt werden, dass der „Critical Spot Eraser“ nicht nach dem Pareto-Prinzip arbeitet, das für die ursprüngliche Datenbank hinsichtlich der ursprünglichen Kriterien noch vollständig erfüllt ist. Dies erscheint aber auch nicht notwendig, da die Bestrahlungsplanung ausschließlich zum Ziel hat, den aus planerischer Sicht bestmöglichen Plan zu generieren, und hierfür bietet der Critical Spot Eraser aus rein pragmatischer Sicht die bestmögliche Einflussmöglichkeit.

Das Verfahren wurde innerhalb des experimentellen multikriteriellen Planungssystems implementiert und am Beispiel der Bestrahlungsplanung für einen Schädelbasistumor mit den Risikoorganen rechter und linker Sehnerv, Hirnstamm und Rückenmark klinisch evaluiert. Es konnte die Erwartungen für diesen Testfall voll erfüllen und einen Hotspot außerhalb des Zielvolumens entfernen, ohne den restlichen Plan an anderen Stellen wesentlich zu verändern.

Für die Einzelheiten des mathematischen Setups, der konkreten Implementierung und der Arbeitsweise des Werkzeugs sei auf die angehängte Originalpublikation verwiesen.

Die Vorteile des neu entwickelten Planungswerkzeugs zur lokalen Dosiskorrektur gegenüber der klassischen inversen Planung mit Hilfsvolumina sind:

- Keine manuelle Konturierung von Hilfsvolumina mehr nötig, stattdessen erfolgt die Markierung des Spots mit einem Mausklick.
- Da im Optimierungsproblem die größtmögliche Ähnlichkeit zur ursprünglichen Dosisverteilung integriert ist, werden überraschend neu auftretende Hot- oder Cold-Spots in weiter Entfernung vom zu korrigierenden Bereich, die ihrerseits wieder zeitaufwändig korrigiert werden müssten, vermieden.
- Auch wenn die lokale Zielvorgabe sehr drastisch war und unerwünschte Effekte auf Nachbarregionen hatte, müssen keinen weiteren Lösungen mehr berechnet werden, denn durch Echtzeitinterpolation mit interaktiver Navigation lassen sich alle Zwischenpläne bis hin zum Ursprungsplan erreichen.
- Völlig neu ist die Möglichkeit, die Änderungen auf den Gesamtplan so lokal wie möglich zu halten oder auf einen größeren Bereich auszudehnen, und auch hier alle Zwischenstufen interaktiv in Echtzeit zu explorieren.

Das in dieser Arbeit entwickelte und evaluierte Tool zur lokalen Dosiskorrektur hat damit das Potenzial, in der klinischen Routine zu einem Standardwerkzeug im letzten Schritt der Bestrahlungsplanung zu werden.

2.1.3. *Weitere, thematisch verbundene eigene Arbeiten*

Es wurde ein Verfahren zur Beschleunigung der Dosisberechnung entwickelt, um den Optimierungsprozess zeitlich praktikabel zu halten [A1]. Ein neues Modell der EUD, das auf der maximalen und der mittleren Dosis im Risikoorgan basiert, wurde vorgeschlagen und an publizierte Toleranzdosen von Risikoorganen angepasst [A2]. Der grundsätzliche Planungsablauf in der MCO mit Vorberechnung des Lösungsraums und anschließender interaktiver Navigation wurde entwickelt [A3]. Die Berücksichtigung der EUD in der Optimierung wurde ermöglicht mit Hilfe der Projektion auf konvexe Mengen (projection onto convex sets, POCS) [A4]. Die Stratifizierung, d.h. die Überführung der in der Optimierung bestimmten kontinuierlichen Bixelintensitäten in diskrete Intensitätsstufen zur Umsetzung in praktisch abstrahlbare Sequenzen, wurde verbessert durch Definition des Optimierungsziels als minimale Dosisdifferenz zwischen ursprünglicher und stratifizierter Intensitätsverteilung [A5]. Die interaktive Exploration des MCO-Lösungsraums, die wegen der Interpolation von Stützplänen und separater Optimierung der Bewegungen im Lösungsraum eine eigenständige, algorithmisch komplexe Herausforderung darstellt, wurde konzeptionell entwickelt und prototypisch implementiert [A6]. Zur Analyse des Einflusses von Parametern auf das Optimierungsergebnis ohne wiederholte Neuberechnungen wurden Konzepte der Elastizität und Sensitivität eingeführt und an einem artifiziellen Beispielfall evaluiert [A7]. Die effiziente Generierung des Lösungsraums klinisch relevanter Lösungen wurde durch Einführung von sog. Trade-Off Bounds unterstützt [A8]. Neue Methoden für den Vergleich von Paretofronten für den multikriteriell basierten Vergleich zweier verschiedener Techniken, z.B. unterschiedlicher Anzahl von Einstrahlrichtungen oder Photonen- und Protonentherapie, wurden entwickelt und evaluiert [A9].

A1. **Thieke C**, Nill S, Oelfke U, Bortfeld T. Acceleration of intensity-modulated radiotherapy dose calculation by importance sampling of the calculation matrices. *Med Phys* 2002; 29:676-81

A2. **Thieke C**, Bortfeld T, Kuefer KH. Characterization of dose distributions through the max and mean dose concept. *Acta Oncol* 2002; 41:158-161

A3. Kuefer KH, Scherrer A, Monz M, Alonso F, Trinkaus H, Bortfeld T, **Thieke C**. Intensity-modulated radiotherapy – a large scale multi-criteria programming problem. *OR Spectrum* 2003; 25:223-249

A4. **Thieke C**, Bortfeld T, Niemierko A, Nill S. From physical dose constraints to equivalent uniform dose constraints in inverse radiotherapy planning. *Med Phys* 2003, 30:2332-2339

A5. Süss P, Küfer KH, **Thieke C**. Improved stratification algorithms for step-and-shoot MLC delivery in intensity-modulated radiation therapy. *Phys Med Biol* 2007; 52:6039-51

A6. Monz M, Küfer KH, Bortfeld TR, **Thieke C**. Pareto navigation: algorithmic foundation of interactive multi-criteria IMRT planning. *Phys Med Biol* 2008; 53:985-98

A7. Krause M, Scherrer A, **Thieke C**. On the role of modeling parameters in IMRT plan optimization. *Phys Med Biol* 2008; 53:4907–26

A8. Serna JI, Monz M, Küfer KH, **Thieke C**. Trade-off bounds for the Pareto surface approximation in multi-criteria IMRT planning. *Phys Med Biol* 2009; 54:6299-311

A9. Teichert K, Süss P, Serna JI, Monz M, Küfer KH, **Thieke C**. Comparative analysis of Pareto surfaces in multi-criteria IMRT planning. *Phys Med Biol*. 2011;56(12):3669-84

2.2. Funktionelle und molekulare Bildgebung für die Strahlentherapie

2.2.1. *Askoxylakis V, Dinkel J, Eichinger M, Stieltjes B, Sommer G, Strauss LG, Dimitrakopoulou-Strauss A, Kopp-Schneider A, Haberkorn U, Huber PE, Bischof M, Debus J,* ***Thieke C****: Multimodal hypoxia imaging and intensity modulated radiation therapy for unresectable non-small-cell lung cancer: the HIL trial. Radiat Oncol. 2012 14;7:157*

Diese Publikation beschreibt eine prospektive Studie, die den Stellenwert der Hypoxiebildgebung mittels FMISO-PET und der Perfusions-MRT im Rahmen der intensitätsmodulierten Strahlentherapie des nichtkleinzelligen Bronchialkarzinoms (non small cell lung cancer, NSCLC) untersuchen sollte. Die Untersuchungen waren geplant für 15 Patienten mit NSCLC Stadium III an jeweils 3 Zeitpunkten im Verlaufe der Therapie: Zunächst im Rahmen der Bestrahlungsplanung, dann in der 5. Woche der fraktionierten Strahlentherapieserie, und schließlich im Rahmen der ersten strahlentherapeutischen Nachsorgeuntersuchung 6 Wochen nach Strahlentherapieende. Die Therapie selbst sollte im Rahmen dieser Studie durch die zusätzlichen Untersuchungen nicht beeinflusst werden. Ziel war vielmehr die Gewinnung von Informationen, inwiefern die Hypoxiebildgebung später in der Bestrahlungsplanung eingesetzt werden könnte, wie sich die Bildgebung im Therapieverlauf verändert, und schließlich ob die Hypoxiebildgebung eine prognostische Aussagekraft besitzt und sich eventuell für die Stratifizierung der NSCLC-Patienten in unterschiedliche Gruppen eignet.

Ein positives Votum der lokalen Ethikkommission wurde eingeholt, und die Studie wurde unter der Protokoll-ID NCT01617980 auf ClinicalTrials.gov registriert. Die Patientenrekrutierung begann im April 2012. Leider stellte sich diese als schwierig heraus, sowohl hinsichtlich der Identifizierung grundsätzlich geeigneter Patienten als auch bei der Einholung der freiwilligen Zustimmung zur Teilnahme. Hinzu kam ein bereits beschriebener Effekt des FDG-PET, das im Rahmen der Bestrahlungsplanung das Staging komplettieren sollte: Zuvor als Stadium III klassifizierte Patienten zeigten im FDG-PET Metastasen, waren also im Stadium IV und fielen damit bereits nach dem ersten Untersuchungszeitpunkt aus der Studie heraus. Dies war bei insgesamt 6 von initial 13 eingeschlossenen Patienten der Fall. Die Studie wurde schließlich wegen zu langsamer Rekrutierung im März 2014 geschlossen.

Trotz dieses vorzeitigen Studienendes konnten wertvolle Erkenntnisse über die Planung und Durchführung derartiger Studien gewonnen werden. Zudem erfolgte eine Vergleichsanalyse

der akquirierten FDG- und FMISO-PET Untersuchungen, siehe folgenden Abschnitt unter der Referenz B6.

2.2.2. *Weitere, thematisch verbundene eigene Arbeiten*

Die zeitaufgelöste Volumendarstellung im MRT wurde zur Analyse der Bewegung sowohl von Lungentumoren als auch der Prostata eingesetzt [B1, B2]. Die bei multimodaler Bildgebung erforderliche Registrierung wurde durch softwaregestütztes Definieren von in allen Bildern identifizierbaren Landmarken untersucht [B3]. Die diffusionsgewichtete MRT (diffusion weighted imaging, DWI) wurde genutzt für ein neuartiges Verfahren der Einteilung von Hirntumor-Arealen mit niedriger und hoher Proliferationsrate [B4]. Die MR-Spektroskopie (MRS) der Prostata wurde durch ein automatisiertes Verfahren mit Mustererkennung zur Unterscheidung intraprostatischer Areale in tumorsuspekte und nicht suspekte Anteile eingeführt und durch Vergleich mit manueller Klassifikation der Spektren evaluiert [B5]. Die PET schließlich wurde auf Basis der in 2.2.1 beschriebenen Studiendaten untersucht hinsichtlich der Identifikation hypoxischer Anteile von Lungentumoren mittels FMISO-PET, und die Ergebnisse mit FDG-PET verglichen [B6].

B1. Dinkel J, Hintze C, Tetzlaff R, Huber PE, Herfarth K, Debus J, Kauczor HU, **Thieke C**. 4D-MRI analysis of lung tumor motion in patients with hemidiaphragmatic paralysis. *Radiother Oncol* 2009; 91:449-54

B2. Dinkel J, **Thieke C**, Plathow C, Zamecnik P, Prüm H, Huber PE, Kauczor HU, Schlemmer HP, Zechmann CM. Respiratory-induced prostate motion: characterization and quantification in dynamic MRI. *Strahlenther Onkol*. 2011;187(7):426-32

B3. Prüm H, Gerigk L, Hintze C, **Thieke C**, Floca R. Software-guided standardization of manual landmark data in medical images. *Z Med Phys*. 2011;21(1):42-51

B4. Simon D, Fritzsche KH, **Thieke C**, Klein J, Parzer P, Weber MA, Stieltjes B. Diffusion-weighted imaging-based probabilistic segmentation of high- and low-proliferative areas in high-grade gliomas. *Cancer Imaging*. 2012;12:89-99

B5. Zechmann CM, Menze BH, Kelm BM, Zamecnik P, Ikinger U, Giesel FL, **Thieke C**, Delorme S, Hamprecht FA, Bachert P. Automated vs. manual pattern recognition of 3D (1)H MRSI data of patients with prostate cancer. *Acad Radiol*. 2012;19(6):675-84

B6. Sachpekidis C, **Thieke C**, Askoxylakis V, Nicolay NH, Huber PE, Thomas M, Dimitrakopoulou G, Debus J, Haberkorn U, Dimitrakopoulou-Strauss A. Combined use of (18)F-FDG and (18)F-FMISO in unresectable non-small cell lung cancer patients planned for radiotherapy: a dynamic PET/CT study. *Am J Nucl Med Mol Imaging*. 2015 15;5(2): 127-42

2.3. Bildführung im Bestrahlungsraum

2.3.1. Thieke C*, Malsch U, Schlegel W, Debus J, Huber P, Bendl R, Thilmann C: Kilovoltage CT using a linac-CT scanner combination. Br J Radiol 2006 Sep;79 Spec No 1:79-86*

Am Deutschen Krebsforschungszentrum wurde im Jahre 2002 ein einzeiliger CT-Scanner (Typ Siemens Somatom) im Bestrahlungsraum installiert, der den gleichen Patiententisch wie der im gleichen Raum installierte Linearbeschleuniger Siemens Primus (später Siemens Artiste) nutzt. Zwischen CT-Untersuchung und Bestrahlung wird der Tisch um 90° gedreht.

Die hier vorliegende Arbeit befasst sich mit der systematischen Einführung und klinischen Erprobung von bildgeführter, adaptiver Strahlentherapie auf Basis dieser kV-basierter Volumenbildgebung. Verschiedene Levels der adaptiven Strahlentherapie werden definiert:

Level 0: Bestrahlungsplanung basierend auf multipler Bildgebung ohne spätere Plananpassungen, entweder patientenindividuell oder populationsbasiert

Level 1: Offline-Korrekturen von interfraktionellen Abweichungen nach multipler Bildgebung (erfasst systematische Abweichungen)
1A: durch Zielpunktkorrektur (wenn rigide Transformationen ausreichen)
1B: durch Re-Planung (wenn elastische Transformationen benötigt werden)

Level 2: Online-Korrektur von interfraktionellen Abweichungen direkt nach dem CT-Scan und noch vor der direkt folgenden Bestrahlung (erfasst neben den systematischen auch die täglich wechselnden, zufälligen Abweichungen)
2A: durch Zielpunktkorrektur
2B: durch Re-Planung

Level 3: Korrektur intrafraktioneller Abweichungen, z.B. durch Gating oder Tracking

Die bildgeführte Therapie von Prostatatumoren (10 Patienten), paraspinalen Tumoren (7 Patienten) und Kopf-Hals-Tumoren (1 Patient) wurde klinisch durchgeführt und quantitativ ausgewertet. Da nur rigide Registrierungsalgorithmen zur Verfügung standen, wurde das bestrahlte Volumen in mehrere Teilvolumina aufgeteilt, die unabhängig voneinander rigide registriert wurden. Durch Vergleich der Translationsvektoren konnte festgestellt werden, ob die rigide Registrierung insgesamt ausreichend war: Bei nahezu gleichen Translationsvektoren für die verschiedenen Subvolumina ist eine einfache globale Zielpunktkorrektur ausreichend, bei größeren Abweichungen ist unter Umständen eine Neukonturierung des CT-Datensatzes mit anschließender Re-Planung erforderlich.

Es zeigte sich, dass bei Prostatatumoren mit Beschränkung auf die knöcherne Anatomie als Lagerungskriterium die einfache Zielpunktkorrektur ausreichend ist. Auch bei paraspinalen Tumoren gab es keine klinisch relevanten elastischen Verformungen im Zielgebiet, so dass eine Zielpunktkorrektur ausreichend ist. Beim Kopf-Hals-Patienten konnte schließlich gezeigt werden, dass die Abweichungen deutlich variabler ausfallen können und eine einfache rigide Registrierung mit anschließender Zielpunktkorrektur nicht immer ausreicht. Dies wurde nicht nur rein geometrisch gezeigt, sondern auch anhand einer dosimetrischen Analyse vor und nach einer Re-Planung mit angepasster Konturierung. Hierbei wurde der Vorteil der In-Room CT-Bildgebung genutzt, dass die Daten im Gegensatz zum mittlerweile klinisch etablierten Cone-Beam CT direkt auch für die Dosisberechnung und Bestrahlungsplanung eingesetzt werden können.

Die hier beschriebenen klinischen Prozeduren stellen bis heute im Wesentlichen den aktuellen Standard in der Routine dar, wobei allerdings statt In-Room-CTs in der Regel am Beschleuniger montierte kV-Cone-Beam-CTs verwendet werden. Diese stellen geringere Anforderungen an die Größe des Bestrahlungsraums, erfordern keine manuelle Tischdrehung zwischen Bildgebung und Bestrahlung, sind günstiger in der Anschaffung haben prinzipiell das Potenzial zur Bildgebung während der Bestrahlung (Level 3), bringen aber auch eine höhere Dosisbelastung für die Bildgebung bei zugleich schlechterer Bildqualität mit sich und sind nicht ohne weiteres für die Dosisberechnung und Re-Planung verwendbar. Es ist allerdings zu erwarten, dass in den kommenden Jahren auch der Level 2B und zunehmend auch der Level 3 in klinischen Routinebehandlungen erreicht werden wird, nicht zuletzt durch die Entwicklung der MR-/Linac-Hybridgeräte, die neben den dafür nötigen technischen Entwicklungen auch eine deutliche Weiterentwicklung den Bereichen Bildregistrierung, Rekonturierung, Dosisakkumulation, Re-Planung und Echtzeitkorrektur mit sich bringen könnten.

2.3.2. *Stoiber EM, Lechsel G, Giske K, Muenter MW, Hoess A, Bendl R, Debus J, Huber PE,* ***Thieke C****: Quantitative assessment of image-guided radiotherapy for paraspinal tumors.* Int J Radiat Oncol Biol Phys 2009; 75:933-40

Die Bestrahlung paraspinaler Tumoren ist besonders kritisch, da hier durch das Rückenmark als strahlensensible Risikostruktur schwerwiegende Nebenwirkungen in Form von Sensibilitätsstörungen und Lähmungserscheinungen im Falle einer Fehllagerung drohen. Auf der anderen Seite muss das Tumorzielvolumen mit der höchstmöglichen Dosis behandelt werden, da dieselben Auswirkungen auch durch lokal nicht kontrolliertes Tumorwachstum drohen.

In dieser Arbeit wurde daher die bildgeführte intensitätsmodulierte Strahlentherapie paraspinaler Tumoren sorgfältig untersucht, um die bestmögliche klinische Behandlungsprozedur zu bestimmen. Dazu wurden 45 Patienten mit paraspinalen Tumoren im Bereich der zervikalen, thorakalen und lumbalen Wirbelsäule analysiert, die insgesamt 321 Kontroll-CTs erhalten haben.

Durch Aufteilung des Registrierungsvolumens auf drei Teilbereiche und Vergleich der Translationsvektoren konnte gezeigt werden, dass eine rigide Registrierung mit anschließender Zielpunktkorrektur bei der verwendeten Patientenfixierung in einer Scotch-Cast-Körperschale ausreichend ist. Es konnte allerdings auch gezeigt werden, dass trotz der strikten äußeren Fixierung das Rückenmark in einzelnen Fraktionen ohne Korrektur durch Lagerungsvariationen im Bereich des Hochdosis-Zielvolumens lokalisiert war, so dass in kritischen Fällen die Online-Korrektur (Level 2A) mit täglicher Bildgebung empfohlen wird.

Durch diese Arbeit konnte eine sichere und zugleich klinisch praktikable Behandlungsprozedur für die Bestrahlung paraspinaler Tumoren etabliert werden.

2.3.3. *Weitere, thematisch verbundene eigene Arbeiten*

Ein erster Prototyp eines kV-ConeBeam CTs wurde klinisch implementiert und evaluiert [C1]. Ein Algorithmus für die schnelle elastische Registrierung der täglichen In-Room CT-Bildgebung mit dem BPL-CT wurde entwickelt und getestet [C2]. Das „Plan of the Day“-Konzept wurde realisiert bei einem Patienten mit Ösophaguskarzinom, dessen Ösophagus sich an verschiedenen Tagen irregulär auf der einen oder der anderen Seite der Aorta befand [C3]. Eine quantitative geometrische Analyse der fraktionierten Therapie von Kopf-Hals-Tumoren auf Basis wöchentlicher bzw. täglicher In-Room CTs wurde durchgeführt [C4]. Im Bereich der Dosisakkumulation wurden sowohl registrierungsbedingte statistische Unsicherheiten untersucht [C5] als auch Verfahren zur Dosisberechnung von Protonenplänen auf Basis der kV-ConeBeam CT realisiert [C6].

C1. Thilmann C, Nill S, Tucking T, Hoss A, Hesse B, Dietrich L, Bendl R, Rhein B, Haring P, **Thieke C**, Oelfke U, Debus J, Huber P. Correction of patient positioning errors based on in-line cone beam CTs: clinical implementation and first experiences. *Radiat Oncol* 2006; 24:1-16

C2. Malsch U, **Thieke C**, Huber PE, Bendl R. An enhanced block matching algorithm for fast elastic registration in adaptive radiotherapy. *Phys Med Biol* 2006; 51:4789-806

C3. Jensen AD, Grehn C, Nikoghosyan A, **Thieke C**, Krempien R, Huber PE, Debus J, Münter MW. Catch me if you can--the use of image guidance in the radiotherapy of an unusual case of esophageal cancer. *Strahlenther Onkol*. 2009; 185:469-73

C4. Giske K, Stoiber EM, Schwarz M, Stoll A, Muenter MW, Timke C, Roeder F, Debus J, Huber PE, **Thieke C**, Bendl R. Local setup errors in image-guided radiotherapy for head and neck cancer patients immobilized with a custom-made device. *Int J Radiat Oncol Biol* Phys. 2011; 80(2):582-9

C5. Hub M, **Thieke C**, Kessler ML, Karger CP. A stochastic approach to estimate the uncertainty of dose mapping caused by uncertainties in b-spline registration. *Med Phys*. 2012;39(4):2186-92

C6. Landry G, Nijhuis R, Dedes G, Handrack J, **Thieke C**, Janssens G, Orban de Xivry J, Reiner M, Kamp F, Wilkens JJ, Paganelli C, Riboldi M, Baroni G, Ganswindt U, Belka C, Parodi K. Investigating CT to CBCT image registration for head and neck proton therapy as a tool for daily dose recalculation. Med Phys. 2015 Mar;42(3):1354-66

2.4. Quantitative Analyse des Therapieansprechens

***2.4.1. Thieke C**, Nicolay NH, Sterzing F, Hoffmann H, Roeder F, Safi S, Debus J, Huber PE: Long-term results in malignant pleural mesothelioma treated with neoadjuvant chemotherapy, extrapleural pneumonectomy and intensity-modulated radiotherapy. Radiat Oncol. 2015; 10:267*

Die Behandlung des malignen Pleuramesothelioms (MPM) ist bestimmt durch die schlechte Prognose palliativ behandelter und unbehandelter Patienten einerseits und die Toxizität intensivierter Therapieschemata andererseits. Eines der intensivsten Therapieschemata des MPM ist die trimodale Therapie, bestehend aus einer neoadjuvanten Chemotherapie über mehrere Zyklen, der operativen Entfernung einer Lungenhälfte inklusive des anhängenden Zwerchfells und Perikards, und der adjuvanten Bestrahlung des betroffenen Hemithorax. Die Risikoorgane bei der Bestrahlung sind das Herz, das Rückenmark, die kontralaterale Lunge, die Nieren und die Leber. Erst mit Einführung der IMRT konnten therapeutische Zieldosen im Bereich von über 40 Gy erreicht werden. Die wichtigste unerwünschte Nebenwirkung ist dabei die strahlenbedingte Pneumonitis der kontralateralen Lunge, die lebensbedrohlich sein kann.

In der hier vorgestellten Arbeit wurde die trimodale Therapie auf Effektivität und Toxizität hin retrospektiv analysiert, wobei der Schwerpunkt auf der adjuvanten Strahlentherapie (durchgeführt als Tomotherapie und als Step&Shoot-IMRT) lag. Erfasst wurden die Toxizität gemäß CTC und die Kaplan-Meier-Kurven für das Gesamtüberleben, die lokoregionäre Kontrolle und die distale Kontrolle.

Mit 62 Patienten und einer medianen Nachbeobachtungszeit von 17 Monaten, wobei nur 6 Patienten zum Zeitpunkt der Analyse noch am Leben waren, handelt es sich um eine der größten Studien mit einer der längsten Nachbeobachtungszeiten bei MPM überhaupt. Bei keinem der Patienten trat nach IMRT eine Nebenwirkung der Schweregrade 4 oder 5 auf. Damit konnte gezeigt werden, dass die IMRT sicher anwendbar ist. Zugleich waren die erreichten Überlebens- und Kontrollraten im Bereich der besten bisher in der Literatur berichteten Werte. Es gab dabei dosimetrisch und hinsichtlich der klinischen Ergebnisse keinen signifikanten Unterschied zwischen der Tomotherapie und der Step&Shoot-IMRT, so dass beide Techniken bei MPM als gleichwertig angesehen werden können.

Die hier dokumentierten Daten belegen die sichere Durchführbarkeit der IMRT bei MPM und stellen eine Referenz dar, an denen sich alternative, aktuelle und zukünftige, Therapieverfahren messen lassen können.

***2.4.2.** Weitere, thematisch verbundene eigene Arbeiten*

Klassische retrospektive Auswertungen zeigen das klinische Potenzial der IMRT für Riesenzelltumoren [D1], Nasopharynx-Tumoren [D2] und rezidivierten Kopf-Hals-Tumoren [D3, D4]. Die MR-Bildgebung als Modalität zur Nachsorge von bestrahlten Prostatakarzinom-Patienten wurde untersucht [D5, D6]. Weiterhin wurden Methoden zur Visualisierung der Unsicherheiten

radiobiologischer Modelle entwickelt [D7]. Eine für die quantitative, ortsaufgelöste und dosisbasierte Analyse von Therapieverläufen geeignete Softwarebibliothek wurde entwickelt und als Open Source der wissenschaftlichen Community zugänglich gemacht [D8].

D1. Roeder F, Timke C, Zwicker F, Thieke C, Bischof M, Debus J, Huber PE. Intensity modulated radiotherapy (IMRT) in benign giant cell tumors--a single institution case series and a short review of the literature. *Radiat Oncol*. 2010; 5:18

D2. Roeder F, Zwicker F, Saleh-Ebrahimi L, Timke C, **Thieke C**, Bischof M, Debus J, Huber PE. Intensity modulated or fractionated stereotactic reirradiation in patients with recurrent nasopharyngeal cancer. *Radiat Oncol*. 2011;6:22

D3. Zwicker F, Roeder F, Hauswald H, **Thieke C**, Timke C, Schlegel W, Debus J, Münter MW, Huber PE. Reirradiation with intensity-modulated radiotherapy in recurrent head and neck cancer. *Head Neck*. 2011;33(12):1695-702

D4. Zwicker F, Roeder F, **Thieke C**, Timke C, Münter MW, Huber PE, Debus J. IMRT reirradiation with concurrent cetuximab immunotherapy in recurrent head and neck cancer. *Strahlenther Onkol*. 2011; 187(1):32-8

D5. Zechmann CM, Aftab K, Didinger B, Giesel FL, Zamecnik P, **Thieke C**, Fütterer JJ, Kopp-Schneider A, Kauczor HU, Delorme S. Changes of prostate gland volume with and without androgen deprivation after intensity modulated radiotherapy - A follow-up study. *Radiother Oncol* 2009; 90:408-12

D6. Zechmann CM, Simpfendörfer T, Giesel FL, Zamecnik P, **Thieke C**, Hielscher T, Meinzer HP, Delorme S. Comparison of peripheral zone and central gland volume in patients undergoing intensity-modulated radiotherapy. *J Comput Assist Tomogr*. 2010; 34(5):739-45

D7. Zhang L, Hub M, **Thieke C**, Floca RO, Karger CP. A method to visualize the uncertainty of the prediction of radiobiological models. *Phys Med*. 2013;29(5):556-61

D8. Zhang L, Hub M, Mang S, **Thieke C**, Nix O, Karger CP, Floca RO. Software for quantitative analysis of radiotherapy: overview, requirement analysis and design solutions. *Comput Methods Programs Biomed*. 2013;110(3):528-37

3. Zusammenfassung und Ausblick

Die in dieser Habilitationsschrift vorgestellten Arbeiten befassen sich mit unterschiedlichen Methoden und Werkzeugen, die ein gemeinsames Ziel haben: Das Potenzial der intensitätsmodulierten Strahlentherapie zum Nutzen des Patienten bestmöglich auszuschöpfen.

Dies betrifft zum einen die inverse Bestrahlungsplanung, bei der die Entwicklung der multikriteriellen Optimierung (MCO) mit interaktiver Entscheidungsunterstützung die mathematische Komplexität des Problems besser beherrschbar macht und daher in der klinischen Routine sowohl eine deutliche Zeitersparnis als auch eine bessere Planqualität erwarten lässt. Das Planungssystem RayStation der Firma RaySearch Laboratories hat dieses Optimierungsprinzip als erstes in einem kommerziellen Planungssystem realisiert, und die Firma Varian wird ihre Planungsstationen ebenfalls mit dieser Funktionalität ausstatten. Es erscheint daher möglich, dass sich die MCO auf breiter Basis in der klinischen Praxis durchsetzen wird. Die Entwicklung geht dabei beständig weiter; so könnten in Zukunft neben Dosiskenngrößen auch weitere Qualitätskriterien zur Beurteilung und Navigation der Bestrahlungspläne herangezogen werden, wie z.B. die Bestrahlungszeit. Auch die Übertragung und Erweiterung der Methoden von der photonenbasierten Step&Shoot IMRT auf die Planung von VMAT-IMRT und Partikeltherapie, z.B. mit Protonen, ist Gegenstand aktueller Forschung und Entwicklung.

Die funktionelle und molekulare Bildgebung für die Strahlentherapie ist ein weiteres Feld mit hohem Potenzial, die Behandlungsqualität weiter zu verbessern. Klinische Studien in diesem Bereich sind zwar logistisch und hinsichtlich der nötigen Patientenzahlen eine große Herausforderung, aber unverzichtbar für die routinemäßige Etablierung neuer Verfahren. Auch bei den grundlegenden Modalitäten sind in Zukunft für die Strahlentherapie hochrelevante Neuerungen zu erwarten, so z.B. neue MRT-Sequenzen und neue PET-Tracer wie z.B. das prostataspezifische Membranantigen, PSMA.

Die bildgeführte Strahlentherapie ist mittlerweile fester Bestandteil der klinischen Routine. Dabei wird aktuell meist ein an der Beschleunigergantry montiertes Flat-Panel in Verbindung mit einer Röntgenröhre (Cone Beam-CT) eingesetzt. Weitere Ansätze der Bildführung wie z.B. mit Ultraschall oder optischen Kameras sind speziellen Einsatzzwecken und Entitäten vorbehalten. Der nächste, universell einsatzbare Schritt könnte die Einführung der MRT anstelle der CT als bildführende Modalität sein, wie sie von der Firma ViewRay und demnächst auch weiteren Firmen kommerziell angeboten wird. Viele der auf CT-Basis entwickelten Prozeduren, Verfahren und Algorithmen werden auch im MRT-Setting Gültigkeit haben und Verwendung finden, andere werden speziell an die neue Modalität adaptiert werden müssen, und wieder andere eventuell ganz ersetzt werden. In jedem Fall ist dieser Bereich ein hochaktives Feld aktueller Forschung und Entwicklung.

Auch in der computergestützten Analyse und Verlaufsbeobachtung sind für die Zukunft deutliche Veränderungen und Verbesserungen zu erwarten. Professionelle, für klinische Studien gemäß den Richtlinien der Good Clinical Practice (GCP) geeignete Datenbanksysteme werden zunehmend in der klinischen Forschung eingesetzt. Die einzelnen onkologischen Fachabteilungen und auch mehrere Kliniken bzw. Krebszentren werden untereinander vernetzt, womit die Zahl der auswertbaren Patienten, die Größe der Datenbasis und damit die Aussagekraft der gewonnenen Ergebnisse steigt. Neue Werkzeuge zur Bildverarbeitung und Dosisanalyse werden zunehmend etabliert, so dass neben den weiterhin wichtigen Parametern wie Gesamtüberleben und Lokalkontrolle zusätzlich auch ortsaufgelöste Verlaufsinformationen zur Verfügung stehen werden und neue Ansätze für eine personalisierte Strahlentherapie liefern.

4. Abkürzungsverzeichnis

BPL-CT	Bestrahlungsplanungs-Computertomographie
BTV	Biological Target Volume
CT	Computertomographie
CTC	Common Toxicity Criteria
CTV	Clinical Target Volume
DKFZ	Deutsches Krebsforschungszentrum
DWI	Diffusion Weighted Imaging
EUD	Equivalent Uniform Dose
FDG-PET	Fluorodeoxyglucose - Positronenemissionstomographie
FMISO-PET	Fluoromisonidazole – Positronenemissionstomographie
GCP	Good Clinical Practice
GTV	Gross Tumor Volume
ICRU	International Commission on Radiation Units & Measurements
IMRT	Intensitätsmodulierte Radiotherapie
ITV	Internal Target Volume
ITWM	Fraunhofer-Institut für Techno- und Wirtschaftsmathematik
MCO	Multicriterial Optimization
MPM	Malignes Pleuramesotheliom
MRS	Magnetic Resonance Spectroscopy
MRT	Magnetresonanztomographie
NCI	National Cancer Institute
NSCLC	Non Small Cell Lung Cancer
NTCP	Normal Tissue Complication Probability
PET	Positronenemissionstomographie
POCS	Projection Onto Convex Sets
PSMA	Prostataspezifisches Membranantigen
TCP	Tumor Control Probability
VMAT	Volumetric Arc Therapy

5. Literaturverzeichnis

[1] Aerts HJ, Velazquez ER, Leijenaar RT, Parmar C, Grossmann P, Carvalho S, Bussink J, Monshouwer R, Haibe-Kains B, Rietveld D, Hoebers F, Rietbergen MM, Leemans CR, Dekker A, Quackenbush J, Gillies RJ, Lambin P. Decoding tumour phenotype by noninvasive imaging using a quantitative radiomics approach. Nat Commun. 2014; 5:4006

[2] Bortfeld T, Boyer AL, Schlegel W, Kahler DL, Waldron TJ. Realization and verification of three-dimensional conformal radiotherapy with modulated fields. Int J Radiat Oncol Biol Phys. 1994; 30(4):899-908

[3] Bortfeld T, Bürkelbach J, Boesecke R, Schlegel W. Methods of image reconstruction from projections applied to conformation radiotherapy. Phys Med Biol. 1990; 35(10):1423-34

[4] Bortfeld T. IMRT: a review and preview. Phys Med Biol. 2006; 51(13):R363-79

[5] Bortfeld TR, Kahler DL, Waldron TJ, Boyer AL. X-ray field compensation with multileaf collimators. Int J Radiat Oncol Biol Phys. 1994; 28(3):723-30

[6] Brahme A, Roos JE, Lax I. Solution of an integral equation encountered in rotation therapy. Phys Med Biol. 1982; 27(10):1221-9

[7] Chen YJ, Suh S, Nelson RA, Liu A, Pezner RD, Wong JY. Setup variations in radiotherapy of anal cancer: advantages of target volume reduction using image-guided radiation treatment. Int J Radiat Oncol Biol Phys. 2012; 84(1):289-95

[8] Chi A, Nguyen NP, Welsh JS, Tse W, Monga M, Oduntan O, Almubarak M, Rogers J, Remick SC, Gius D. Strategies of dose escalation in the treatment of locally advanced non-small cell lung cancer: image guidance and beyond. Front Oncol. 2014; 4:156

[9] Eiland RB, Maare C, Sjöström D, Samsøe E, Behrens CF. Dosimetric and geometric evaluation of the use of deformable image registration in adaptive intensity-modulated radiotherapy for head-and-neck cancer. J Radiat Res. 2014; 55(5):1002-8

[10] Hanahan D, Weinberg RA. Hallmarks of cancer: the next generation. Cell. 2011; 144(5):646-74

[11] ICRU Report 83 (2010). Prescribing, Recording and Reporting Photon-Beam Intensity-Modulated Radiation Therapy (IMRT). International Commission on Radiation Units and Measurements, Bethesda, MD

[12] Jaffray DA. Image-guided radiotherapy: from current concept to future perspectives. Nat Rev Clin Oncol. 2012; 9(12):688-99

[13] Korreman S, Rasch C, McNair H, Verellen D, Oelfke U, Maingon P, Mijnheer B, Khoo V. The European Society of Therapeutic Radiology and Oncology-European Institute of Radiotherapy (ESTRO-EIR) report on 3D CT-based in-room image guidance systems: a practical and technical review and guide. Radiother Oncol. 2010; 94(2):129-44

[14] Ling CC, Humm J, Larson S, Amols H, Fuks Z, Leibel S, Koutcher JA. Towards multidimensional radiotherapy (MD-CRT): biological imaging and biological conformality. Int J Radiat Oncol Biol Phys. 2000; 47(3):551-60

[15] Nabavizadeh N, Elliott DA, Chen Y, Kusano AS, Mitin T, Thomas CR Jr, Holland JM. Image Guided Radiation Therapy (IGRT) Practice Patterns and IGRT's Impact on Workflow and Treatment Planning: Results From a National Survey of American Society for Radiation Oncology Members. Int J Radiat Oncol Biol Phys. 2016; 94(4):850-7

[16] Webb S. Optimisation of conformal radiotherapy dose distributions by simulated annealing. Phys Med Biol. 1989 Oct;34(10):1349-70. Review. Erratum in: Phys Med Biol 1990; 35(2):297

6. Lebenslauf

Zur Person

Name:	Dr.med. Dr.rer.nat. Christian Friedrich Thieke
Privatanschrift:	Albert-Roßhaupter-Str. 105 81369 München Tel.: +49 (0)176 / 652 720 66 Email: c.thieke@gmail.com
Dienstanschrift:	Klinik und Poliklinik für Strahlentherapie und Radioonkologie Klinikum der Universität München Marchioninistr. 15 81377 München Tel.: +49 (0)89 / 4400 74528 Email: christian.thieke@med.uni-muenchen.de
Geboren:	am 26.02.1970 in Hann.-Münden
Nationalität:	deutsch
Familienstand:	verheiratet mit Dr. Katia Parodi, Universitätsprofessorin

Aktuelle Position

seit 02/2014 Wissenschaftlicher Koordinator für Strahlentherapie, Radiologie und Nuklearmedizin am Klinikum der Universität München

Beruflicher Werdegang

03/1995 – 09/2000 Wissenschaftlicher Mitarbeiter am Institut für Medizinische Physik und Biophysik, Universität Göttingen

1995 – 2000 Studienbegleitend:
- Dozent für „Fachbezogene Physik und Chemie“ an der Krankenpflegeschule des Albert-Schweitzer-Krankenhauses Northeim
- Dozent für „Physik“ und „Allgemeine Krankheitslehre“ an der Hebammenschule Göttingen

10/2000 – 12/2003 Wissenschaftlicher Mitarbeiter in der Abt. Medizinische Physik, DKFZ

01/2002 – 09/2002 Visiting Research Fellow am Department of Radiation Oncology, Massachusetts General Hospital and Harvard Medical School, Boston, MA, USA

12/2003 – 01/2014 Wissenschaftlicher Mitarbeiter in der Klinischen Kooperationseinheit Strahlentherapie am DKFZ und Assistenzarzt an der Klinik für Radioonkologie und Strahlentherapie des Universitätsklinikums Heidelberg

03/2009 – 01/2014 Leiter der klinischen Forschungsgruppe „Adaptive Strahlentherapie“ am DKFZ

05/2011 – 01/2014	Wissenschaftlicher Koordinator des Heidelberger Instituts für Radioonkologie (HIRO)
2012 – 2014	Stellvertretendes Mitglied im Kompetenzverbund Strahlenforschung (KVSF)

Ausbildung

Schulbildung

1989	Abitur am Christian-Gymnasium Hermannsburg

Wehrdienst

06-1989 -08/1990	Grundwehrdienst in Celle-Scheuen

Physik

10/1990 -11/1995	Studium der Physik an der Georg-August-Universität Göttingen
11/1995	Diplom im Fach Physik
10/2000 -12/2002	Dissertation Physik am Deutschen Krebsforschungszentrum (DKFZ), Abt. Medizinische Physik (Prof. Dr. W. Schlegel), Titel „Multicriteria optimization in inverse radiotherapy planning“ (Betreuer: Prof. Dr. T. Bortfeld)
01/2003	Promotion zum Dr. rer. nat. (summa cum laude) an der Universität Heidelberg

Medizin

10/1992 -11/2003	Studium der Humanmedizin an der Georg-August-Universität Göttingen und Ruprecht-Karls-Universität Heidelberg
11/2003	Ärztliche Prüfung / 3. Staatsexamen
04/1996 -12/1998	Dissertation Medizin an der Universität Göttingen, Institut für Medizinische Physik und Biophysik (Prof. Dr. D. Harder), Titel „Analyse der Chromosomenaberrationen menschlicher Lymphozyten mittels ‚premature chromosome condensation’ nach Alphateilchen-Bestrahlung“ (Betreuer: Prof. Dr. D. Harder)
01/2004	Promotion zum Dr. med. (magna cum laude) an der Universität Göttingen

Preise und Auszeichnungen

2003 ESTRO-Varian Research Award (Physics)
Europäische Gesellschaft für Strahlentherapie

2004 Young Medical Investigator Award
Medizinische Fakultät Heidelberg

2005 Richtzenhain-Preis für Krebsforschung
Deutsches Krebsforschungszentrum

2016 Wissenschaftspreis „Forschung im Verbund“
Stifterverband für die Deutsche Wissenschaft

(gemeinsam mit Karl-Heinz Küfer, Michael Bortz, Alexander Scherrer, Philipp Süss und Katrin Teichert vom Fraunhofer-ITWM, Thomas Bortfeld vom Massachusetts General Hospital und der Harvard Medical School, Wolfgang Schlegel vom Deutschen Krebsforschungszentrum, und Jürgen Debus vom Universitätsklinikum Heidelberg)

Drittmittel

- „Multikriterielle Optimierung und Entscheidungsunterstützung bei der Planung konformierender Strahlentherapie – Entwicklung und Erprobung eines klinischen Systems“
  Fördersumme: ca. 280.000 EUR (Deutsche Krebshilfe), Förderzeitraum 10/2004-09/2007
  Eigene Rolle: Koordinator für die Bereiche Strahlentherapie und klinische Modellierung
- „Softwareplattform für die multimodale Diagnostik onkologischer Erkrankungen und Therapieoptimierung durch molekulare Bildgebung – DOT-MOBI“
  Fördersumme: gesamt ca. 6,9 Mio EUR (BMBF), Förderzeitraum 01/2009-06/2012
  Eigene Rolle: Antragsteller und Projektleiter am DKFZ (1,7 Mio EUR) und am Universitätsklinikum Heidelberg (417 kEUR)
- „Softwareplattform für die Adaptive Multimodale Radio- und Partikeltherapie mit Autarker Erweiterbarkeit – SPARTA“
  Fördersumme: gesamt ca. 8 Mio EUR (BMBF), Förderzeitraum 04/2013 – 03/2016
  Eigene Rolle: Antragsteller und bis 01/2014 Projektleiter am DKFZ (1,7 Mio EUR)

Tätigkeiten als Reviewer

Medical Physics
Physics in Medicine and Biology
Radiation Oncology
Radiotherapy and Oncology
Strahlentherapie und Onkologie

2008 Mitglied des Ph.D.-Auswahlkomitees der Helmholtz International Graduate School for Cancer Research

Fort- und Weiterbildungen

08/1998 – 06/1999	Studienbegleitende Fortbildung zum Microsoft Certified Systems Engineer (MCSE) für Planung, Implementierung und Wartung unternehmensweiter Netzwerke
12/2003 – 12/2009	Ärztliche Weiterbildung an der Klinik für Radioonkologie und Strahlentherapie des Universitätsklinikums Heidelberg (Ärztl. Direktor Prof. Dr. Dr. M. Wannenmacher / Prof. Dr. Dr. J. Debus) und in der Klinischen Kooperationseinheit Strahlentherapie am DKFZ (Prof. Dr. Dr. J. Debus/Prof. Dr. Dr. P. Huber)
05/2006	Qualifikation zum Prüfarzt in klinischen Studien
09/2009	Fachkunde im Strahlenschutz Strahlentherapieplanung einschließlich CT
12/2009	Fachkunde im Strahlenschutz Strahlentherapie, Gesamtgebiet (Teletherapie und Brachytherapie)
01/2010	Facharzt für Strahlentherapie
05-07/2011	Helmholtz-Akademie für Führungskräfte Durchgeführt vom Malik Management Zentrum 3 jeweils 3-tägige Fortbildungen in Führung, Organisation und Strategie
05/2012	Malik SuperSyntegration, St. Gallen, Schweiz Thema: Zukünftige Governance-Struktur des DKFZ 3-tägiger Workshop mit 40 ausgewählten Mitarbeitern des DKFZ
04/2012 – 01/2013	Junior Professional Management (JPM) für Führungskräfte Zentrum für Wissenschaftsmanagement e.V., Speyer 6 jeweils 3-tägige Fortbildungen in Wissenschaftsmanagement

7. Eigene wissenschaftliche Publikationen

Übersicht

Dr. Dr. Christian Thieke

Stand: Mai 2017

1. Originalarbeiten als Erst- oder Letztautor:	16
2. Originalarbeiten als Koautor:	35
3. Kasuistiken / Case Reports :	1
4. Übersichtsartikel / Reviews :	2
5. Buchkapitel / Book Chapters :	3
6. Sonstige Veröffentlichungen :	2

7.1. Originalarbeiten als Erst- oder Letztautor

1-1. **Thieke C**, Nicolay NH, Sterzing F, Hoffmann H, Roeder F, Safi S, Debus J, Huber PE. Long-term results in malignant pleural mesothelioma treated with neoadjuvant chemotherapy, extrapleural pneumonectomy and intensity-modulated radiotherapy. *Radiat Oncol*. 2015;10:267
IF 2015: 2.83

1-2. Süss P, Bortz M, Küfer KH, **Thieke C**. The critical spot eraser-a method to interactively control the correction of local hot and cold spots in IMRT planning. *Phys Med Biol*. 2013;58(6):1855-67
IF 2013: 2.922

1-3. Askoxylakis V, Dinkel J, Eichinger M, Stieltjes B, Sommer G, Strauss LG, Dimitrakopoulou-Strauss A, Kopp-Schneider A, Haberkorn U, Huber PE, Bischof M, Debus J, **Thieke C**. Multimodal hypoxia imaging and intensity modulated radiation therapy for unresectable non-small-cell lung cancer: the HIL trial. *Radiat Oncol*. 2012 14;7:157
IF 2012: 2.107

1-4. Teichert K, Süss P, Serna JI, Monz M, Küfer KH, **Thieke C**. Comparative analysis of Pareto surfaces in multi-criteria IMRT planning. *Phys Med Biol*. 2011;56(12):3669-84
IF 2011: 2.829

1-5. Dinkel J, Hintze C, Tetzlaff R, Huber PE, Herfarth K, Debus J, Kauczor HU, **Thieke C**. 4D-MRI analysis of lung tumor motion in patients with hemidiaphragmatic paralysis. *Radiother Oncol* 2009; 91:449-54
IF 2009: 4.343

1-6. Stoiber EM, Lechsel G, Giske K, Muenter MW, Hoess A, Bendl R, Debus J, Huber PE, **Thieke C**. Quantitative assessment of image-guided radiotherapy for paraspinal tumors. *Int J Radiat Oncol Biol Phys* 2009; 75:933-40
IF 2009: 4.592

1-7. Serna JI, Monz M, Küfer KH, **Thieke C**. Trade-off bounds for the Pareto surface approximation in multi-criteria IMRT planning. *Phys Med Biol* 2009; 54:6299-311
IF 2009: 2.781

1-8. Krause M, Scherrer A, **Thieke C**. On the role of modeling parameters in IMRT plan optimization. *Phys Med Biol* 2008; 53:4907–26
IF 2008: 2.784

1-9. Monz M, Küfer KH, Bortfeld TR, **Thieke C**. Pareto navigation: algorithmic foundation of interactive multi-criteria IMRT planning. *Phys Med Biol* 2008; 53:985-98
IF 2008: 2.784

1-10. Süss P, Küfer KH, **Thieke C**. Improved stratification algorithms for step-and-shoot MLC delivery in intensity-modulated radiation therapy. *Phys Med Biol* 2007; 52:6039-51
IF 2007: 2.528

1-11. **Thieke C**, Küfer KH, Monz M, Scherrer A, Alonso F, Oelfke U, Huber PE, Debus J, Bortfeld T. A new concept for interactive radiotherapy planning with multicriteria optimization: first clinical evaluation. *Radiother Oncol* 2007; 85:292-8
IF 2007: 4.074

1-12. **Thieke C**, Malsch U, Schlegel W, Debus J, Huber P, Bendl R, Thilmann C. Kilovoltage CT using a linac-CT scanner combination. *Br J Radiol* 2006 Sep;79 Spec No 1:79-86
IF 2006: 1.279

1-13. Kuefer KH, Scherrer A, Monz M, Alonso F, Trinkaus H, Bortfeld T, **Thieke C**. Intensity-modulated radiotherapy – a large scale multi-criteria programming problem. *OR Spectrum* 2003; 25:223-249
IF 2003: 0.49

1-14. **Thieke C**, Bortfeld T, Niemierko A, Nill S. From physical dose constraints to equivalent uniform dose constraints in inverse radiotherapy planning. *Med Phys* 2003, 30:2332-2339
IF 2003: 2.305

1-15. **Thieke C**, Nill S, Oelfke U, Bortfeld T. Acceleration of intensity-modulated radiotherapy dose calculation by importance sampling of the calculation matrices. *Med Phys* 2002; 29:676-81
IF 2002: 2.39

1-16. **Thieke C**, Bortfeld T, Kuefer KH. Characterization of dose distributions through the max and mean dose concept. *Acta Oncol* 2002; 41:158-161
IF 2002: 1.909

7.2. Originalarbeiten als Koautor

2-1. Berndt B, Landry G, Schwarz F, Tessonnier T, Kamp F, Dedes G, **Thieke C**, Würl M, Kurz C, Ganswindt U, Verhaegen F, Debus J, Belka C, Sommer W, Reiser M, Bauer J, Parodi K. Application of single- and dual-energy CT brain tissue segmentation to PET monitoring of proton therapy. *Phys Med Biol*. 2017; 62(6): 2427-2448
IF 2016 (2017 not yet available): 2.60

2-2. Haehnle J, Süss P, Landry G, Teichert K, Hille L, Hofmaier J, Nowak D, Kamp F, Reiner M, **Thieke C**, Ganswindt U, Belka C, Parodi K, Küfer KH, Kurz C. A novel method for interactive multi-objective dose-guided patient positioning. *Phys Med Biol*. 2017; 62(1): 165-185
IF 2016 (2017 not yet available): 2.60

2-3. Kurz C, Kamp F, Park YK, Zöllner C, Rit S, Hansen D, Podesta M, Sharp GC, Li M, Reiner M, Hofmaier J, Neppl S, **Thieke C**, Nijhuis R, Ganswindt U, Belka C, Winey BA, Parodi K, Landry G. Investigating deformable image registration and scatter correction for CBCT-based dose calculation in adaptive IMPT. *Med Phys*. 2016; 43(10): 5635
IF 2015 (2016 not yet available): 2.496

2-4. Hudobivnik N, Schwarz F, Johnson T, Agolli L, Dedes G, Tessonnier T, Verhaegen F, **Thieke C**, Belka C, Sommer WH, Parodi K, Landry G. Comparison of proton therapy treatment planning for head tumors with a pencil beam algorithm on dual and single energy CT images. *Med Phys*. 2016; 43(1):495
IF 2015 (2016 not yet available): 2.496

2-5. Kurz C, Nijhuis R, Reiner M, Ganswindt U, **Thieke C**, Belka C, Parodi K, Landry G. Feasibility of automated proton therapy plan adaptation for head and neck tumors using cone beam CT images. *Radiat Oncol*. 2016; 11:64
IF 2016: 2.83

2-6. Schmid S, Landry G, **Thieke C**, Verhaegen F, Ganswindt U, Belka C, Parodi K, Dedes G. Monte Carlo study on the sensitivity of prompt gamma imaging to proton range variations due to interfractional changes in prostate cancer patients. *Phys Med Biol*. 2015; 60(24):9329-47
IF 2015: 2.60

2-7. Kurz C, Dedes G, Resch A, Reiner M, Ganswindt U, Nijhuis R, **Thieke C**, Belka C, Parodi K, Landry G. Comparing cone-beam CT intensity correction methods for dose recalculation in adaptive intensity-modulated photon and proton therapy for head and neck cancer. *Acta Oncol*. 2015 Jul 22:1-7
IF 2015: 1.53

2-8. Sachpekidis C, **Thieke C**, Askoxylakis V, Nicolay NH, Huber PE, Thomas M, Dimitrakopoulou G, Debus J, Haberkorn U, Dimitrakopoulou-Strauss A. Combined use of (18)F-FDG and (18)F-FMISO in unresectable non-small cell lung cancer patients planned for radiotherapy: a dynamic PET/CT study. *Am J Nucl Med Mol Imaging*. 2015; 5(2): 127-42
IF 2015 (unofficial): 2.520

2-9. Landry G, Nijhuis R, Dedes G, Handrack J, **Thieke C**, Janssens G, Orban de Xivry J, Reiner M, Kamp F, Wilkens JJ, Paganelli C, Riboldi M, Baroni G, Ganswindt U, Belka C, Parodi K. Investigating CT to CBCT image registration for head and neck proton therapy as a tool for daily dose recalculation. *Med Phys*. 2015; 42(3):1354-66
IF 2015: 2.496

2-10. Zwicker F, Swartman B, Roeder F, Sterzing F, Hauswald H, **Thieke C**, Weber KJ, Huber PE, Schubert K, Debus J, Herfarth K. In vivo measurement of dose distribution in patients' lymphocytes: helical tomotherapy versus step-and-shoot IMRT in prostate cancer. *J Radiat Res*. 2015;56(2):239-47
IF 2015: 1.01

2-11. Zhang L, Hub M, Mang S, **Thieke C**, Nix O, Karger CP, Floca RO. Software for quantitative analysis of radiotherapy: overview, requirement analysis and design solutions. *Comput Methods Programs Biomed*. 2013;110(3):528-37
IF 2013: 1.093

2-12. Zhang L, Hub M, **Thieke C**, Floca RO, Karger CP. A method to visualize the uncertainty of the prediction of radiobiological models. *Phys Med*. 2013;29(5):556-61
IF 2013: 1.849

2-13. Zechmann CM, Menze BH, Kelm BM, Zamecnik P, Ikinger U, Giesel FL, **Thieke C**, Delorme S, Hamprecht FA, Bachert P. Automated vs. manual pattern recognition of 3D (1)H MRSI data of patients with prostate cancer. *Acad Radiol*. 2012;19(6):675-84
IF 2012: 1.914

2-14. Simon D, Fritzsche KH, **Thieke C**, Klein J, Parzer P, Weber MA, Stieltjes B. Diffusion-weighted imaging-based probabilistic segmentation of high- and low-proliferative areas in high-grade gliomas. *Cancer Imaging*. 2012;12:89-99
IF 2012: 1.594

2-15. Hub M, **Thieke C**, Kessler ML, Karger CP. A stochastic approach to estimate the uncertainty of dose mapping caused by uncertainties in b-spline registration. *Med Phys*. 2012;39(4):2186-92
IF 2012: 2.911

2-16. Prüm H, Gerigk L, Hintze C, **Thieke C**, Floca R. Software-guided standardization of manual landmark data in medical images. *Z Med Phys*. 2011;21(1):42-51
IF 2011: 1.212

2-17. Giske K, Stoiber EM, Schwarz M, Stoll A, Muenter MW, Timke C, Roeder F, Debus J, Huber PE, **Thieke C**, Bendl R. Local setup errors in image-guided radiotherapy for head and neck cancer patients immobilized with a custom-made device. *Int J Radiat Oncol Biol* Phys. 2011; 80(2):582-9
IF 2011: 4.105

2-18. Zwicker F, Roeder F, **Thieke C**, Timke C, Münter MW, Huber PE, Debus J. IMRT reirradiation with concurrent cetuximab immunotherapy in recurrent head and neck cancer. *Strahlenther Onkol*. 2011; 187(1):32-8
IF 2011: 3.561

2-19. Zwicker F, Roeder F, Hauswald H, **Thieke C**, Timke C, Schlegel W, Debus J, Münter MW, Huber PE. Reirradiation with intensity-modulated radiotherapy in recurrent head and neck cancer. *Head Neck*. 2011;33(12):1695-702
IF 2011: 2.403

2-20. Roeder F, Zwicker F, Saleh-Ebrahimi L, Timke C, **Thieke C**, Bischof M, Debus J, Huber PE. Intensity modulated or fractionated stereotactic reirradiation in patients with recurrent nasopharyngeal cancer. *Radiat Oncol*. 2011;6:22
IF 2011: 2.321

2-21. Zwicker F, Swartman B, Sterzing F, Major G, Weber KJ, Huber PE, **Thieke C**, Debus J, Herfarth K. Biological in-vivo measurement of dose distribution in patients' lymphocytes by gamma-H2AX immunofluorescence staining: 3D conformal-vs. step-and-shoot IMRT of the prostate gland. *Radiat Oncol*. 2011;6:62
IF 2011: 2.321

2-22. Dinkel J, **Thieke C**, Plathow C, Zamecnik P, Prüm H, Huber PE, Kauczor HU, Schlemmer HP, Zechmann CM. Respiratory-induced prostate motion: characterization and quantification in dynamic MRI. *Strahlenther Onkol*. 2011;187(7):426-32
IF 2011: 3.561

2-23. Zechmann CM, Simpfendörfer T, Giesel FL, Zamecnik P, **Thieke C**, Hielscher T, Meinzer HP, Delorme S. Comparison of peripheral zone and central gland volume in patients undergoing intensity-modulated radiotherapy. *J Comput Assist Tomogr*. 2010; 34(5):739-45
IF 2010: 1.358

2-24. Zwicker F, Hauswald H, Nill S, Rhein B, **Thieke C**, Roeder F, Timke C, Zabel-du Bois A, Debus J, Huber PE. New multileaf collimator with a leaf width of 5 mm improves plan quality compared to 10 mm in step-and-shoot IMRT of HNC using integrated boost procedure. *Strahlenther Onkol*. 2010; 186(6):334-43
IF 2010: 3.567

2-25. Roeder F, Timke C, Zwicker F, **Thieke C**, Bischof M, Debus J, Huber PE. Intensity modulated radiotherapy (IMRT) in benign giant cell tumors--a single institution case series and a short review of the literature. *Radiat Oncol*. 2010; 5:18
IF 2010: 2.409

2-26. Zechmann CM, Aftab K, Didinger B, Giesel FL, Zamecnik P, **Thieke C**, Fütterer JJ, Kopp-Schneider A, Kauczor HU, Delorme S. Changes of prostate gland volume with and without androgen deprivation after intensity modulated radiotherapy - A follow-up study. *Radiother Oncol* 2009; 90:408-12
IF 2009: 4.343

2-27. Plathow C, Klopp M, **Thieke C**, Herth F, Thomas A, Schmaehl A, Zuna I, Kauczor HU. Therapy response in malignant pleural mesothelioma-role of MRI using RECIST, modified RECIST and volumetric approaches in comparison with CT. *Eur Radiol* 2008;18:1635-43
IF 2008: 3.651

2-28. Sterzing F, Sroka-Perez G, Schubert K, Münter MW, **Thieke C**, Huber P, Debus J, Herfarth KK. Evaluating target coverage and normal tissue sparing in the adjuvant radiotherapy of malignant pleural mesothelioma: helical tomotherapy compared with step-and-shoot IMRT. *Radiother Oncol* 2008; 86:251-7
IF 2008: 3.99

2-29. Malsch U, **Thieke C**, Huber PE, Bendl R. An enhanced block matching algorithm for fast elastic registration in adaptive radiotherapy. *Phys Med Biol* 2006; 51:4789-806
IF 2006: 2.873

2-30. Plathow C, Klopp M, Schoebinger M, **Thieke C**, Fink C, Puderbach M, Ley S, Weber MA, Sandner A, Claussen CD, Herth F, Tuengerthal S, Meinzer HP, Kauczor HU. Monitoring of Lung Motion in Patients With Malignant Pleural Mesothelioma Using Two-Dimensional and Three-Dimensional Dynamic Magnetic Resonance Imaging: Comparison With Spirometry. *Invest Radiol* 2006; 41:443-8
IF 2006: 3.398

2-31. Thilmann C, Nill S, Tucking T, Hoss A, Hesse B, Dietrich L, Bendl R, Rhein B, Haring P, **Thieke C**, Oelfke U, Debus J, Huber P. Correction of patient positioning errors based on in-line cone beam CTs: clinical implementation and first experiences. *Radiat Oncol* 2006; 24:1-16
IF 2010 (first available): 2.409

2-32. Poppe B, **Thieke C**, Beyer D, Kollhoff R, Djouguela A, Ruhmann A, Willborn KC, Harder D. DAVID-a translucent multi-wire transmission ionization chamber for in vivo verification of IMRT and conformal irradiation techniques. *Phys Med Biol* 2006; 51:1237-48
IF 2006: 2.873

2-33. Thilmann C, Haring P, Thilmann L, Unkelbach J, Rhein B, Nill S, Huber P, Janisch E, **Thieke C**, Debus J. The influence of breathing motion on intensity modulated radiotherapy in the step-and-shoot technique: phantom measurements for irradiation of superficial target volumes. *Phys Med Biol* 2006; 51:N117-26
IF 2006: 2.873

2-34. Greinert R, **Thieke C**, Detzler E, Boguhn O, Frankenberg D, Harder D. Chromosome Aberrations Induced In Human Lymphocytes by 3.45 MeV Alpha Particles Analyzed by Premature Chromosome Condensation. *Radiat Res* 1999; 152:412-20
IF 1999: 2.807

2-35. Bartels A, **Thieke C**, Harder D, Greinert R. Fokus-Optimierung eines Slit-Scan-Flußzytometers zur morphologischen Analyse von Chromosomen in Suspension. *Z Med Phys* 1996; 6:194-200
IF 1996: -

7.3. Kasuistiken / Case Reports

3-1. Jensen AD, Grehn C, Nikoghosyan A, **Thieke C**, Krempien R, Huber PE, Debus J, Münter MW. Catch me if you can--the use of image guidance in the radiotherapy of an unusual case of esophageal cancer. *Strahlenther Onkol*. 2009; 185:469-73
IF 2009: 3.776

7.4. Übersichtsartikel / Reviews

4-1. Askoxylakis V, **Thieke C**, Pleger ST, Most P, Tanner J, Lindel K, Katus HA, Debus J, Bischof M. Long-term survival of cancer patients compared to heart failure and stroke: a systematic review. BMC Cancer. 2010;10:105
IF 2010: 3.153

4-2. Dinkel J, Hintze C, Rochet N, **Thieke C**, Biederer J. Computed tomography of the lungs - A step into the fourth dimension. Radiologe 2009; 49:698-704
IF 2009: 0.481

7.5. Buchkapitel / Book Chapters

5-1. Parodi K, **Thieke C**. Imaging Instrumentation and Techniques for Precision Radiotherapy. In: *Handbook of Particle Detection and Imaging*. Grupen C and Buvat I (eds), ISBN 978-3-642-13270-4, Springer 2012, 1153-1179

5-2. **Thieke C**, Bortfeld T, Levegrün S, Ton L: Plan optimization. In: *3D Conformal Radiation Therapy. A multimedia introduction to methods and techniques*, 2nd edition, Schlegel W, Mahr A (eds), Springer 2007

5-3. Bortfeld T, **Thieke C**: Optimization of Treatment Plans, Inverse Planning. In: *New Technologies in Radiation Oncology*. Schlegel W, Bortfeld T, Grosu AL (eds), Springer 2005, 205-18

7.6. Sonstige Veröffentlichungen

6-1. Weschke C, **Thieke C**. Partnerships Between Research Institutes and Industry: Information and Communication as the Cornerstones of Success. *Imaging Management*. 2009; 8(5): 16-7

6-2. Biederer J, Hintze C, **Thieke C**, Kauczor H-U. Diagnostische Bildgebung für eine fortschrittliche Strahlentherapie bei Lungenkrebs. Medical Solutions Dezember 2006:71-78 (Siemens AG, Medical Solutions, Erlangen; ISSN 0340-5389)

8. Danksagung

Mein Dank gilt an erster Stelle Herrn Professor Claus Belka für die Betreuung dieser Habilitation, seine großzügige Unterstützung meiner wissenschaftlichen Arbeit und auch für die damit verbundenen gewährten Freiheiten.

Herzlich bedanken möchte ich mich bei Herrn Professor Peter Bartenstein und Herrn Professor Maximilian Reiser für die Übernahme des Fachmentorats und für die sehr gute Zusammenarbeit am Klinikum der Universität München.

Die in dieser Habilitationsschrift vorgestellten Arbeiten wurden im Wesentlichen durchgeführt während meiner Zeit am Deutschen Krebsforschungszentrum (DKFZ) in Heidelberg und am dortigen Universitätsklinikum. Mein besonderer Dank gilt dabei Herrn Professor Jürgen Debus für seine inspirierende Betreuung und Unterstützung in allen Themen der Medizin und der Physik. Mein großer Dank gilt auch Herrn Professor Peter Huber für seine stete Unterstützung und die vertrauensvolle Zusammenarbeit über viele Jahre. Ebenfalls ganz herzlich bedanken möchte ich mich bei Herrn Professor Wolfgang Schlegel und Herrn Professor Heinz-Peter Schlemmer, die als Sprecher des Forschungsschwerpunktes „Bildgebung und Radioonkologie“ am DKFZ immer wichtige und hilfsbereite Ansprechpartner für mich waren.

Die Interdisziplinarität der bearbeiteten Themen hat mich über die Jahre mit vielen Kollegen aus den Bereichen Medizin, Physik, Mathematik und Informatik zusammengebracht. Von diesen habe ich fachlich und persönlich viel gelernt und mit diesen mit großer Freude zusammengearbeitet, wofür ich tiefe Dankbarkeit empfinde. Stellvertretend für alle diese Kollegen möchte ich namentlich nennen: Herrn PD Dr. Vasileios Askoxylakis, Herrn Professor Jürgen Biederer, Herrn Dr. Tilman Bostel, Herrn Professor Julien Dinkel, Herrn Dr. Christian Hintze, Herrn PD Dr. Dr. Nils Nicolay, Herrn PD Dr. Falk Röder, Herrn Dr. Bram Stieltjes, Herrn PD Dr. Christian Zechmann, Herrn Dr. Felix Zwicker, den leider verstorbenen Herrn Professor Ludwig Strauss, und seine Frau Professorin Antonia Dimitrakopoulou-Strauss. Besonders bedanken möchte ich mich bei Herrn Dr. Ralf Floca für die herausragende Unterstützung im Bereich der medizinischen Informatik.

Die Begeisterung für medizinisch-medizinphysikalische Themen in mir geweckt haben Professor Thomas Bortfeld und Professor Dietrich Harder. Als Betreuer meiner physikalischen und meiner medizinischen Dissertation waren sie mir immer ein Vorbild und sind bis heute freundschaftliche Ansprechpartner, wofür ich ihnen sehr dankbar bin.

Eine besondere wissenschaftliche Kooperation verbindet mich mit Mathematikern des Fraunhofer-Instituts für Techno- und Wirtschaftsmathematik (ITWM) in Kaiserslautern. Die Kollegen des ITWM haben als erste vorgeschlagen, die multikriterielle Optimierung auf das Problem der Strahlentherapieplanung anzuwenden. Daraus entstand eine nunmehr 17 Jahre währende, äußerst fruchtbare und angenehme Zusammenarbeit über Städte- und Ländergrenzen hinweg, die hoffentlich noch mindestens ebenso lange weiter bestehen bleibt. Vielen Dank an Herrn Professor Karl-Heinz Küfer, Herrn Dr. Michael Bortz, Herrn Dr. Alexander Scherrer, Herrn Dr. Philipp Süss, Frau Dr. Katrin Teichert, und an die mittlerweile an andere Stelle gewechselten Herren Dr. Jonas Hähnle und Dr. Michael Mronz!

Zu guter Letzt möchte ich mich bei meiner Familie, allen voran meinen Eltern und meiner Frau Katia, bedanken, die mich immer unterstützt und begleitet haben.

9. Eidesstattliche Erklärung

Hiermit versichere ich an Eides statt, dass ich meine Habilitationsleistung selbständig und ohne andere als die angegebenen Hilfsmittel angefertigt habe, zudem die Herkunft des verwendeten und zitierten Materials ordnungsgemäß kenntlich gemacht habe.

Des Weiteren erkläre ich, dass ich mich weder anderweitig habilitiert, noch bereits Habilitationsversuche unternommen habe und dass mir kein akademischer Grad entzogen wurde oder ein Verfahren gegen mich anhängig ist, welches zur Entziehung eines akademischen Grades führen könnte.

München, 03.05.2017

Dr.med. Dr.rer.nat. Christian Thieke

10. Faksimile der themenrelevanten Arbeiten

Radiotherapy and Oncology 85 (2007) 292—298
www.thegreenjournal.com

Treatment planning

A new concept for interactive radiotherapy planning with multicriteria optimization: First clinical evaluation☆

Christian Thieke[a,b,*], Karl-Heinz Küfer[c], Michael Monz[c], Alexander Scherrer[c], Fernando Alonso[c], Uwe Oelfke[d], Peter E. Huber[a,b], Jürgen Debus[b], Thomas Bortfeld[e]

[a]*Department of Radiation Oncology, Deutsches Krebsforschungszentrum, Heidelberg, Germany,* [b]*Department of Radiooncology and Radiation Therapy, University Clinic, Heidelberg, Germany,* [c]*Department of Optimization, Fraunhofer-Institute for Industrial Mathematics, Kaiserslautern, Germany,* [d]*Department of Medical Physics in Radiation Oncology, Deutsches Krebsforschungszentrum, Heidelberg, Germany,* [e]*Department of Radiation Oncology, Massachusetts General Hospital and Harvard Medical School, Boston, MA, USA*

Abstract

***Background and purpose*: Currently, inverse planning for intensity-modulated radiotherapy (IMRT) can be a time-consuming trial and error process. This is because many planning objectives are inherently contradictory and cannot reach their individual optimum all at the same time. Therefore in clinical practice the potential of IMRT cannot be fully exploited for all patients. Multicriteria (multiobjective) optimization combined with interactive plan navigation is a promising approach to overcome these problems.**

***Patients and methods*: We developed a new inverse planning system called ''Multicriteria Interactive Radiotherapy Assistant (MIRA)''. The optimization result is a database of patient specific, Pareto-optimal plan proposals. The database is explored with an intuitive user interface that utilizes both a new interactive element for plan navigation and familiar dose visualizations in form of DVH and isodose projections. Two clinical test cases, one paraspinal meningioma case and one prostate case, were optimized using MIRA and compared with the clinically approved planning program KonRad.**

***Results*: Generating the databases required no user interaction and took approx. 2—3 h per case. The interactive exploration required only a few minutes until the best plan was identified, resulting in a significant reduction of human planning time. The achievable plan quality was comparable to KonRad with the additional benefit of having plan alternatives at hand to perform a sensitivity analysis or to decide for a different clinical compromise.**

***Conclusions*: The MIRA system provides a complete database and interactive exploration of the solution space in real time. Hence, it is ideally suited for the inherently multicriterial problem of inverse IMRT treatment planning.**
 Radiotherapy and Oncology 85 (2007) 292—298.

Keywords: Inverse planning system; IMRT; Interactive; Multicriteria; Multiobjective; Clinical evaluation

The goal of radiotherapy is to achieve local tumor control without causing severe side effects in the surrounding normal tissue. In other terms, high radiation doses should conform closely to the target volume while the rest of the patient's body should get as low doses as possible. The most conformal technique for external photon therapy today is intensity-modulated radiotherapy (IMRT). In current inverse planning systems for IMRT, the intensity profiles are determined in a computerized optimization process based on certain dose prescriptions for targets and organs at risk, whereby so-called weight factors have to be assigned to each structure. The quality of a plan is measured by a single number by adding up the deviations from the prescriptions, and the optimization result is simply the treatment plan with the best number. The problem is that often the resulting compromise between the contradictory planning goals is clinically not acceptable, and several optimization runs with different parameters are needed until an acceptable compromise is found [7]. This trial and error process can be very time consuming, and even when a plan is accepted for treatment it is not clear whether there would have been a better plan for the patient if only the planner would have tried some more parameter settings. There is additional risk of suboptimal treatment plans if the optimization only considers upper and lower dose constraints, because then doses to structures already below or above these constraints are not further improved. All these problems add up to the fact that for some patients the potential of IMRT is not exploited to its full extent because of limitations of the inverse planning process.

☆ The basis of this work was presented 2003 at 7th Biennial ESTRO Physics Meeting and received the ESTRO Varian Research Award (Physics).

0167-8140/$ - see front matter doi:10.1016/j.radonc.2007.06.020

To overcome the current situation, multicriteria (also called multiobjective) optimization (MCO) is a promising approach. The optimization result is no longer a single plan, but rather a whole database of plans, each of them representing a so-called Pareto-optimal solution [14] which cannot be improved in one criterion without worsening at least one other criterion. By exploring the database interactively, the planner can experience the sensitivity to changes in certain structures and decide for the clinically optimal compromise.

The Pareto concept and MCO in the radiotherapy context were utilized for the optimization of beam angles [3], for brachytherapy [10], radiosurgery [23] and external radiotherapy [1,2,5,20], mainly in a research context.

In 2000, a collaborative effort of the Fraunhofer-Institute for Industrial Mathematics, the German Cancer Research Center and the Massachusetts General Hospital was started to develop a new planning system based on multicriteria optimization for IMRT that can be used in real clinical practice. Single aspects of our approach are described in previous publications [4,8,9,11,17,21,22]. These efforts resulted in the realization of a new IMRT planning system which we call MIRA — Multicriteria Interactive Radiotherapy Assistant. In this paper, we give an overview of the complete MIRA system, discuss the objective functions currently used, describe the clinical workflow and present the first results for two clinical test cases.

Patients and methods

General workflow

We propose a two-stage planning process: in a first stage, the computer generates Pareto-optimal plans for the patient-individual planning problem and stores them in a database. Since many plans have to be generated, the computation time can be considerably longer compared to current systems. However, this step requires no user interaction and as such does not increase the workload of the treatment planner. In a second stage, the treatment planner interactively explores the Pareto front and decides for the plan that is in his opinion the best clinical compromise for the patient. Here it is important to give the planner quick and intuitive access to the database.

First stage — generating the Pareto front

Preparatory manual steps

As in current inverse planning systems, the organs at risk (OAR_i) and target structures (T_i) have to be outlined based on tomographic images. In our case, this is done in the conventional forward planning system VIRTUOS which is an in-house development of DKFZ Heidelberg [6]. Also the number and directions of the treatment beams are manually defined in this system.

Dose calculation

Based on the predefined beam geometry, the computer calculates the dose contribution D_{ij} of each single beam element (bixel) j to each volume element (voxel) i inside the patient for unit fluence. The dose for arbitrary intensity-modulated beams can then be calculated by $d_i = \sum_j w_j D_{ij}$ or in short $\mathbf{d} = \mathbf{D}\mathbf{w}$. At the moment we use a pencil beam dose algorithm to generate the matrix $\mathbf{D}$ [13]. Since the matrix has to be computed only once, more accurate dose algorithms will add only the time of a single dose computation to the total running time and can be integrated easily. Superposition algorithms were already implemented [18], and also Monte Carlo algorithms can be used [19].

Building the database

Optimization objectives. During the optimization, the bixel intensities $\mathbf{w}$ have to be varied according to the planning goals for the resulting dose distribution $\mathbf{d}$. The dose distribution thereby is evaluated separately for the target structures T_i and organs at risk OAR_i. For each of these structures an objective function F_i has to be defined. One option is the generalized equivalent uniform dose (EUD) as proposed by Niermierko [12] which is basically the p-Norm of the dose distribution of the respective organ at risk:

$$F_i(\mathbf{d}(\mathrm{OAR}_i)) = \mathrm{EUD}_p(\mathbf{d}(\mathrm{OAR}_i)) = \left(\frac{1}{N}\sum_{j=1}^{N} d_j^p\right)^{1/p} = |\mathbf{d}(\mathrm{OAR}_i)|_p$$

with $p \in [1.0, \ldots, \infty[$ as organ-specific parameter and N the number of voxels of OAR_i. For parallel organs, the EUD equals the mean dose ($p = 1$), and for serial organs p is high since here the highest doses are most important. The EUD does allow very high doses to small volumes of a parallel organ, and in test calculations we observed very high maximum doses in parallel organs like the lung. Because this does not resemble treatment plans common in clinical routine, we decided to use a convex combination with two norm parameters p and q:

$$F_i(\mathbf{d}(\mathrm{OAR}_i)) = k * |\mathbf{d}(\mathrm{OAR}_i)|_p + (1-k) * |\mathbf{d}(\mathrm{OAR}_i)|_q, \quad k \in [0,1].$$

This allows for a better control of both the mean dose (for $p = 1$) and the highest doses (for high values of q) of an organ at risk. The convex parameter k determines which component is more dominant. Note that this function cannot be called EUD anymore.

Modelling the target dose distribution requires a different approach. As usually described in clinical protocols, it should be above a certain minimum dose and at the same time be as homogeneous as possible. Therefore two objective functions for each target seem appropriate. Two different approaches are implemented at the moment:

Using the mean dose and the standard deviation,

$$F_{i,1}(\mathbf{d}(T_i)) = \overline{\mathbf{d}(T_i)} \text{ and } F_{i,2}(\mathbf{d}(T_i)) = \sigma(\mathbf{d}(T_i))$$

or describing the dose values below and above predefined dose thresholds,

$$F_{i,1}(\mathbf{d}(T_i)) = \left(\frac{1}{N}\sum_{j=1}^{N}[L - d_j]_+^p\right)^{1/p} \quad \text{and}$$

$$F_{i,2}(\mathbf{d}(T_i)) = \left(\frac{1}{N}\sum_{j=1}^{N}[d_j - U]_+^q\right)^{1/q}$$

with $p,q \in [1.0,\ldots,\infty[$ as norm parameters, N the number of voxels of T_i, and L und U the lower and upper dose limit in Gy. $[x]_+$ is a function that equals x for $x \geqslant 0$ and 0 for $x < 0$.

Each treatment plan is then characterized by a vector **F** containing all objective function values F_i.

Database structure. Strictly mathematically spoken there are an infinite number of Pareto-optimal solutions. Even discretization in a computer would lead to unacceptable time and storage requirements. Therefore we implemented a twofold strategy to build a database that is as compact as possible albeit still able to deliver all relevant treatment plans in the final exploration process: (1) *Restrict the planning horizon:* although Pareto optimal, many solutions are not of any clinical relevance. One example is no irradiation at all, since any dose improvement to the target would worsen the result in the organs at risk due to inevitable scatter dose. Therefore the solution set covered by the database can be reduced. So-called extreme compromises are defining the planning horizon. (2) *Store only representative solutions:* many solutions will be so close to each other that there will be no visual difference in terms of isodoses or dose—volume-histograms, so it would be redundant to store all of them. The distance between neighbouring solutions in the database can be further enlarged by real-time interpolation during the interactive exploration. Fig. 1 illustrates this strategy for a schematized two-dimensional case.

Optimization algorithm. In a first prototype system [21,22], we implemented EUD optimization into a research version of the existing inverse planning system KonRad developed at DKFZ [15] and generated the database by nested loops over the different optimization criteria. Although this approach demonstrated the feasibility of multicriteria optimization for radiotherapy planning, it turned out to be too slow for daily clinical routine purposes. Therefore a completely new optimization engine was developed. Except the restriction of the intensities to non-negative values, all optimization objectives are modelled by differentiable penalty functions that are combined to a scalar auxiliary function. The $2^n - 1$ (with n the number of criteria) extreme compromises defining the planning horizon are calculated by successively optimizing all combinations of criteria (first each criterion F_i individually, then all combinations of 2 criteria and so forth) while relaxing all remaining criteria up to a predefined constraint. In this concept no user-defined weight factors occur, and the constraints defining the planning horizon are not critical because they can be defined quite generously. Additional intermediate solutions that complete the representative system are placed stochastically. Adaptive clustering in the voxel domain was implemented for drastically reducing the calculation time without compromising the optimization result [17].

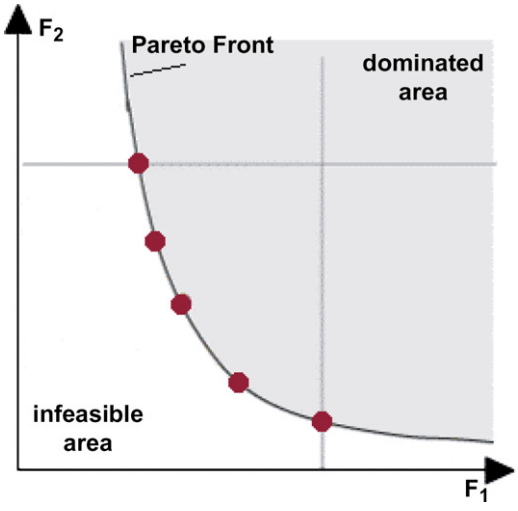

Fig. 1. Schematic example of a two-dimensional problem. Improving parameter F_1 by moving along the Pareto front inevitably leads to worsening F_2. Dots represent solutions stored in the database. Solutions not on the Pareto front are either physically not feasible or dominated.

Second stage — exploring the Pareto front

After computing the database, it is interactively explored by the treatment planner, and the decision for a specific plan is made. The user interface is shown in Fig. 2. The right side of the interface presents the current plan in a familiar way, i.e. as dose—volume-histogram (DVH) and as isodoses or colorwash in three projections (transverse, sagittal and coronal). The left side of the interface shows the new navigation instrument: Here, each structure of the treatment plan is represented by its own axis. The organs at risk are grouped together to form a so-called navigation star, and the target structures are plotted independently below. A marker on each axis gives the criterion value of the currently selected plan. All current marker positions are connected and are forming a polygon. Also targets are represented by a single axis per structure. The start and end values of each axis are giving the planning horizon, i.e. the lowest and highest values covered by the database.

If the planner wants to improve one aspect (one objective) of the current plan, he/she simply points with the computer mouse at the respective marker and drags it in the desired direction. Internally, the computer will identify the plans in the database that are better in the selected criterion than the current one. Then a fast online interpolation is carried out, and a new plan is presented to the planner. The values of all other indicators and the dose visualization as DVH and isodose/colorwash projections are updated. We would like to stress the fact that because of the pre-computed database no optimization of treatment plans is necessary, and because of the interpolation the navigation is a smooth process with real-time feedback to the planner's actions. In mathematical terms, plan navigation is equivalent to moving along the Pareto front. Due to the Pareto optimality of each presented plan, it is clear that improving one part of the plan will simultaneously deteriorate at least one of the other criteria. To prevent a certain criterion from getting worse because of the improvement in another criterion, it is possible to set ''locks''. This will result in a reduced planning horizon, which is indicated by a different shade of

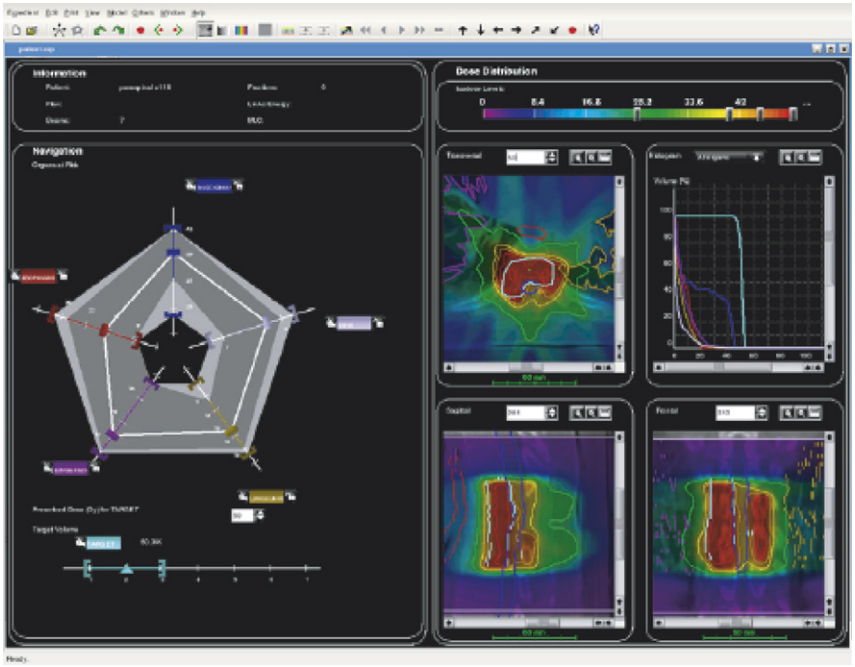

Fig. 2. Navigator interface. The left side shows the navigation elements for all plan criteria, and the right side shows the actual treatment plan as the dose distribution in colorwash and the dose–volume-histogram.

grey of the navigation star. An example is shown in Fig. 2: here a lock is active for a maximum target dose standard deviation, and consequently the planning horizon for the organs at risk is reduced. Of course, it is possible to release the locks anytime to regain access to all solutions in the database. Adding one criterion to the optimization problem simply adds one axis in the navigation interface, in contrast to projecting the solution space to two-dimensional planes which becomes rapidly more complex with each additional criterion [20]. The navigation star can be simplified by removing axes of non-critical organs at risk.

The planning process ends when the planner decides for a specific plan that is in his opinion the best clinical compromise for the patient.

Clinical test cases

Paraspinal case

This is a case of a 71-year-old woman with recurrent spinal meningioma near the thoracic vertebrae 8/9 who was treated with IMRT at the German Cancer Research Center (DKFZ). Fig. 3(left) shows the rendered contours as outlined by the treatment planner. Fig. 3(right) shows a typical CT slice where the delicate proximity of the target volume to the spinal cord becomes apparent. Other organs at risk were the left and right lung, the esophagus and the unclassified tissue. The irradiation geometry consisted of 7 coplanar 6 MV photon beams, as indicated in Fig. 3(right).

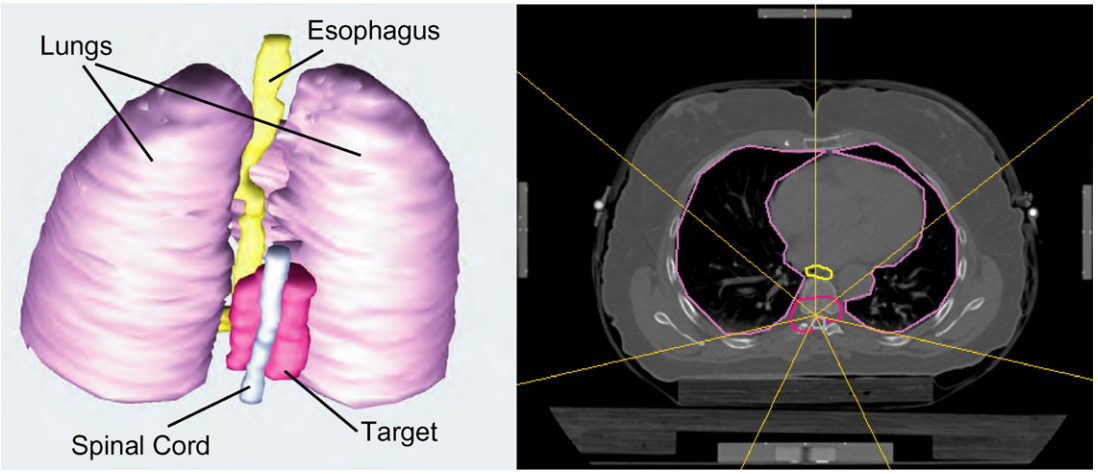

Fig. 3. 3D-rendered structures (left side) and exemplary CT slice with beam arrangement (right side) of the paraspinal case.

Treatment was carried out in step-and-shoot-technique with a Siemens Primus linear accelerator (leaf size 1 cm at the isocenter, bixel size 1×1 cm^2) using a treatment plan generated with the commercial inverse planning system KonRad (Siemens OCS, Heidelberg). The mean dose and the standard deviation were used to optimize the target dose in MIRA. All plans were normalized to a median target dose of 50.4 Gy, to be delivered in 28 fractions with a fraction dose of 1.8 Gy.

Prostate case

This 68-year-old patient received primary treatment with IMRT because of prostate cancer of intermediate risk. The biopsy was positive with a Gleason Score of 7 (3 + 4), the initial PSA 11.3 ng/ml. According to our standard outlining scheme for prostate IMRT treatments at DKFZ, the complete macroscopic prostate as seen on CT was defined as GTV, a margin of 5 mm (while sparing rectum and bladder) was added to obtain the CTV, and an additional margin of 5 mm was added for the PTV. The organs at risk were rectum, bladder, both femoral heads and the unclassified tissue. Also in this case 7 coplanar, equispaced beams were used, and treatment was carried out with the Siemens Primus linac based on a KonRad plan. For target evaluation in MIRA we used the under-/overdosage model. All plans were normalized to a median dose of 76 Gy to the GTV, to be delivered in 38 fractions with a fraction dose of 2 Gy.

Results

The test cases were taken from clinical routine at DKFZ and could be processed by MIRA without further modifications. The calculation time for building the database was approx. 3 h for the paraspinal case and approx. 2 h for the prostate case. A standard PC (2.8 GHz Pentium D with 2 GB RAM running Linux) was used. The voxel resolution was $2.5 \times 2.5 \times 3$ mm^3. Bigger cases would require at least 4 GB RAM or reduced voxel resolutions.

The exploration of the database and decision for a specific plan could be done quickly, of the order of 10 min. In comparison, a single optimization run in KonRad took approx. 3–4 min, and several runs were needed. Until an acceptable treatment plan was found with KonRad, an experienced treatment planner was occupied for approx. 1 h for each case.

Fig. 4 shows three plans taken as snapshots from the MIRA navigation process (solid lines) together with the KonRad reference plan (dotted lines) for the paraspinal case. Since the lungs and the unclassified tissue were well below their tolerance dose for all plans, we show only the target, spinal cord and esophagus. The two major structures determining the clinical compromise are the target volume and the spinal cord. As one extreme, Fig. 5a shows a plan that homogeneously delivers the dose to the target, however at the cost of giving almost the same dose to the spinal cord. Here the DVH of the spinal cord even show some steps that correspond to the 1 cm leaf width of the multileaf collimator. In Fig. 5c the other extreme stored in the database is shown where the spinal cord is spared to a great extent, but at the same time the target dose has to be largely sacrificed. From a clinical point of view, a plan somewhere in between these extremes seems to be most appropriate. This is shown in Fig. 5b, and it can be seen that MIRA is able to resemble the original KonRad plan quite closely.

We strongly encourage the reader to watch the movie that is available on the journal's website as Supporting electronic material. It shows the interactive navigation along the spinal cord's axis which leads to better and better sparing of the spinal cord at the cost of target dose homogeneity. Only by watching the movie one can directly experience the fundamental difference of MIRA compared to conventional inverse planning.

The same evaluation was done for the prostate case, shown in Fig. 5. Here the major tradeoff has to be made between the doses to the three target volumes vs. the bladder and the rectum. Again, a plan (shown in Fig. 5b) could be found in the database that is very similar to the reference KonRad plan.

Discussion

We showed that for both the paraspinal and the prostate case databases could be created which enclose the clinical

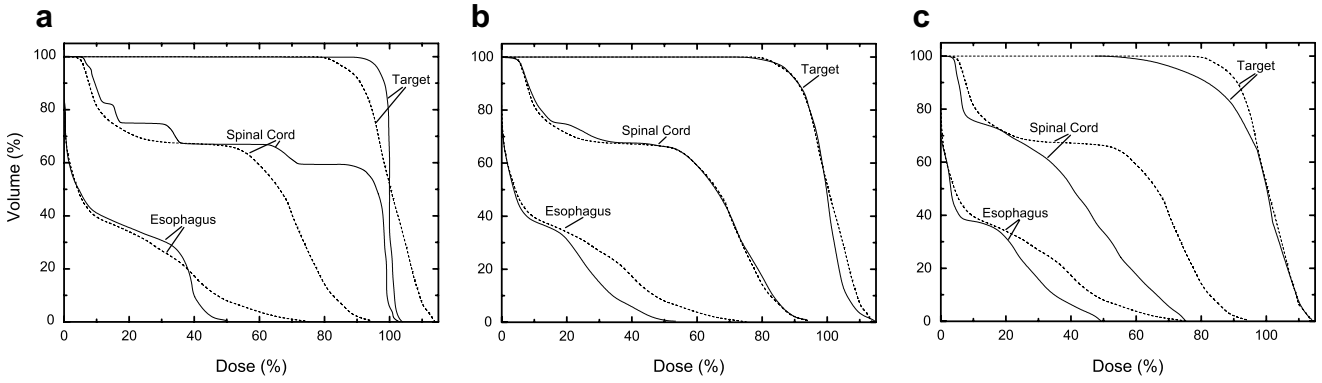

Fig. 4. Plans for the paraspinal case from MIRA (solid lines) together with the KonRad plan (dotted lines, same in all subfigures). (a) Good target coverage of the MIRA plan with high doses to the spinal cord. (b) KonRad and MIRA with similar plans, and (c) spinal cord sparing, sacrificing target coverage.

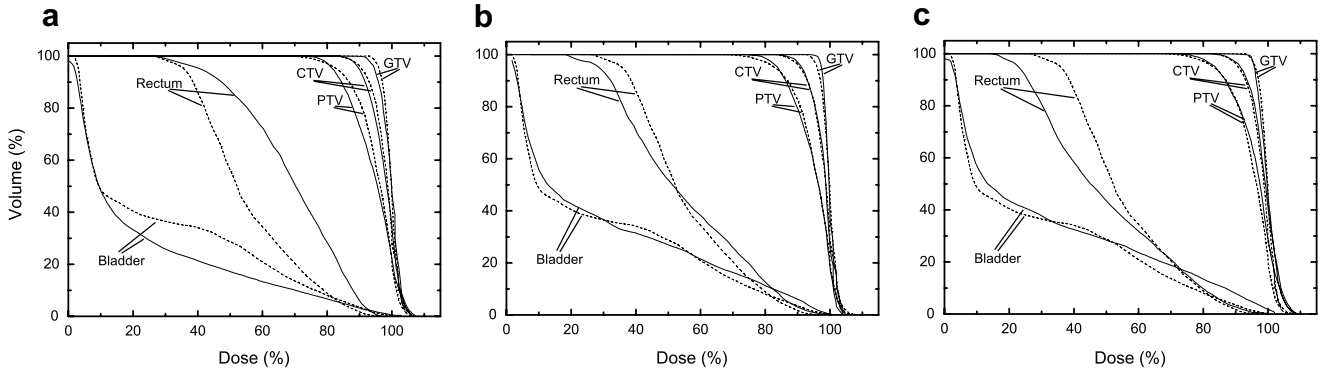

Fig. 5. Plans for the prostate case from MIRA (solid lines) together with the KonRad plan (dotted lines, same in all subfigures). The plan in (b) closely resembles the reference KonRad plan.

relevant part of the multi-dimensional Pareto-optimal solution space. The calculation time in the range of 2–3 h seems well tolerable since it does not require user intervention. The time requirements for the treatment planner could be drastically reduced. However, it has to be noted that the time requirements for inverse planning vary greatly depending on many factors, e.g. the tumor site, the specific case, and the experience of the planner. Therefore our results here can only give a rough first assessment of how much time can potentially be saved.

Besides the time aspect, the second major improvement of MIRA over current systems is that the planner is provided with much more information about the patient-individual planning problem. By interactive exploration of the solution space, the sensitivity of the problem, i.e. how much changes in one structure affect the doses to all other structures, can be directly experienced.

Naturally, a prerequisite for the concept of a pre-computed database to work is that the database does indeed include the best clinical compromise. Although this was the case for the examples shown in this paper (at least in terms of the state-of-the-art inverse planning system KonRad), it remains to be verified that the planning horizon is always wide enough. As an additional caveat, the interpolation between representative solutions can only work accurately if the Pareto front between the interpolation partners does not have steep gradients. The placement of the representative solutions is only done stochastically at the moment and does not guarantee optimal placement at strong curvatures of the Pareto front.

MIRA is closely integrated into the clinical workflow at DKFZ Heidelberg. However, before replacing current inverse planning systems in clinical routine, MIRA will be tested extensively on different clinical entities. In contrast to the rough, qualitative assessment of the treatment plan quality performed in this paper, these studies need to perform detailed quantitative analyses to assure the robustness of the new system and to further clarify its benefits in terms of time savings and plan quality.

In addition to the clinical implementation and evaluation, the MIRA system will serve as a basis for further research. Even with MCO the optimization result depends on the used objective function. It is not clear which function will deliver the ''best'' databases from a clinical point of view. As stated above, our experience so far did not warrant the use of the standard EUD model because of very high maximum doses in parallel organs at risk, so a rather artificial (p, q, k)-norm was introduced which has the disadvantage of not having a direct clinical meaning. The ultimate goal would be to operate on tumor/organ specific TCP and NTCP functions; unfortunately, limited clinical data do not allow the routine use of such functions. Fortunately, the choice for a specific objective function in a multicriteria setting is less critical, since many objective functions are equivalent in terms of the resulting Pareto front [16] and often the geometry of the planning problem is so restricting that even different objective functions lead to similar plans, like for the cases shown here.

The predefined beam arrangement also determines the solution space to some extent. We are currently investigating the integrated optimization of the beam number and angles.

In a restricted sense, even current inverse planning programs can be called ''multicriterial'' since they produce a single Pareto-optimal solution in each optimization run. In our opinion, the next major evolution in inverse planning will be the precomputation of all clinically relevant Pareto-optimal plans and their real-time exploration. We think that especially the interactive character of the decision making process is an irrevocable new aspect in radiotherapy planning that will become more and more important in the future.

We set up a dedicated webpage, http://www.project-mira.net, where the reader can find more information about the MIRA project and related efforts. This webpage will be constantly updated.

Conclusion

We developed a new radiotherapy planning system called MIRA that precomputes all clinically relevant solutions for a patient-specific IMRT planning problem and provides a graphical user interface for real-time, interactive exploration of the solution space. It could be shown for two clinical test

cases that the achievable plan quality was at least equal to the reference planning program KonRad, while the time requirements for the treatment planner could be reduced.

Acknowledgements

We thank following people for their support: Dr. S. Nill gave invaluable help for utilizing existing software components at DKFZ for the MIRA project. D. Maleike developed a script that organizes all relevant software packages in one graphical user interface. M. Uhrig tested the optimizer software and pointed out some stability issues. This research was supported in part by the Deutsche Krebshilfe, Project No. 106425, and in part by the National Cancer Institute of the United States under Grant R01-CA103904.

Appendix A. Supplementary data

Supplementary data associated with this article can be found, in the online version, at doi:10.1016/j.radonc.2007.06.020.

* **Corresponding author. Christian Thieke**, Department of Radiation Oncology, E050, German Cancer Research Center, Im Neuenheimer Feld 280, 69120 Heidelberg, Germany. *E-mail address:* c.thieke@dkfz.de

Received 15 December 2006; received in revised form 2 April 2007; accepted 13 June 2007; Available online 24 September 2007

References

[1] Cotrutz C, Lahanas M, Kappas K, Baltas D. A multiobjective gradient based dose optimization algorithm for external beam conformal radiotherapy. Phys Med Biol 2001;46:2161–75.
[2] Craft DL, Halabi TF, Shih HA, Bortfeld TR. Approximating convex Pareto surfaces in multiobjective radiotherapy planning. Med Phys 2006;33:3399–407.
[3] Haas OCL, Burnham KJ, Mills JA. Optimization of beam orientation in radiotherapy using planar geometry. Phys Med Biol 1998;43:2179–93.
[4] Hamacher HW, Küfer KH. Inverse radiation therapy planning – a multiple objective optimization approach. Discrete Appl Math 2002;118:145–61.
[5] Hoffmann AL, Siem AY, den Hertog D, Kaanders JH, Huizenga H. Derivative-free generation and interpolation of convex Pareto optimal IMRT plans. Phys Med Biol 2006;51:6349–69.
[6] Höss A, Debus J, Bendl R, Engenhart-Cabillic R, Schlegel W. Computerized procedures in 3-dimensional radiotherapy planning. Radiologe 1995;35:583–6.
[7] Hunt MA, Hsiung CY, Spirou SV, et al. Evaluation of concave dose distributions created using an inverse planning system. Int J Radiat Oncol Biol Phys 2002;54:953–62.
[8] Küfer KH, Hamacher HW, Bortfeld TR. A multicriteria optimization approach for inverse radiotherapy planning. In: Bortfeld TR, Schlegel W, editors, Proceedings of the XIIIth ICCR, Heidelberg, Germany; 2000. p. 26–9.
[9] Küfer KH, Scherrer A, Monz M, et al. Intensity modulated radiotherapy – a large scale multicriteria programming problem. OR Spectrum 2003;25:223–49.
[10] Lahanas M, Baltas D, Zamboglou N. Anatomy-based three-dimensional dose optimization in brachytherapy using multiobjective genetic algorithms. Med Phys 1999;26:1904–18.
[11] Monz M. Pareto Navigation – interactive multiobjective optimisation and its application in radiotherapy planning. Ph.D. thesis, Faculty for Mathematics, University Kaiserslautern, 2006.
[12] Niemierko A. A generalized concept of equivalent uniform dose. Med Phys 1999;26:1100.
[13] Nill S, Bortfeld T, Oelfke U. Inverse planning of intensity modulated proton therapy. Z Med Phys 2004;14:35–40.
[14] Pareto V. Manual of political economy. New York, New York: A.M. Kelley; 1971 [Translation of Manuale di economia politica 1906].
[15] Preiser K, Bortfeld T, Hartwig K, Schlegel W, Stein J. A new program for inverse radiotherapy planning. In: Leavitt DD, Starkschall G, editors. 12th international conference on the use of computers in radiation therapy, Med Phys 1997; 425–8.
[16] Romeijn HE, Dempsey JF, Li JG. A unifying framework for multi-criteria fluence map optimization models. Phys Med Biol 2004;49:1991–2013.
[17] Scherrer A, Küfer KH, Bortfeld T, Monz M, Alonso F. IMRT planning on adaptive volume structures – a decisive reduction in computational complexity. Phys Med Biol 2005;50:2033–53.
[18] Scholz C, Nill S, Oelfke U. Comparison of IMRT optimization based on a pencil beam and a superposition algorithm. Med Phys 2003;30:1909–13.
[19] Scholz C, Oelfke U. IMRT planning based on various photon dose calculation inhomogeneous media. Med Phys 2005;32:2071.
[20] Schreibmann E, Lahanas M, Xing L, Baltas D. Multiobjective evolutionary optimization of number of beams, their orientation and weights for IMRT. Phys Med Biol 2004;49:747–70.
[21] Thieke C. Multicriteria Optimization in Inverse Radiotherapy Planning. Ph.D. thesis, Combined Faculties for the Natural Sciences and for Mathematics, University of Heidelberg, 2003.
[22] Thieke C, Bortfeld T, Niemierko A, Kuefer KH, Nill S. Multicriteria optimization in inverse radiotherapy planning. In: 7th Biennial ESTRO Meeting on Physics and Radiation Technology for Clinical Radiotherapy, Geneva, Switzerland. Radiother Oncol 2003;68 (Suppl. 1):44.
[23] Yu Y, Zhang JB, Cheng G, Schell MC, Okunieff P. Multiobjective optimization in radiotherapy: applications to stereotactic radiosurgery and prostate brachytherapy. Artif Intell Med 2000;19:39–51.

IOP Publishing Physics in Medicine and Biology

Phys. Med. Biol. **58** (2013) 1855–1867 doi:10.1088/0031-9155/58/6/1855

The critical spot eraser—a method to interactively control the correction of local hot and cold spots in IMRT planning

Philipp Süss[1], **Michael Bortz**[1], **Karl-Heinz Küfer**[1] **and Christian Thieke**[2]

[1] Fraunhofer Institute for Industrial Mathematics (ITWM), Kaiserslautern, Germany
[2] Department of Radiation Oncology, German Cancer Research Center and University Clinic Heidelberg, Heidelberg, Germany

E-mail: philipp.suess@itwm.fraunhofer.de

Received 7 December 2012, in final form 27 January 2013
Published 27 February 2013
Online at stacks.iop.org/PMB/58/1855

Abstract

Common problems in inverse radiotherapy planning are localized dose insufficiencies like hot spots in organs at risk or cold spots inside targets. These are hard to correct since the optimization is based on global evaluations like maximum/minimum doses, equivalent uniform doses or dose–volume constraints for whole structures. In this work, we present a new approach to locally correct the dose of any given treatment plan. Once a treatment plan has been found that is acceptable in general but requires local corrections, these areas are marked by the planner. Then the system generates new plans that fulfil the local dose goals. Consequently, it is possible to interactively explore all plans between the locally corrected plans and the original treatment plan, allowing one to exactly adjust the degree of local correction and how the plan changes overall. Both the amount (in Gy) and the size of the local dose change can be navigated. The method is introduced formally as a new mathematical optimization setting, and is evaluated using a clinical example of a meningioma at the base of the skull. It was possible to eliminate a hot spot outside the target volume while controlling the dose changes to all other parts of the treatment plan. The proposed method has the potential to become the final standard step of inverse treatment planning.

(Some figures may appear in colour only in the online journal)

1. Introduction

IMRT treatment plans are mainly evaluated based on their virtually predicted 3D dose distribution in the patient, either by visually inspecting the overlay of the dose over the planning structures or by judging aggregated forms such as a dose–volume histogram (DVH) or global indicators measuring critical structure sparing (e.g. the equivalent uniform dose

function (EUD) (Brahme 1984, Niemierko 1997)) or conformality of dose in targets (e.g. functions measuring deviations of individual dose points from a prescribed reference dose (Bortfeld *et al* 1990, Mageras and Mohan 1993, Webb 1989, Xing and Chen 1996), see (1) below). Modern treatment planning systems (TPS) provide routines to optimize treatment plans where such global indicators and DVH specifications are formulated as objectives to optimize and constraints to force their values to lie within certain limits. In most planning systems treatment plans are obtained iteratively by modifying the resulting optimization problem in some form. Some modern systems, such as the prototype planning system by ITWM[3] have adapted a multicriteria decision-making framework in which the plan optimization is done offline and the resulting solution space is interactively explored, again guided by global or aggregating indicators which were formulated for the optimization (Küfer *et al* 2009).

In this paper we address the situation when, at some point during the interaction with a TPS, the user was able to create a treatment plan that is acceptable regarding the balance of all global indicators and DVHs but which suffers from local insufficiencies in the 3D dose distribution. More specifically, when there are regions (not necessarily connected) in the patient volume where the dose is either to high (hot spots) or too low (cold spots). This is not necessarily a shortcoming of the numerical method used to solve the IMRT optimization problem and could arise from several situations. It could be that such local insufficiencies have a negative impact on a global indicator, albeit a very small one so that they do not play a significant role in the optimization. Another reason for such occurrences is when the treatment plan of a previous fraction is evaluated on a newly obtained image and the target and critical volumes have changed their sizes or have shifted a little. Yet another possibility is the acquisition of new functional images and the definition of more detailed sub-volume boost targets during the planning stage.

Such an almost acceptable plan should be locally improved without losing its overall characteristics. More specifically, the previously established trade-offs between critical structure sparing and targets conformality and the overall 3D dose distribution (with the exception of the local insufficiency) should be preserved. However, any modification made to the beam arrangement or the fluence modulation of the current treatment plan could lead to big changes in the dose distribution and, therefore, to *a priori* unknown changes to global indicators and DVHs. At this point the user faces a trade-off situation concerning how much the plan may change to correct the identified local deficiencies.

Cotrutz and Xing (2002, 2003) first described this problem in general and applied their method in the context of functional image-guided IMRT planning (Xing *et al* 2002). Their method is based on a quadratic objective (Bortfeld *et al* 1990, Mageras and Mohan 1993, Webb 1989, Xing and Chen 1996) defined by

$$f := \sum_{k \in K} r_{\sigma(k)} \left(d_k(x) - D_k^0 \right)^2 \tag{1}$$

where $k \in K$ are all voxel indices in the body, $r_{\sigma(k)}$ is an *importance factor* for a structure σ to which the voxel k belongs, $d_k(x)$ is the dose value at voxel k as a function of the treatment plan parameters x (beam directions, fluence modulation, etc) and D_k^0 is the prescription value for the dose at voxel k. They then extend the formulation by voxel-specific 'local importance factors' r_k for the deviation terms which are then empirically modified to place more weight on certain regions and the function (1) minimized to obtain new plans until after the user's visual inspection and clinical evaluation an acceptable plan is found. In Lougovski *et al* (2010) an automatic procedure is introduced to adaptively vary the prescriptions D_k^0 to render them

[3] The RayStation® by RaySearch Laboratories is the only commercial planning tool available supporting this technology for radiotherapy planning.

more or less important in subsequent optimizations of (1) depending on the magnitude of deviation of the individual doses d_k. In both approaches the user has to play an active role in the stepwise generation of alternative treatment plans, which are inspected and judged turn by turn. The preservation of the original plan characteristics is controlled only by keeping the original structure-dependent importance factors $r_{\sigma(k)}$ and influenced strongly by the empirically determined local importance factors r_k as in Cotrutz and Xing (2002, 2003), Xing *et al* (2002) or the automatically modified prescriptions D_k^0 as in Lougovski *et al* (2010). That is, the magnitude and type of change is beyond the direct influence of the user and could lead to several manual backtracking steps if an observed 'price' for recovering a local deficiency was too steep.

In this work, we introduce a framework to offer a *continuous* plan change based on an almost acceptable plan and one or more alternative plans which have in some way removed specifically marked local insufficiencies in the dose. By manipulating slider controls on the screen, the user is able to explore the trade-off between retaining the old plan and recovering local deficiencies while inspecting the change in the dose distribution and DVHs in real time. This approach is reminiscent of the multicriteria decision-making framework introduced in Küfer *et al* (2009) where the (partially extreme) compromises are determined first and then the whole space between these extremes is explored.

First we describe how to obtain such alternative plans in a fairly generic setting. We formulate an optimization problem to explicitly try to preserve the original plan characteristics. Then we describe the interaction mechanisms that allow the decision maker to intuitively explore the trade-offs between correcting the dose locally and retaining the original treatment plan characteristics. In the results section, we demonstrate these techniques on real patient data.

2. Methods and materials

Here we describe the initial situation we assume for our framework and how to obtain alternative treatment plans which correct local deficiencies present in the original plan. However, the interactive manipulation of treatment plans described later in section 2.2 does not make any assumptions how alternative plans were generated.

2.1. Obtaining locally corrected plans

For this part we assume that the formulation of the solved optimization problem by the TPS and its achieved global indicator values (objectives and constraints) represent well the essential clinical trade-offs of the original treatment plan. These function evaluations of the thus obtained plan will serve as an anchor for our method. Together with the formulated wish for new bounds on the dose in some marked subvolume(s), we formulate a new optimization problem to obtain alternative plans. In general form, the original, possibly multicriteria IMRT planning problem (MCO) can be formulated as follows

$$\text{MCO} \quad \text{`min'}\{f_i(x)\}_{i\in I} \tag{2}$$

$$s.t. \quad g_j(x) \leqslant 0 \quad j \in J \tag{3}$$

$$x \in \mathcal{X} \tag{4}$$

where x are the treatment plan parameters (beam directions, fluence modulation, etc) and the functions f_i and g_j each measure the quality of the dose in separate planning structures or subvolumes as a function of the plan parameters x (e.g. EUD or DVH objectives/constraints)

or they measure some aspect of the parameters themselves (e.g. some measure of complexity on the fluence modulation). Non-negativity constraints for the fluence modulation and other physical delivery constraints are treated separately by enforcing $x \in \mathcal{X}$. We make no further assumptions about the mathematical structure of the functions or the calculation of the 3D dose distribution dependent on x except that MCO can be solved by the TPS. It is possible that f_i and g_j are the same function for some i and j if a quality measure should be both optimized and constrained to lie within a certain range. MCO is a multicriteria problem if the cardinality of I is greater than 1. Then the 'min' condition amounts to finding efficient treatment plans and another (possibly interactive) step (e.g. weighting the objectives with importance factors) is necessary to solve MCO numerically. We assume from here on that a treatment plan x^* has been found by solving MCO and we define our 'anchor' qualities $f_i^A := f_i(x^*)$ and doses $d_k^A := d_k(x^*)$. With these we formulate our 'critical region correction' (CRC) problem as follows

$$\text{CRC} \quad \min_x \sum_{i \in I} \left(f_i(x) - f_i^A\right)^2 \tag{5}$$

$$+ \sum_{j \in J} \pi_j \cdot \max(0, g_j(x)) \tag{6}$$

$$+ \sum_{k \in K} r_k \cdot \left(d_k(x) - d_k^A\right)^2 \tag{7}$$

$$s.t.\, l_c \leqslant d_c(x) \leqslant u_c \quad c \in C \tag{8}$$

$$x \in \mathcal{X} \tag{9}$$

where $\pi_j \geqslant 0$ are new (fixed) weights for every original constraint g_j, $r_k \geqslant 0$ are voxel-specific weights (i.e. 'local importance factors' as in Cotrutz and Xing (2002, 2003), Xing *et al* (2002) and C is the set of voxels defining the critical region(s) in which newly formulated bounds l_c and u_c are not fulfilled in x^*. The bounds l_c and u_c can be set to 0 or ∞, respectively if such a constraint is not of interest for some voxel c. Note the following about CRC.

(i) Part (5) explicitly measures the deviation of the new treatment plan from the original objectives. Note that potential improvements in the objectives over the anchor are penalized in this formulation. We argue that if f_i^A was an efficient compromise in the multicriteria sense a 'net gain' in the objectives would not be possible anyway. Then (5) is responsible to preserve the original (acceptable) trade-off between the objectives as much as possible. To truly enforce this, the ∞-norm instead of the 2-norm could be used in (5) to measure the deviation of the new objectives from the anchor. Alternatively, the originally used scalarization (e.g. the weighted sum $\sum_{i \in I} w_i^* f_i$) used to obtain x^* could be used. Then it is implicitly assumed that the specific parameters of the scalarization (e.g. the weights w_i^*) carry some information about the trade-offs in x^*. If a function like (1) was used to obtain x^*, then it should be split as discussed at the end of this section.

(ii) The second term (6) in the objective of CRC corresponds to a so-called *exact penalty term* (Bazaraa *et al* 1993) involving the original model constraints of MCO. Note that the physical constraints such as the non-negativity of the intensities are not treated this way as they must be observed at all times. The presence of some of the constraints g_j in MCO probably had a significant role in obtaining the original almost acceptable treatment plan x^*. There are two main reasons for treating the formerly hard constraints in this now 'softer' manner. The intention of CRC is to obtain a new treatment plan with some identified local deficiencies completely removed. We therefore do not allow any other restriction other than those of physical nature. Also, retaining a treatment plan feasible

to the original constraints g_j can be controlled by setting high values for the penalty variables π_j, although this can be difficult to guarantee numerically. As second reason the authors argue that hard restrictions on global indicators and resulting function evaluations $g_j(x^*)$ only possess limited clinical meaning as often they are merely correlated with the clinical objectives of IMRT. If an original constraint is active in x^*, that is $g_j(x^*) = 0$ for some j, then it is not clear if a small violation is preferable over the identified local dose insufficiencies. If $g_j(x^*) < 0$ for some j, then the constraint might yet have played a role in the numerical optimization to balance out the other constraints and objectives of MCO. In both cases the clinical worth of truly keeping them as constraints is questionable and hence we don't enforce them in CRC. We mention how to find suitable values for π_j below.

(iii) While it is the job of the first two objective terms to retain the global characteristics of x^*, part (7) is meant to retain the shape of the 3D dose distribution itself. It is known that for a rather large class of optimization problems in IMRT planning the solutions can be varied rather strongly without changing global indicators f_i and g_j too much (Alber *et al* 2002). However, aside from the identified local dose deficiencies, all local plan characteristics from x^* should be maintained as well. Strategies for setting voxel weights r_k in (7) are given below.

(iv) The most important goal of CRC is to create alternative treatment plans which have local deficiencies in x^* removed. The unwanted hot spots are removed by applying upper bounds u_c and local cold spots are eliminated by enforcing lower bounds l_c. Note that if constraints (8) were satisfied by x^*, then this original plan is an optimal solution for CRC and it is only by explicitly constraining new plans to observe the newly formulated bounds that we guarantee to get exactly what we wanted.

It is conceivable that instead of a quadratic norm some other norms are used in (5) and (7) or to use a different penalty scheme for (6). Although it seems more complex at first glance, CRC is not harder to solve numerically than the original IMRT planning problem originating from MCO because its main structures are with f_i and g_j identical. Also note that x^* is an excellent starting point for finding alternative treatment plans as the (violated) constraints (8) should only be confined to small regions. What remains is how to set the weights π_j and r_k.

From mathematical programming (Bazaraa *et al* 1993) it follows that the optimal dual variables from the original IMRT planning problem resulting from MCO should be used for π_j as this retains best the original balance between the original objective values f_i and constraints g_j. This is especially true if x^* is a saddle point of the original IMRT planning problem (Kallio and Rosa 1999). If these optimal dual variables can not be estimated, then π_j should be treated in the standard way how penalty variables are treated in mathematical optimization and adjusted adaptively or empirically, see Bazaraa *et al* (1993).

With the help of r_k the burden of necessary change in the 3D dose distribution can be controllably distributed over the entire planning region. For example, the weights r_k can be increased with increasing distance of a voxel k to a critical region to force the changes in the dose to remain 'local' to the critical regions. It is also possible to set these weights depending on the correspondence of the voxel to a planning structure to allow more or less change in certain risk or target structures. As in Cotrutz and Xing (2002, 2003), Xing *et al* (2002), these weights have to be determined empirically and possibly be set by the user. However, their role and, therefore, the importance of choosing 'correct' values for r_k is diminished in CRC as part (7) is only one of several aims of this optimization problem.

It should be mentioned that if the TPS minimizes only a single function similar to the conventional quadratic function (1), then the deviation from an 'anchor' (5) should be formulated on a planning structure level. That is, to obtain a greater stability in the global trade-offs, instead of summing over the entire volume as in equation (1), the problem should be understood as a multicriteria optimization problem with involved objectives

$$f_\sigma(x) := \sum_{k \in K_\sigma} r_\sigma \left(d_k(x) - D_k^0\right)^2$$

for every planning structure σ (K_σ denotes the voxels in structure σ). Otherwise the burden of change necessary to solve CRC could be spread over too many voxels to retain only one function score for (1) for x^*. That is, if the TPS employs (1) as objective and no further hard constraints, the objective (lines (5)–(7)) of CRC should read

$$\min_x \sum_\sigma \left(\left(\sum_{k \in K_\sigma} r_\sigma \left(d_k(x) - D_k^0\right)^2 \right) - f_\sigma^A \right)^2,$$

where $f_\sigma^A := f_\sigma(x^*)$ are the separate evaluations of the weighted dose deviations for planning structures σ under the original plan. The original dose deviation terms given by line (7) can be omitted, as f_σ already measure dose differences.

2.2. Continuous plan change

At this point we assume that aside from the original, almost acceptable plan x^* one or two alternative plans have been generated which have some identified local deficiencies of x^* removed and are otherwise fairly similar to x^*. Although CRC is ideal for obtaining such plans, no assumptions about the derivation of such alternative treatment plans are made for the remainder of this paper. The planer now finds himself confronted with the conflict of how much change in the characteristics of x^* is acceptable to obtain some local improvements. Since the magnitude of change is impossible to determine *a priori*, that is, before the alternative plans are generated, this conflict should be explored interactively to give the user maximum control over the change. From experience with Pareto treatment plan navigation (Küfer *et al* 2009) for the exploration of global trade-offs the authors learned that the direct and continuous plan manipulation and real-time visualization of thus resulting plan changes is an invaluable planning instrument. There, previously calculated treatment plans are interpolated to obtain a new plan.

We propose to use one slider to interactively explore the conflict between locally corrected deficiencies and retaining plan characteristics. In the case where only one alternative plan $\tilde{x}$ was calculated, one end position of this slider corresponds to the original treatment plan x^* and the other end position corresponds to the alternative. Any position in between corresponds to a mix of both. The slider simply controls the combination coefficient $0 \leqslant \alpha \leqslant 1$ to obtain a new plan $\hat{x} := \alpha x^* + (1-\alpha)\tilde{x}$. If, for example by varying the voxel weights r_k in CRC, there are two alternative plans $\tilde{x}^1$ and $\tilde{x}^2$, a second slider can be used to control how much the necessary change should be spread over the planning region. The new plan is now given by $\hat{x} := \alpha x^* + (1-\alpha)(\beta\tilde{x}^1 + (1-\beta)\tilde{x}^2)$ with $0 \leqslant \beta \leqslant 1$ as well. In the numerical results section, we will use a constant weight $r_k = 1$ to obtain $\tilde{x}^1$, whereas $\tilde{x}^2$ is calculated by exponentially increasing the voxel weights with increasing geometrical distance to the identified critical regions. We then present two sliders: one to control the 'degree of correction α' of the local insufficiencies, and another to control the mix of the two alternative treatment plans, in our case the 'locality of allowed change β'. Figure 1 illustrates the set of plans that can be obtained by this mechanism.

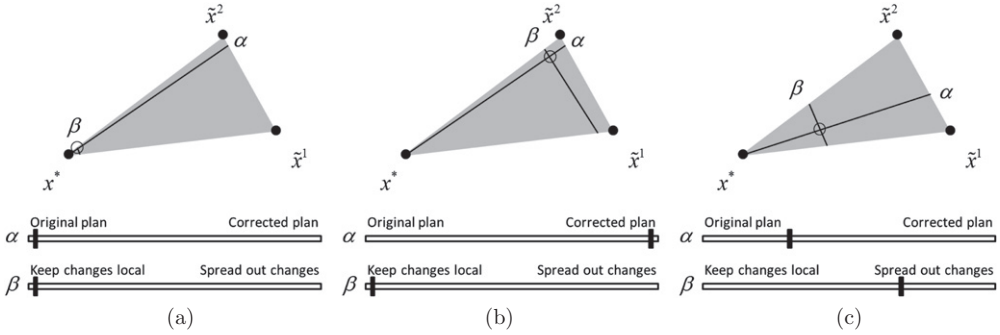

Figure 1. Set of plans reachable by the proposed mechanism and the corresponding slider positions. The lines indicate the plans attainable by sliding α or β from the current position marked by the circle. (a) Very close to x^*. (b) Very close to $\tilde{x}^2$. (c) A compromise solution.

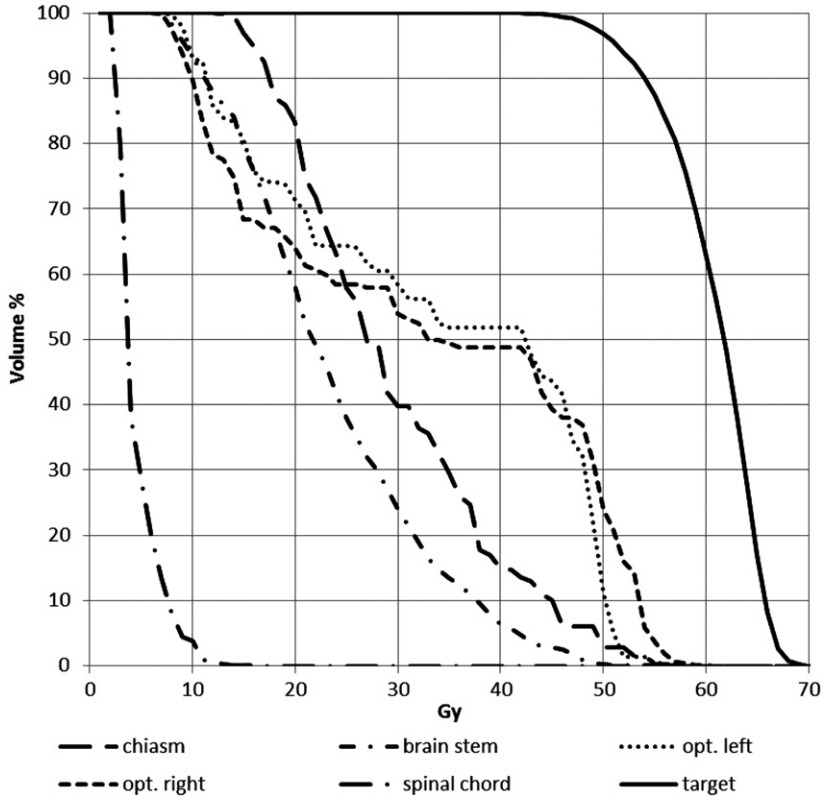

Figure 2. DVH curves of the original plan.

Note that interpolated solutions obtained by this mixing mechanism do not exhibit any optimality properties. They are in general neither efficient for the original problem MCO nor optimal for any variant of the correction problem CRC. The aim is to provide a smooth transition between plans exhibiting favourable properties. A strong advantage of the linear

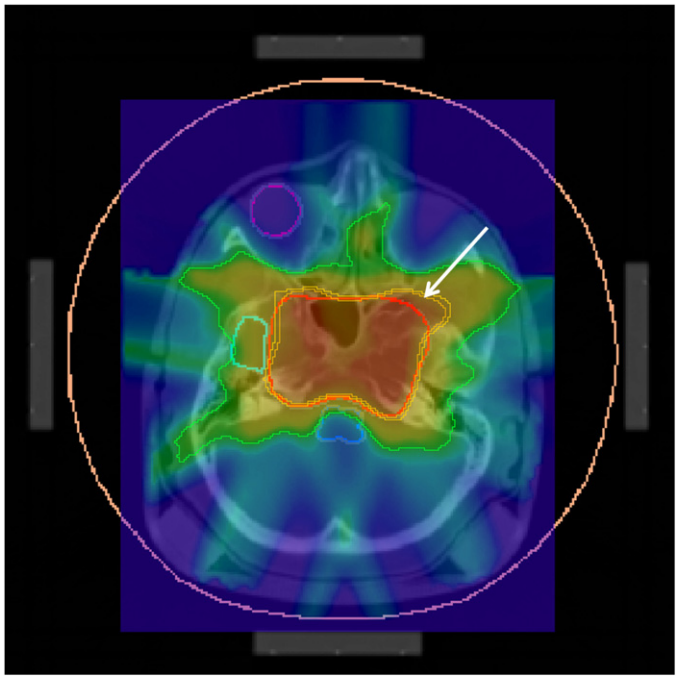

Figure 3. Slice of the original dose. Isolines correspond to the 50%, 90% and 95% volumes of the reference dose (set at 57.6 Gy). The marked area is the identified hot spot.

interpolation is that the dose in the critical spot can be controlled exactly if the dose calculation $d(x)$ is linear—there is a direct connection between the dose in the critical spot and the position of the correction slider for α.

3. Results and discussion

We demonstrate the results on a meningioma case at the base of the skull. The original MCO problem consisted of EUD objectives for all risk structures, one objective to minimize the underdosage under prescription in the target and one objective to minimize the overdosage over prescription in the target. Both objectives for the target were also hard constrained to lie within reasonable limits. Multicriteria navigation (Küfer *et al* 2009) was used to obtain a plan that had similar overall characteristics to the actually delivered treatment plan. This was done by visually comparing the DVH curves and selected views of the 3D dose distribution. The prototype software developed by the Fraunhofer ITWM was used for all calculations.

Figure 2 show the DVH curves and figure 3 a transversal cut of the dose colour wash of a slice close to the isocentre. The image shows the contours of the target volume, the brain stem, the right temporal lobe and the right eye. The marked spot in figure 3 where the high dose enters the unclassified tissue is the hot spot to eliminate using the techniques from above.

The software allows clicking in any display of the dose to select a critical region. The width of the region (in number of dose voxels in each dimension) and whether to exclude

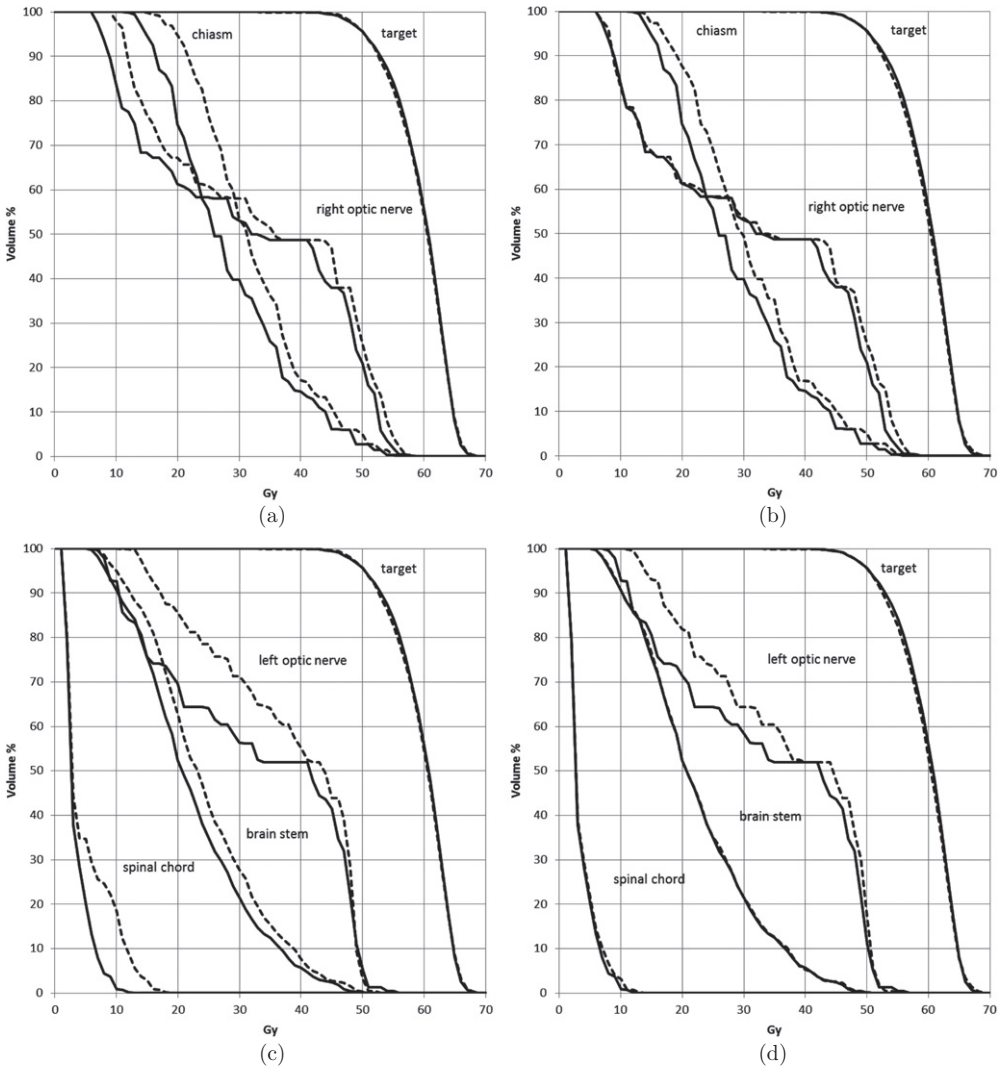

Figure 4. The DVH curves of the newly created plans. Figures (a) and (c) belong to the same plan where changes are allowed to spread out and figures (b) and (d) are from the plan where changes are kept local. The curves are split over two diagrams for better visualization. The solid lines are from the original solution and the dashed lines are from the corrected solutions.

voxels which overlay with the target volumes from the critical region can also be specified. Clicking the point marked with the white arrow in figure 3 revealed a dose of 56.9 Gy (about 99% of prescription) in the clicked voxel, and a minimum of 45.5 and maximum of 60.8 Gy in a roughly $3 \times 3 \times 3$ voxels (or $9 \times 9 \times 9\,\mathrm{mm}^3$) subvolume around the clicked region, excluding any voxel associated with the target. In this case, 4 voxels of that region also overlap with the target contour, leaving a total of 23 voxels (instead of 27) as the critical region.

The CRC problem was formulated and solved as described above using an interior point method described in detail in Süss (2008), once with unit voxel weights in line (7) and once

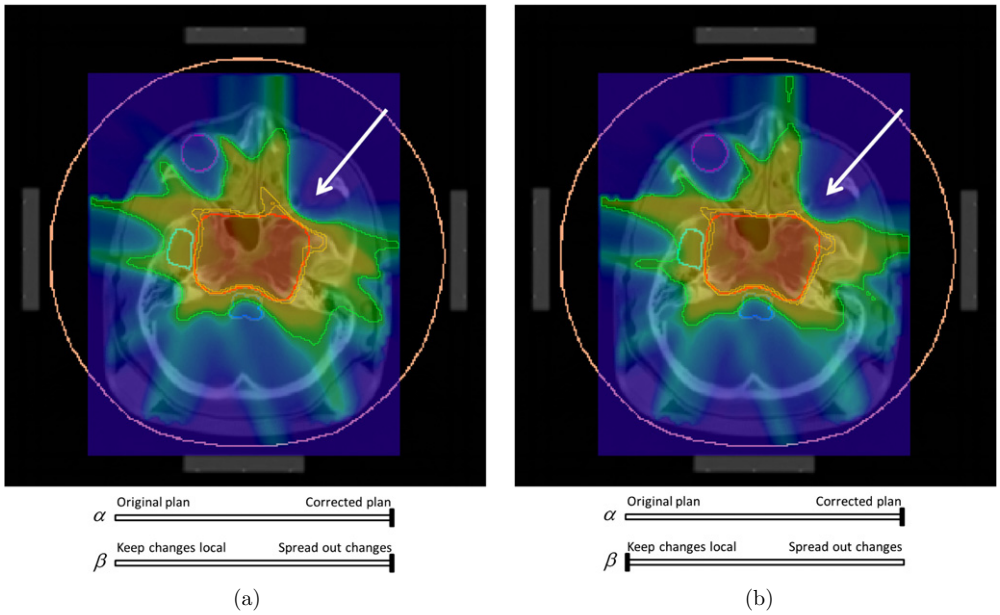

Figure 5. Dose colour washes of the newly created plans. The marked area is the declared hot spot where the dose has been reduced significantly. (a) Spread out changes. (b) Keep changes local.

with weights increasing as the distance to the hot spot increased. An upper limit of 30 Gy was set for all 23 voxels in the hot spot. This corresponds to the ambitious goal of reducing the dose by 30 Gy locally. It was found that it is better to specify such ambitious goals since the degree of correction can be interactively controlled at a later stage. The critical spot constraints were regularized using smooth functions to guarantee differentiability. That is, instead of requiring

$$d(x)_c \leqslant 30 \quad \forall c \in C,$$

we use

$$\ln(e^{d(x)_c \cdot a}) \leqslant \ln(e^{30 \cdot a}) \quad \forall c \in C$$

for some small positive a. This means that the exactness of the constraint is forfeit numerically in favour of a faster convergence of our optimizer and one of the new solutions was 4 Gy off this mark. However, this is compensated by specifying ambitious goals. In both cases, the CRC problem could be solved without violating the original underdose and overdose constraints. Figure 4 shows the DVH plots of the two newly calculated plans. These represent the extreme endpoints of the set of plans that can be generated by the interactive manipulation. The target curves have barely changed due to the penalty weighting scheme in CRC (line (6)). Figure 4 also shows that the dose in structures far away from the hot spot (i.e. right optic nerve, spinal cord and brain stem) is changed significantly more in the plan where changes were allowed to spread out further by using uniform weights for the weights r_k.

The isolines for both alternative plans are shown in figure 5. Since both new plans are somewhat extreme corrections (a reduction from 60 to 40 Gy as the maximum dose over all 23 hot spot voxels), we are more interested in a mix of these plans and the original. Figure 6 shows what happens to some descriptive statistics as the correction slider for the α parameter

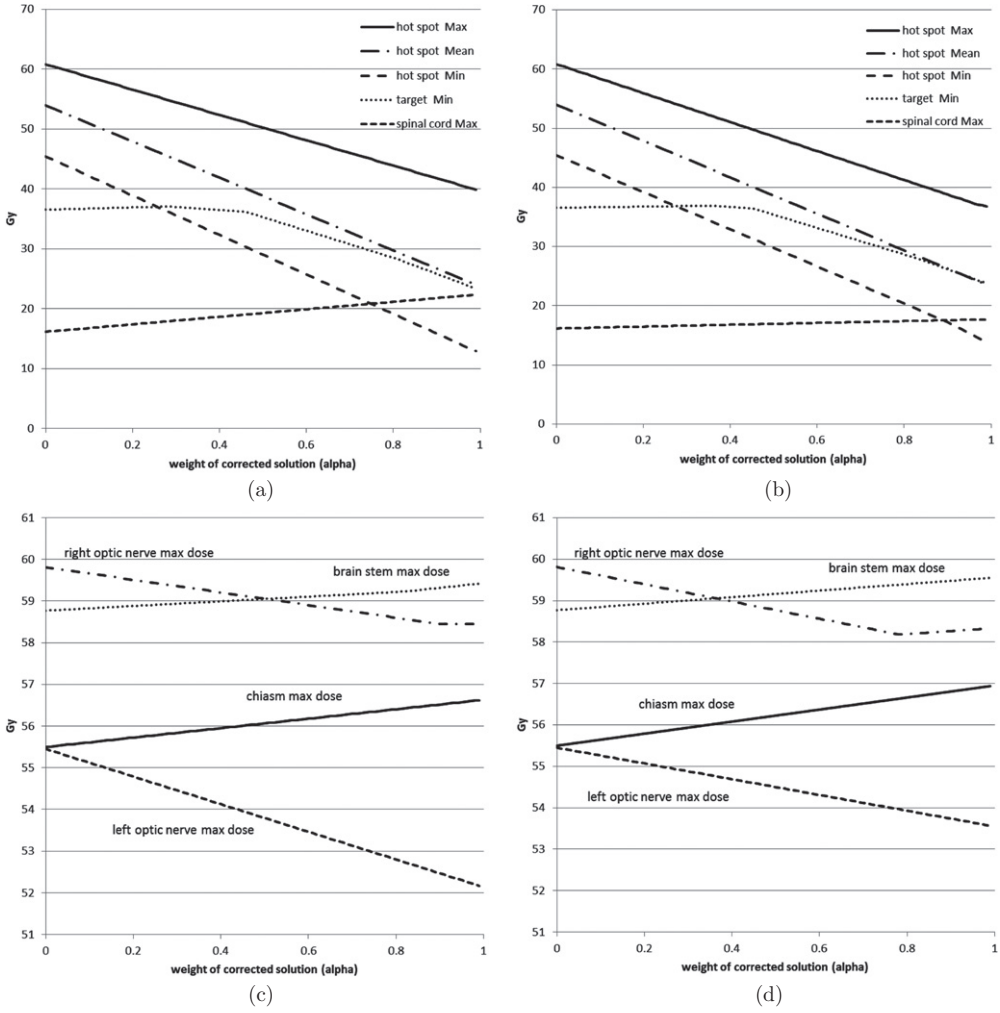

Figure 6. Dose values as a function of the slider values for α. (a) and (c) Spread out changes. (b) and (d) Keep changes local.

is moved. In both cases the minimum dose in the target only begins to deteriorate when the slider is moved about half the way, corresponding to an almost equal mix between the original solution of the alternative plans. Because the progression is virtually identical in both solutions, this will be true for any mixing factor β between the new alternatives, too.

Therefore, the dose in the hot spot can be reduced by 10 Gy without reducing the minimum dose in the target. The maximum dose in the delineated brain structures remains largely unchanged. The maximum dose for the spinal cord increases significantly for the solutions where changes are spread out over larger areas. The mean doses for all risk structures show a slight and steady increase as the correction slider is pulled. The decrease in the maximum dose of the left optical nerve is due to its geometrical proximity to the hot spot.

Figure 7 shows a compromise where the dose was reduced by about 20 Gy.

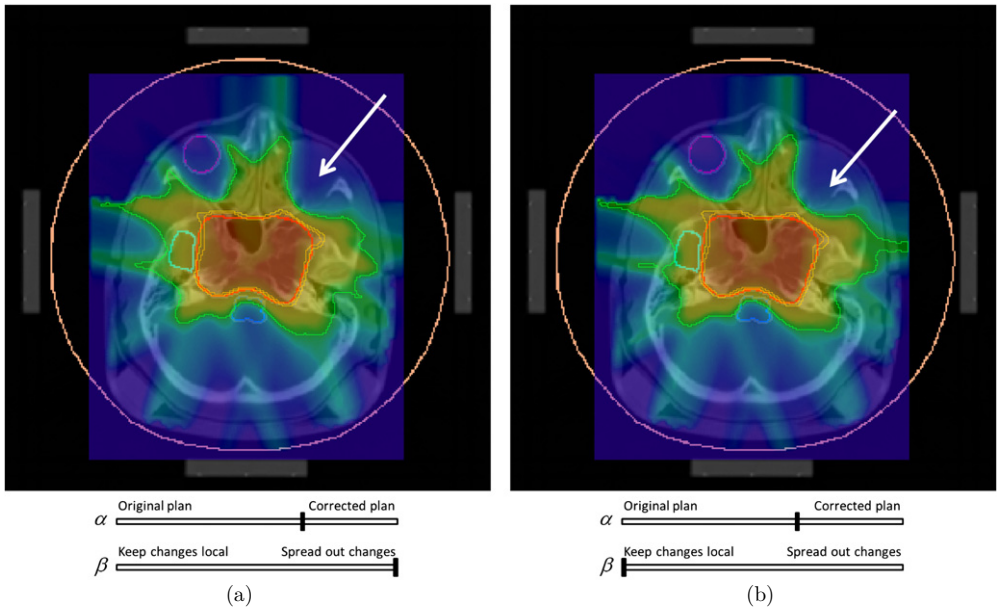

Figure 7. Two compromise plans. (a) Spread out changes. (b) Keep changes local.

4. Conclusion

We introduced and tested a method to correct for local dose insufficiencies like cold or hold spots in inverse treatment planning. New plans are calculated to allow for an interactive adjustment of local and global trade-offs by navigating both the amount and the size of the local dose change. The proposed method has the potential to become the final standard step of inverse treatment planning.

Acknowledgment

This work was partially supported by the DOT-MOBI grant (01 IS 08002D) of the Bundesministerium für Bildung und Forschung.

References

Alber M, Meedt G, Nüsslin F and Reemtsen R 2002 On the degeneracy of the IMRT optimization problem *Med. Phys.* **29** 2584–89

Bazaraa M S, Sherali H D and Shetty C M 1993 *Nonlinear Programming—Theory and Algorithms* (New York: Wiley)

Bortfeld T, Burkelbach J, Boesecke R and Schlegel W 1990 Methods of image reconstruction from projections applied to conformation radiotherapy *Phys. Med. Biol.* **35** 1424–34

Brahme A 1984 Dosimetric precision requirements in radiation therapy *Acta Radiol. Oncol.* **23** 379–91

Cotrutz C and Xing L 2002 Using voxel-dependent importance factors for interactive DVH-based dose optimization *Phys. Med. Biol.* **47** 1659–69

Cotrutz C and Xing L 2003 IMRT dose shaping with regionally variable penalty scheme *Med. Phys.* **30** 544–51

Kallio M and Rosa C 1999 Large-scale convex optimization via saddle point computation *Oper. Res.* **47** 93–101

Küfer K H, Monz M, Scherrer A, Süss P, Alonso F V, Azizi Sultan A S, Bortfeld T and Thieke C 2009 Multicriteria optimization in intensity modulated radiotherapy planning *Handbook of Optimization in Medicine* ed H E Romeijn and P M Pardalos (New York: Springer) pp 123

Lougovski P, LeNoach J, Zhu L, Ma Y, Censor Y and Xing L 2010 Toward truly optimal IMRT dose distribution: inverse planning with voxel-specific penalty *Technol. Cancer Res. Treat.* **9** 629–36 PMCID: PMC3057528

Mageras G S and Mohan R 1993 Application of fast simulated annealing to optimization of conformal radiation treatments *Med. Phys.* **20** 639–47

Niemierko A 1997 Reporting and analyzing dose distributions: a concept of equivalent uniform dose *Med. Phys.* **24** 103–10

Süss P 2008 A primal-dual barrier algorithm for the IMRT planning problem: an application of optimization-driven adaptive discretization *Dissertation,* Technical University Kaiserslautern

Webb S 1989 Optimisation of conformal radiotherapy dose distributions by simulated annealing *Phys. Med. Biol.* **34** 1349–70

Xing L and Chen G T Y 1996 Iterative algorithms for inverse treatment planning *Phys. Med. Biol.* **41** 2107–23

Xing L, Cotrutz C, Hunjan S, Boyer A, Adalsteinsson E and Spielmann D 2002 Inverse planning for functional image-guide intensity-modulated radiation therapy *Phys. Med. Biol.* **47** 3567–78

RADIATION ONCOLOGY

STUDY PROTOCOL Open Access

Multimodal hypoxia imaging and intensity modulated radiation therapy for unresectable non-small-cell lung cancer: the HIL trial

Vasileios Askoxylakis[1,2*], Julien Dinkel[3], Monika Eichinger[3], Bram Stieltjes[4], Gregor Sommer[3], Ludwig G Strauss[5], Antonia Dimitrakopoulou-Strauss[5], Annette Kopp-Schneider[6], Uwe Haberkorn[7], Peter E Huber[1,2], Marc Bischof[1], Jürgen Debus[1,2] and Christian Thieke[1,2]

Abstract

Background: Radiotherapy, preferably combined with chemotherapy, is the treatment standard for locally advanced, unresectable non-small cell lung cancer (NSCLC). The tumor response to different therapy protocols is variable, with hypoxia known to be a major factor that negatively influences treatment effectiveness. Visualisation of tumor hypoxia prior to the use of modern radiation therapy strategies, such as intensity modulated radiation therapy (IMRT), might allow optimized dose applications to the target volume, leading to improvement of therapy outcome. ^{18}F-fluoromisonidazole dynamic positron emission tomography and computed tomography (^{18}F-FMISO dPET-CT) and functional magnetic resonance imaging (functional MRI) are attractive options for imaging tumor hypoxia.

Methods/design: The HIL trial is a single centre study combining multimodal hypoxia imaging with ^{18}F-FMISO dPET-CT and functional MRI, with intensity modulated radiation therapy (IMRT) in patients with inoperable stage III NSCLC. 15 patients will be recruited in the study. All patients undergo initial FDG PET-CT and serial ^{18}F-FMISO dPET-CT and functional MRI before treatment, at week 5 of radiotherapy and 6 weeks post treatment. Radiation therapy is performed as inversely planned IMRT based on 4D-CT.

Discussion: Primary objectives of the trial are to characterize the correlation of ^{18}F-FMISO dPET-CT and functional MRI for tumor hypoxia imaging in NSCLC and evaluate possible effects of radiation therapy on tumor re-oxygenation. Further objectives include the generation of data regarding the prognostic value of ^{18}F-FMISO dPET-CT and functional MRI for locoregional control, progression free survival and overall survival of NSCLC treated with IMRT, which will form the basis for larger clinical trials focusing on possible interactions between tumor oxygenation and radiotherapy outcome.

Trial registration: The ClinicalTrials.gov protocol ID is NCT01617980

Keywords: Hypoxia, Imaging, Radiotherapy, Non-small-cell lung cancer

* Correspondence: vasileios.askoxylakis@med.uni-heidelberg.de
[1]Department of Radiation Oncology, University of Heidelberg, INF 400, 69120 Heidelberg, Germany
[2]Clinical Cooperation Unit Radiation Oncology, German Cancer Research Center (DKFZ), INF 280, 69120 Heidelberg, Germany
Full list of author information is available at the end of the article

Background

Lung cancer is the leading cause of cancer mortality. The disease is worldwide diagnosed in about 1.35 million patients yearly and is responsible for about 1.18 million deaths yearly [1]. Non-small-cell lung cancer (NSCLC) accounts for 75% of all cases. The treatment of choice is surgery however a radical resection is possible in only 20% of all cases. Radiation therapy alone or combined with chemotherapy are therapeutic alternatives for tumors that are surgically not resectable. Application of 60-66 Gy by external beam radiotherapy results in a mean local tumor control of about 12 months [2], whereas combined radio-chemotherapy, preferably platinum-based, leads to a significant survival improvement compared to irradiation alone [3].

Although there is evidence that dose escalation is related with increased local control and improved overall survival, a higher radiation dose is also related with increased lung toxicity and severe side effects, such as radiation induced pneumonitis and lung fibrosis [4]. To reduce side effects, advanced technologies that allow a more accurate dose delivery to the target volume minimizing healthy tissue toxicity have been developed. A promising technology in this respect is the intensity modulated radiation therapy (IMRT) [5].

Furthermore, use of fluorine-18 deoxyglucose dynamic positron emission tomography and computed tomography (FDG dPET-CT) improved disease staging, whereas the development of four-dimensional computed tomography (4D-CT) enabled a more precise target volume definition [6,7]. 4D-CT can improve radiotherapy targeting, since it provides information about the motion of the target but also about changes of the pulmonary parenchyma as a result of breathing-associated changes in air content [8,9]. In addition, advanced dynamic contrast enhanced magnetic resonance imaging (DCE-MRI) techniques allow a better visualization of tumor heterogeneity, as well as an improved assessment of tumor vascularization and more accurate differentiation between benign processes such as inflammation or atelectasis and malignant tumor lesions [10,11].

However, despite the development of diagnostic and therapeutic modalities, lung tumors still show a variable resistance to available regimens of radio-chemotherapy. One of the factors that increase therapy resistance is hypoxia. Tumor hypoxia is associated with a malignant phenotype, characterized by high invasiveness, increased potential for progression and metastasis and poor prognosis [12,13]. Subphysiologic levels of oxygen are present in the majority of human tumors and lead to an up to 3-fold increase of resistance against antineoplastic strategies [14].

The leading role of hypoxia in radiation resistance reveals the necessity for the development and evaluation of hypoxia imaging assays. Such assays would allow a better characterization of tumor heterogeneity and facilitate the improvement of targeted therapies, as well as the development of novel strategies for prediction of treatment outcome. An extensively investigated tracer for visualization of tumor hypoxia by dynamic positron emission tomography and computed tomography (dPET-CT) is fluorine-18-labeled fluoromisonidazole (^{18}F-FMISO; half time 110 min). Various preclinical and clinical studies have revealed a correlation between oxygen measurements and ^{18}F-FMISO uptake [15]. In metastatic head and neck cancer, the retention of ^{18}F-FMISO was found to be significantly greater in hypoxic tumors, especially at pO_2 values <5 mmHg [16]. A study of 12 patients with head and neck carcinoma, who received FMISO-PET scans before radiotherapy, revealed that the tracer uptake was a prognostic indicator of treatment response [17]. In regard to NSCLC, a study performed in 14 patients demonstrated an association between high tumor-to-muscle FMISO uptake ratios and risk of relapse [18]. Furthermore, a trial of 8 patients with NSCLC who were treated by combined radio-chemotherapy and received serial ^{18}F-FMISO-PET scans showed an association between FMISO uptake decrease post treatment and favourable therapy outcome [19].

Further non-invasive methods for *in vivo* oxygenation monitoring include modern magnetic resonance imaging (MRI) and magnetic resonance spectroscopy (MRS) applications. MRI approaches comprise perfusion functional MRI for evaluation of tissue hemodynamics through characterization of blood flow patterns, as well as approaches based on the effects of local oxygen tension on the magnetic susceptibility effects of oxy- and deoxyhemoglobin and on the effects of paramagnetic oxygen on the relaxation times of tissue water [20].

Aim of the present trial is to investigate the correlation of ^{18}F-FMISO dPET-CT and functional MRI for tumor hypoxia imaging in patients with inoperable stage III NSCLC, treated with 4D-CT based IMRT. Furthermore, through serial ^{18}F-FMISO dPET-CT and functional MRI investigations prior, during and post treatment, possible effects of radiation therapy on tumor re-oxygenation and their influence on treatment response will be evaluated.

Methods/design

Trial organisation

The HIL-trial has been designed by the study initiators at the Clinical Cooperation Unit Radiation Oncology at the German Cancer Research Center (DKFZ), the Clinical Cooperation Unit Nuclear Medicine at DKFZ, the Department of Radiology at DKFZ and the Department of Radiation Oncology at the University of Heidelberg. The trial is carried out at DKFZ in co-operation with the

Department of Radiation Oncology at the University of Heidelberg.

Coordination

The trial is coordinated by the Clinical Cooperation Unit Radiation Oncology at DKFZ and the Department of Radiation Oncology at the University of Heidelberg. DKFZ is responsible for trial management and quality assurance including reporting and database management.

Study design

The study is designed as a single centre trial with an accrual of 15 patients with inoperable stage III NSCLC. Patients fulfilling the inclusion criteria are treated with intensity modulated radiation therapy (IMRT). All patients undergo serial ^{18}F-FMISO dPET-CT and functional MRI before treatment, at week 5 of radiotherapy and 6 weeks post treatment. The trial workflow is depicted in Figure 1.

Study objectives

Primary aim of the study is to characterize the correlation of ^{18}F-FMISO dPET-CT and functional MRI for tumor hypoxia imaging in patients with stage III NSCLC treated with intensity modulated radiation therapy (IMRT). This will be achieved through correlation between functional MRI parameters, such as diffusion coefficients and ^{18}F-FMISO dPET-CT parameters, such as standard uptake value (SUV) in matched regions of interest. Further objectives are to evaluate changes in ^{18}F-FMISO dPET-CT and functional MRI parameters during radiation treatment and characterize their prognostic value for locoregional control, progression free survival and overall survival.

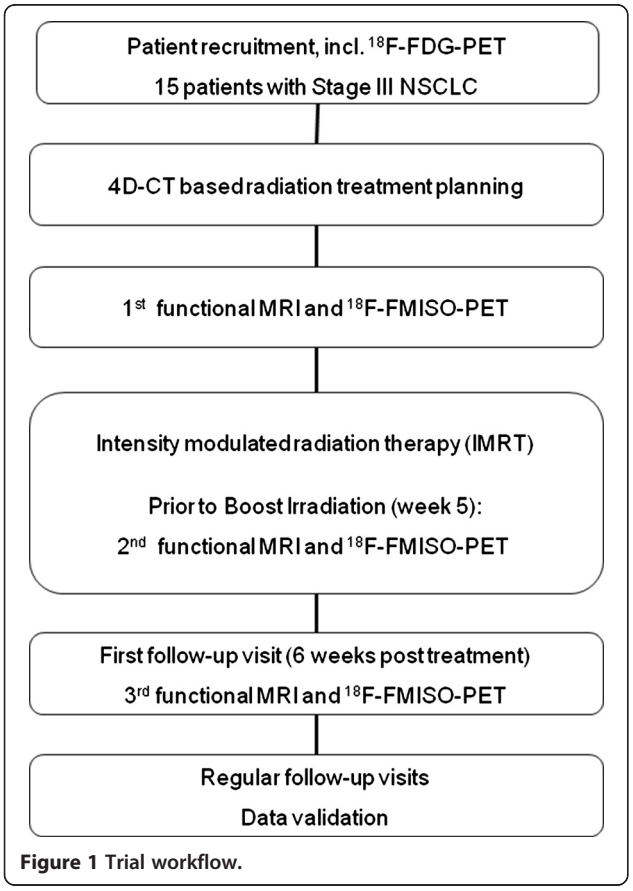

Figure 1 Trial workflow.

Investigators

Patient treatment is performed by radiation oncologists at the Clinical Cooperation Unit Radiation Oncology at DKFZ. 4D-CT and functional MRI scans are performed at the Department of Radiology at DKFZ. dPET-CT studies are carried out at the Clinical Cooperation Unit Nuclear Medicine at DKFZ.

Data handling, storage and archiving

All findings, including clinical and laboratory data, are documented by the investigator or an authorized member of the study team in the subject's medical record. The investigator is responsible for ensuring that all sections are completed correctly and that entries can be verified against source data. All missing data or inconsistencies are reported back to the investigators and clarified by the responsible investigator. If no further corrections are to be made in the database it will be declared closed and used for analysis. The data will be stored and archived according to §13 of the German GCP-Regulation and §28c of the German X-Ray Regulation (RöV) and §87 of the German Radiation Protection Regulation (StrlSchV) for at least 30 years after the initial termination.

Ethics, informed consent and safety

The final protocol was approved by the ethics committee of the University of Heidelberg, Heidelberg, Germany (Nr: S-249/2009). The trial is sponsored by the Federal Ministry of Education and Research (BMBF) of Germany as part of the research fund "DOT-MOBI" (Nr.: 01IB08002B). This study complies with the Helsinki Declaration and its recent German version, the Medical Association code of conduct, the principles of Good Clinical Practice (GCP) and the Federal Data Protection Act. The trial is carried out in keeping with local legal and regulatory requirements. The medical secrecy and the Federal Data Protection Act are followed. The ClinicalTrials.gov protocol ID is NCT01617980.

Patient selection

Inclusion criteria for the trial are:

- Documented inoperable, histologically confirmed NSCLC stage III.

- Sufficient remaining lung function ($FeV_1 > 1.5$ l/s or at least 50% of the respective individual norm value).
- Karnofsky Performance Score of 70% or higher.
- Patients > 18 years of age.
- Adequate haematological function (wbc $> 3000 \times 10^3$ /ml, thc $>100 \times 10^6$ /ml, Hb > 10 g/dl)
- Adequate hepatic and renal function
- Written informed consent

Exclusion criteria for the trial are:

- Patient refusal
- Severe concurrent systemic disease
- Other malignancies
- Hypersensitivity to x-ray contrast medium or ^{18}F-FMISO
- Claustrophobia
- Cardiac pacemaker
- Severe renal or hepatic insufficiency
- Pregnancy or lactation

Study plan

15 patients are included in the study according to the criteria above. Eligible patients are informed about participation in the trial with possible benefits and risks, and written informed consent is obtained. Staging is completed through performance of thoracic CT scan, abdominal ultrasound and ^{18}F-FDG dPET-CT scan.

IMRT treatment planning

After immobilization in a vacuum mattress a contrast-enhanced thoracic CT scan including 4D respiratory triggering is carried out. CT data are synchronized with the recorded respiratory signal and 4D reconstructions are performed to evaluate the motion of the thoracic organs and the tumor during the breathing cycle. Based on the 4D-CT data set, radiation treatment planning is performed as inverse planning. ^{18}F-FMISO dPET-CT and functional MRI data are not included in target volume definition or dose prescription.

Radiation therapy

Radiation therapy is performed as intensity modulated radiation therapy (IMRT). A dose of 50-54 Gy is applied to the primary tumor and mediastinal lymph nodes in daily fractions of 5×2 Gy. Subsequently, the primary tumor and involved lymph nodes are boosted to a total dose of 60-72 Gy in daily fractions of 5×2 Gy. Tolerance doses of thoracic organs at risk are not exceeded.

Treatment is carried out on an out-patient basis unless the condition of the patient requires hospital administration.

^{18}F-FMISO positron emission tomography

^{18}F-FMISO is provided by Iason (Graz, Austria). ^{18}F-FMISO dPET-CT investigations are performed prior to radiotherapy, at week 5 of radiation therapy and at 6 weeks post treatment. dPET-CT examinations are performed after the i.v. injection of ^{18}F-FMISO using an Biograph mCT S128 (Siemens Medical Solutions Co., Erlangen, Germany). The dynamic studies are acquired with a 28-frame protocol for one hour. Quantification is performed following the iterative reconstruction of the dPET-CT data using a dedicated software package. Generally, volumes-of-interest (VOIs) are placed over the tumor and reference regions, followed by a compartment and non-compartment analysis. A two-tissue compartment model is the model of choice and five parameters are obtained. The quantification includes the calculation of the fractional blood volume, also named as vessel density (VD), the parameters k1 and k2, which reflect the influx and efflux of FMISO into and out of the cells, and k3 and k4, which are related to the trapping and re-oxygenation of FMISO. For the input function the mean value of the VOI data obtained from a large arterial vessel like the descending aorta is used. Besides the VOI based analysis, parametric images are calculated to assess dedicated parameters of the FMISO kinetics.

Furthermore, a non-compartment model based on the fractal dimension is used. The fractal dimension (FD) is a parameter for the heterogeneity and is calculated for the time activity data of each individual VOI. The values of the fractal dimension vary from 0 to 2 showing the deterministic or chaotic distribution of the tracer activity. We use a subdivision of 7×7 and a maximal SUV of 20 for the calculation of FD. Details of the quantification of the dPET data have been published elsewhere [21].

Functional MRI

Functional MRI investigations are performed prior to radiation therapy, at week 5 of radiation therapy and at 6 weeks post treatment. All examinations are performed using a clinical 1.5-T MRI scanner (Magnetom Avanto, Siemens Medical Solutions, Erlangen, Germany).

The standard protocol comprises a coronal and a transversal breath-hold TrueFISP, T2w single-shot half-Fourier TSE (HASTE) and T1w 3D-GRE (VIBE) sequence. Afterwards, a navigator triggered transversal T2w-FatSat sequence (T2-FS BLADE) is carried out.

Diffusion weighted imaging (DWI) is performed using an axial single shot echoplanar (EPI) sequence with and without flow-compensation. A total of ten b-values (0, 10, 25, 50, 100, 200, 300, 400, 500 and 800 s/mm2) is acquired, enabling extraction of diffusion and perfusion parameters. DWI parameters are evaluated based on the Intravoxel Incoherent motion (IVIM) model [22],

yielding the parameters perfusion fraction f and diffusion constant D, using in house developed open-source software MITK Diffusion, Version 2011 (downloadable at www.mitk.org). The parameter estimation is based on the assumption that the diffusion measurement is influenced by mainly two effects, a perfusion related effect introduced by the molecules moving in the capillary network (pseudodiffusion coefficient, D*) and extravascular effects of passive diffusion (D). Since a simultaneous nonlinear fit for all parameters D, D*, and the weighting coefficient f can be instable, measurement at b-values greater than 200 s/mm^2 are used in a first step to estimate f and D as described [23]. D* is then calculated in a second step by using exhaustive search.

Lung cancer perfusion is assessed using a spoiled 3D gradient echo sequence after bolus injection of 0.07 mmol/kg body weight of Gd-DTPA. Ten acquisitions in one expiratory breath hold (10 × 2.25 s = 22 s) are followed by 50 navigator-triggered acquisitions under free breathing (total TA 4½ min). After a co-registration of the 3D data sets, a ROI-based visualization of the signal-time curves is performed as described [24].

Furthermore, a time-resolved echoshared gradient echo sequence (TWIST) is performed for assessment of three-dimensional tumor motion (240 × 0.5 s = TA 2 min). A dynamic 2D-TrueFISP sequence acquired in coronal orientation crossing the centre of the tumor provides additional information about lung and tumor motion during the breathing cycle.

Contrast-enhanced sequences breath hold 3D-GRE sequence (VIBE) completes this protocol. The in-room time for the complete protocol is approximately 30 min.

Clinical follow up

The first follow-up is planned 6 weeks post treatment and includes study-related ^{18}F-FMISO dPET-CT and functional MRI examinations. Further regular follow-up visits are scheduled every 3 months for the first 2 years, every 6 months for the following 3 years and thereafter yearly. Individual trial participation is completed three years after patient enrolment or death of the patient.

The therapeutic efficacy will be evaluated through thoracic CT-scan at follow up visits.

Evaluation of local response

Local response evaluation is performed according to the RECIST Criteria (Response Evaluation Criteria in Solid Tumours) [25].

Statistical analysis

The study is a prospective and non-randomized trial with inclusion of 15 patients. Repeated examinations with ^{18}F-FMISO dPET-CT and functional MRI lead to longitudinal data for every patient. The data consists of maps obtained from both measurement devices. Data are quantitative measurements but may be dichotomized or categorized into more than two classes. For all parameters, differences between the site of local relapse and a selected control region are derived and compared by paired tests at 5% level.

All analyses are exploratory. A sample size calculation cannot be performed because neither standard deviation of the differences has been estimated before, nor the relevant difference is known. Therefore, the study will be used to generate hypotheses for future research.

In the frame of the radiation therapy planning study, virtual radiation therapy strategies will be compared to the radiation therapy administered to the patient.

Discussion

Radiation therapy in combination with platinum-based chemotherapy is the treatment of choice for inoperable non-small-cell lung cancer. The development of modern radiation delivery techniques, such as intensity-modulated radiotherapy (IMRT) optimized treatment planning, enabled better sparring of surrounding healthy tissues and decreased treatment-related toxicity [26,27].

Compared with other cancer entities, in case of lung cancer tumor motion during the breathing cycle and variation of the target size due to changes in air content of the pulmonary parenchyma enhance the complexity of issues involved in radiation therapy planning, impede the definition of target volume and limit IMRT. In recent years, major progress has been made, mainly through the development of four dimensional respiratory triggering CT-scan planning modalities and MRI applications that allow a spatial resolution in the assessment of tumor, healthy lung parenchyma, chest wall and diaphragm [28].

The outcome of radiation therapy is however often limited by features of the tumor microenvironment. The therapeutic effect of radiation therapy is known to be negatively influenced by low tumor oxygen levels. Therefore, better understanding of the correlation between radiation resistance enhancing parameter, such as tumor hypoxia, and outcome of radiation therapy applications is of high priority for optimization of radiation therapy strategies and improvement of treatment efficacy.

In this respect, visualization of tumor heterogeneity in regard to hemodynamics and oxygen concentration is necessary. Imaging applications for hypoxia assessment include FMISO PET-CT and functional magnetic resonance imaging. The use of FMISO in hypoxia specific PET approaches is based on its selective reduction in tumor regions with decreased oxygen concentration, and the binding of its metabolites to macromolecules [15]. However, PET imaging is limited mainly through a reduced spatial resolution. MRI provides high spatial

resolution structural and functional information on tumor vasculature and perfusion, including important anatomical details. Therefore, dPET-CT based investigation of variations in FMISO uptake and analysis of functional MRI parameter can provide complementary data about tumor vascularisation, microenvironment, functional and anatomical structures.

Multimodal imaging studies in animal models were combined with tissue section analysis to relate the *in vivo* non-invasive data to the tumor microenvironment. These studies demonstrated a positive correlation between perfusion related, MRI-derived parameter with early FMISO PET intensity and a negative correlation with late FMISO slope, providing evidence for the hypothesis that tumor regions with reduced perfusion are hypoxic [29]. However, the same study also revealed issues which should be considered in multimodal approaches, such as volume averaging effects in PET as a result of its lower spatial resolution and perfusion effects of FMISO accumulation in the tumor [29]. Based on these data, a clinical trial investigated tumor perfusion using MRI and hypoxia measured by FMISO-PET in 13 patients with nodal metastases of head and neck cancer [30]. The results of this study also revealed a negative correlation between FMISO uptake and the perfusion value, supporting the hypothesis that hypoxic tumors are poorly perfused [30].

Major pathophysiological mechanisms for the onset of tumor hypoxia do not only include structural and functional abnormalities of the tumor vasculature, which can be assessed by perfusion protocols, but also adverse molecular diffusion. The diffusion geometry of tumors can be assessed and visualized by diffusion-weighted MRI (DWI). DWI has been successfully applied in various clinical trials for determination and monitoring of treatment response, indicating that lesions with locoregional recurrence during follow-up correlated with significantly lower diffusion [31].

Based on the empiricism of previous trials and on the fact that, although single methods for non-invasive hypoxia imaging are well established, still their complementary potential is not utilized, we designed the HIL trial. Aim of this trial is the evaluation of multimodal tumor hypoxia imaging using ^{18}F-FMISO positron emission tomography and functional MRI in 15 patients with inoperable stage III NSCLC, receiving 4D-planned intensity modulated radiation therapy. We chose for our trial NSCLC because of the major challenges that are associated with this tumor entity, i.e. the tumor motion due to changes in air content, which impedes the exact image co-registration that is however necessary for pixel-by-pixel comparisons. The HIL trial is an exploratory study. Data gained from this pilot investigation of simultaneous, serial, multimodal approaches on hypoxia visualization will form the basis for larger clinical studies characterizing in detail possible interactions between oxygen concentration and radiation outcome.

Competing interests
The authors declare that they have no competing interests.

Authors' contributions
VA, CT, JDi, PEH and JD planned, co-ordinated and conducted the study. VA, CT and MB are responsible for patient recruitment. ME, GS and BS perform CT and MRI scans and analysis. VA, CT, and MB perform planning and radiation therapy. ADS, LGS and UH perform ^{18}F-FMISO and ^{18}F-FDG investigations and analysis. Medical care and follow up is provided by VA and CT. Statistical analysis is performed by AKS. All authors read and approved the final manuscript.

Acknowledgements
This trial is financed by the Federal Ministry of Education and Research (BMBF) of Germany (Project DOT-MOBI, Nr.: 01IB08002B).

Author details
[1]Department of Radiation Oncology, University of Heidelberg, INF 400, 69120 Heidelberg, Germany. [2]Clinical Cooperation Unit Radiation Oncology, German Cancer Research Center (DKFZ), INF 280, 69120 Heidelberg, Germany. [3]Department of Radiology, German Cancer Research Center (DKFZ), INF 280, 69120 Heidelberg, Germany. [4]Quantitative Imaging-based Disease Characterization, German Cancer Research Center (DKFZ), INF 280, 69120 Heidelberg, Germany. [5]Clinical Cooperation Unit Nuclear Medicine, German Cancer Research Center (DKFZ), INF 280, 69120 Heidelberg, Germany. [6]Department for Biostatistics, German Cancer Research Center (DKFZ), INF 280, 69120 Heidelberg, Germany. [7]Department of Nuclear Medicine, University of Heidelberg, INF 400, 69120 Heidelberg, Germany.

Received: 10 July 2012 Accepted: 11 September 2012
Published: 14 September 2012

References
1. Askoxylakis V, Thieke C, Pleger ST, Most P, Tanner J, Lindel K, Katus HA, Debus J, Bischof M: **Long-term survival of cancer patients compared to heart failure and stroke: a systematic review.** *BMC Cancer* 2010, **10:**105.
2. Willner J, Baier K, Caragiani E, Tschammler A, Flentje M: **Dose, volume, and tumor control prediction in primary radiotherapy of non-small-cell lung cancer.** *Int J Radiat Oncol Biol Phys* 2002, **52:**382–389.
3. Anderson CS, Curran WJ: **Combined modality therapy for stage III non-small-cell lung cancer.** *Semin Radiat Oncol* 2010, **20:**186–191.
4. Lee CB, Stinchcombe TE, Moore DT, Morris DE, Hayes DN, Halle J, Rosenman JG, Rivera MP, Socinski MA: **Late complications of high dose (>/=66 Gy) thoracic conformal radiation therapy in combined modality trials in unresectable stage III non-small cell lung cancer.** *J Thorac Oncol* 2009, **4:**74–79.
5. Christian JA, Bedford JL, Webb S, Brada M: **Comparison of inverse-planned three-dimensional conformal radiotherapy and intensity-modulated radiotherapy for non-small-cell lung cancer.** *Int J Radiat Oncol Biol Phys* 2007, **67:**735–741.
6. De Ruysscher D, Nestle U, Jeraj R, Macmanus M: **PET scans in radiotherapy planning of lung cancer.** *Lung Cancer* 2012, **75**(2):141–145.
7. Yaremko BP, Guerrero TM, Noyola-Martinez J, Guerra R, Lege DG, Nguyen LT, Balter PA, Cox JD, Komaki R: **Reduction of normal lung irradiation in locally advanced non-small-cell lung patients, using ventilation images for functional avoidance.** *Int J Radiat Oncol Biol Phys* 2007, **68:**562–571.
8. Ford EC, Mageras GS, Yorke E, Ling CC: **Respiration-correlated spiral CT: a method of measuring respiratory-induced anatomic motion for radiation treatment planning.** *Med Phys* 2003, **30:**88–97.
9. Guerrero T, Sanders K, Castillo E, Zhang Y, Bidaut L, Pan T, Komaki R: **Dynamic ventilation imaging from four-dimensional computed tomography.** *Phys Med Biol* 2006, **51:**777–791.
10. Fujimoto K: **Usefulness of contrast-enhanced magnetic resonance imaging for evaluating solitary pulmonary nodules.** *Cancer imaging* 2008, **3:**36–44.
11. Henzler T, Schmid-Bindert G, Schoenberg SO, Fink C: **Diffusion and perfusion MRI of the lung and mediastinum.** *Eur J Radiol* 2010, **76:**329–336.

12. Demir R, Naschberger L, Demir I, Melling N, Dimmler A, Papadopoulus T, Sturzl M, Klein P, Hohenberger W: **Hypoxia generates a more invasive phenotype of tumour cells: An *in vivo* experimental setup based on the chorioallantoic membrane.** *Pathol Oncol Res* 2009, **15:**417–422.
13. Graves EE, Maity A, Le QT: **The tumor microenvironment in non-small-cell lung cancer.** *Semin Radiat Oncol* 2010, **20:**156–163.
14. Bussink J, Kaanders JH, van der Kogel AJ: **Tumor hypoxia at the micro-regional level: clinical relevance and predictive value of exogenous and endogenous hypoxic cell markers.** *Radiother Oncol* 2003, **67:**3–15.
15. Lee ST, Scott AM: **Hypoxia positron emission tomography imaging with 18f-fluoromisonidazole.** *Semin Nucl Med* 2007, **37:**451–461.
16. Zimny M, Gagel B, Dimartino E, Hamacher K, Coenen HH, Westhofen M, Eble M, Buell U, Reinarzt P: **FDG-a marker of tumour hypoxia? A comparison with [(18 F]fluoromisonidazole and pO (2)-polarography in metastatic head and neck cancer.** *Eur J Nucl Med Mol Imaging* 2006, **33:**1426–1431.
17. Thorwarth D, Eschmann SM, Holzner F, Paulsen F, Alber M: **Combined uptake of [18 F]FDG and [18 F]FMISO correlates with radiation therapy outcome in head-and-neck cancer patients.** *Radiother Oncol* 2006, **80:**151–156.
18. Eschmann SM, Paulsen F, Reimold M, Dittmann H, Welz S, Reischl G, Machulla HJ, Bares R: **Prognostic impact of hypoxia imaging with 18 F-misonidazole PET in non-small cell lung cancer and head and neck cancer before radiotherapy.** *J Nucl Med* 2005, **46:**253–260.
19. Gagel B, Reinarzt P, Demirel C, Kaiser HJ, Zimny M, Piroth M, Pinkawa M, Stanzel S, Asadpour B, Hamacher K, Coenen HH, Buell U, Eble MJ: **[18 F] fluoromisonidazole and [18 F] fluorodeoxyglucose positron emission tomography in response evaluation after chemo-/radiotherapy of non-small-cell lung cancer: a feasibility study.** *BMC Cancer* 2006, **6:**51.
20. Pacheco-Torres J, López-Larrubia P, Ballesteros P, Cerdán S: **Imaging tumor hypoxia by magnetic resonance methods.** *NMR Biomed* 2011, **24:**1–16.
21. Dimitrakopoulou-Strauss A, Hoffmann M, Bergner R, Uppenkamp M, Eisenhut M, Pan L, Haberkorn U, Strauss LG: **Prediction of short-term survival in patients with advanced nonsmall cell lung cancer following chemotherapy based on 2-deoxy-2-[F-18]fluoro-D-glucose-positron emission tomography: a feasibility study.** *Mol Imaging Biol* 2007, **9:**308–317.
22. Lemke A, Laun FB, Simon D, Stieltjes B, Schad LR: **An *in vivo* verification of the intravoxel incoherent motion effect in diffusion-weighted imaging of the abdomen.** *Magn Reson Med* 2010, **64:**1580–1585.
23. Patel J, Sigmund EE, Rusinek H, Oei M, Babb JS, Taouli B: **Diagnosis of cirrhosis with intravoxel incoherent motion diffusion MRI and dynamic contrast- enhanced MRI alone and in combination: preliminary experience.** *J Magn Reson Imaging* 2010, **31:**589–600.
24. Hintze C, Stemmer A, Bock M, Kuder TA, Risse F, Dinkel J, Prüm H, Puderbach M, Fink C, Biederer J, Kauczor HU: **A hybrid breath hold and continued respiration-triggered technique for time-resolved 3D MRI perfusion studies in lung cancer.** *Rofo* 2010, **182:**45–52.
25. Therasse P, Arbuck SG, Eisenhauer EA, Wanders J, Kaplan RS, Rubinstein L, Verweij J, Van Glabbeke M, van Oosterom AT, Christian MC, Gwyther SG, European Organization for Research and Treatment of Cancer, National Cancer Institute of the United States, National Cancer Institute of Canada: **New guidelines to evaluate the response to treatment in solid tumors.** *In J Natl Cancer Inst* 2000, **92**(3):205–216.
26. Sura S, Gupta V, Yorke E, Jackson A, Amols H, Rosenzweig KE: **Intensity modulated radiation therapy (IMRT) for inoperable non-small cell lung cancer: the Memorial Sloan-Kettering Cancer Center (MSKCC) experience.** *Radiother Oncol* 2008, **87:**17–23.
27. Jiang ZQ, Yang K, Komaki R, Wei X, Tucker SL, Zhuang Y, Martel MK, Vedam S, Balter P, Zhu G, Gomez D, Lu C, Mohan R, Cox JD, Liao Z: **Long-term clinical outcome of intensity-modulated radiotherapy for inoperable non-small-cell lung cancer: The MD Anderson experience.** *Int J Radiat Oncol Biol Phys* 2012, **83:**332–339.
28. Napadow VJ, Mai V, Bankier A, Gilbert RJ, Edelman R, Chen Q: **Determination of regional pulmonary parenchymal strain during normal respiration using spin inversion tagged magnetization MRI.** *J Magn Reson Imaging* 2001, **13:**467–474.
29. Cho H, Ackerstaff E, Carlin S, Lupu ME, Wang Y, Rizwan A, O'Donoghue J, Ling CC, Humm JZ, Zanzonico PB, Koutcher JA: **Noninvasive multimodality imaging of the tumor microenvironment: registered dynamic magnetic resonance imaging and positron emission tomography studies of a preclinical tumor model of tumor hypoxia.** *Neoplasia* 2009, **11:**247–259.
30. Jansen JF, Schöder H, Lee NY, Wang Y, Pfister DG, Fury MG, Stambuk HE, Humm JL, Koutcher JA, Shukla-Dave A: **Noninvasive assessment of tumor microenvironment using dynamic contrast-enhanced magnetic resonance imaging and 18 F-fluoromisonidazole positron emission tomography imaging in neck nodal metastases.** *Int J Radiat Oncol Biol Phys* 2010, **77:**1403–1410.
31. Dirix P, Vandecaveye V, De Keyzer F, Stroobants S, Hermans R, Nuyts S: **Dose painting in radiotherapy for head and neck squamous cell carcinoma: value of repeated functional imaging with (18)F-FDG PET, (18)F-fluoromisonidazole PET, diffusion-weighted MRI, and dynamic contrast-enhanced MRI.** *J Nucl Med* 2009, **50:**1020–1027.

doi:10.1186/1748-717X-7-157
Cite this article as: Askoxylakis *et al.*: Multimodal hypoxia imaging and intensity modulated radiation therapy for unresectable non-small-cell lung cancer: the HIL trial. *Radiation Oncology* 2012 **7**:157.

The British Journal of Radiology, 79 (2006), S79–S86

Kilovoltage CT using a linac-CT scanner combination

[1]C THIEKE, MD, PhD, [2]U MALSCH, MS, [2]W SCHLEGEL, PhD, [1]J DEBUS, MD, PhD, [1]P HUBER, MD, PhD, [2]R BENDL, PhD and [1]C THILMANN, MD, MS

[1]*Department of Radiation Oncology, University Hospital of Heidelberg and German Cancer Research Center, Heidelberg and* [2]*Department of Medical Physics, German Cancer Research Center, Heidelberg, Germany*

ABSTRACT. Modern radiotherapy techniques such as intensity modulation are capable of generating complex dose distributions whose high dose areas tightly conform to the tumour target volume, sparing critical organs even when they are located in close proximity. This potential can only be exploited to its full extent when the accumulated dose actually delivered over the complete treatment course is sufficiently close to the dose computed on the initial CT scan used for treatment planning. Exact patient repositioning is mandatory, but also other sources of error, *e.g.* changes of the patient's anatomy under therapy, should be taken into account. At the German Cancer Research Center, we use a combination of a linear accelerator and a CT scanner installed in one room and sharing the same couch. It allows the quantification and correction of interfractional variations between planning and treatment delivery. In this paper, we describe treatments of prostate, paraspinal and head and neck tumours. All patients were immobilized by customized fixation devices and treated in a stereotactic setup. For each patient, frequent CT scans were taken during the treatment course. Each scan was compared with the original planning CT using manual checks and automatic rigid matching algorithms. Depending on the individual case, the adaptation to variations was carried out offline after several fractions or in real-time between the CT scan and linac irradiation. We discuss the techniques for detecting and correcting interfractional errors and outline the procedural steps of a linac-CT scanner-supported radiation treatment course.

Received 22 August 2005
Revised 6 January 2006
Accepted 25 January 2006

DOI: 10.1259/bjr/88849490

CT has been used in radiotherapy for decades and plays a decisive role in the development of conformal radiation treatment. Computer science, physics and engineering have had a tremendous impact on radiotherapy. The most obvious progress has been achieved in treatment planning and treatment delivery. Here, we are close to the limits of what can be reached with high energy photons. Modern irradiation techniques such as stereotactic radiotherapy and intensity-modulated radiotherapy (IMRT) are capable of generating complex dose distributions whose high dose areas tightly conform to the tumour target volume. Exact repositioning of the target is mandatory to ensure that the dose actually delivered at treatment time is as close as possible to the dose computed on the initial CT scan used for treatment planning. Despite great efforts, this is the weak point of high precision radiotherapy especially in the trunk region. Available fixation devices reduce interfraction and intrafraction motion. For example, our in-house developed combination of a body cast and head mask system in a rigid stereotactic body frame ensures non-invasive patient fixation for fractionated extracranial stereotactic radiotherapy and IMRT [1]. It provides precise and reliable positioning with regard to bony structures [2]. Nevertheless, internal soft tissue structures may deviate considerably from what we expect. When treating internal targets in the body region, the target position cannot be guaranteed with external immobilization devices. No further improvement of repositioning can be achieved by more rigid fixation. Additionally, a CT examination for treatment planning is a snapshot of anatomical structures and is gathered several days before treatment. Especially in high conformal radiotherapy with dose escalation and conformal avoidance of critical structures requiring a high degree of positional accuracy, the daily position of the target needs to be confirmed before irradiation by a reliable imaging modality.

There are different approaches to image guidance aimed at the reduction of uncertainties of target position. For acquisition of 3D anatomic information in the treatment position, megavoltage CT [3] and cone beam kilovoltage CT fixed at the gantry [4] or a separate in-room CT scanner [5–7] has been tested so far. When using an in-room CT, the system consists of a linear accelerator (linac) and a conventional CT scanner connected via a conventional treatment couch. The CT scanner is mounted on rails. The obvious advantage of this system is that all components are separately established for clinical application. The accuracy has been demonstrated by Cheng and coworkers [8].

We would like to point out three particularities of the system. (1) The patient is immobilized in the usual way on the treatment couch and CT scanning is performed for confirmation of the correct isocentre and patient (target) position. By using a gantry mounted on rails, scanning is

performed without either couch or patient movement, eliminating reductions in accuracy. After performing the scan, the treatment couch is rotated to the linac side for irradiation. (2) The kilovoltage technique allows an image quality with high soft-tissue contrast. This is a requirement for detecting deviations of soft tissue targets from their position at the initial CT scan used for treatment planning, even when bony landmarks are repositioned correctly. (3) The CT data set can be used without any transformation for treatment planning and dose calculation. The basic input for radiotherapy planning systems considering tissue heterogeneities is the relationship between CT Hounsfield units and electron densities, which is determined using common CT-calibration methods. Thus the in-room CT is well suited for target point verification, correction of setup errors and interfraction target deviations due to organ motion, as well as for recalculation of the dose actually given. The simplest correction is to correct the target point without changing the treatment plan. Beyond this, systematic changes of the patient's anatomy under therapy (*e.g.* weight loss, tumour mass reduction) can be considered and, if necessary, the radiation treatment plan can be re-optimized until the next fraction. The highest level of adaptation achievable with a linac-CT combination is the adaptation/optimization of the treatment plan to the actual given situation, *i.e.* between the CT scan and the linac irradiation. Since a CT scan is not possible in treatment position, the described system cannot be used to detect intrafraction motion.

The purpose of this study is to demonstrate the potential of an integrated linac-CT scanner system for different tumour sites and to derive a workflow which is reasonable for clinical routine with target point correction and re-optimization of the dose distribution.

Materials and methods

Treatments at DKFZ with the linac-CT scanner Siemens Primatom

Since October 2002, the Siemens Primatom (Siemens OCS, Concorde, CA) has been in clinical use at the German Cancer Research Center (DKFZ) in Heidelberg, Germany. It consists of a 6 MV Siemens Primus linear accelerator and a single-slice spiral CT scanner Siemens Emotion, which are set 90° apart and share the same couch (Figure 1). Depending on the treatment room, a 180° design can also be used [6, 8]. Almost all fractionated treatments at DKFZ are carried out as IMRT. The indicated treatments are prostate cancer, head and neck cancer, paraspinal tumours, base of skull tumours, breast cancer and, more recently, pleural mesothelioma, oesophageal cancer and pancreatic cancer. Radiosurgery is used for arteriovenous malformations, lung tumours and liver metastases.

Patient fixation

Every patient at DKFZ is treated in an individually customized fixation device. For fractionated treatment of intracranial targets, a head mask made of Scotch

Figure 1. Treatment room with the Siemens Primatom at DKFZ Heidelberg. The linear accelerator and the CT scanner on rails share the same couch, which is rotated by 90° to switch between CT scanning and treatment position.

therefore cast is produced [9]. For intracranial radiosurgery we use either an invasive ring or the Scotch (3M, St Paul, MN) cast mask. For extracranial targets, we use either a wrap-around body cast [2] made from the same material as the head mask or a vacuum pillow [2]. Both extracranial fixation devices are complemented by a head mask to eliminate head rotations, which might translate into movements of the spine, and for single-fractionated treatment of lung and liver an additional abdominal pressure plate reduces the respiratory motion.

Treatment

For all single-fractionated treatments, a control CT scan is performed directly prior to irradiation. By comparing the control CT scan to the CT scan made for treatment planning, any translational displacement is detected and the target point corrected accordingly.

For fractionated treatment of intracranial targets, the repositioning accuracy of the patient's head with the customized head mask was found to be better than 2 mm in all three dimensions [9]. We usually therefore include a 2 mm safety margin in the planning target volume (PTV), and apart from the verification of the target point on the first fraction, we do not perform further control CT scans.

Fractionated treatment of extracranial targets is accompanied by frequent CT control scans during the treatment course, since even with a rigid fixation significant interfractional discrepancies are observed (see results below). The scan frequency depends on the individual case and is between once weekly for unproblematic cases, up to daily CT scans for patients with large repositioning errors and critical proximity of target structures to organs at risk.

Analysis of CT scans

All CT scans generated with the Siemens Primatom are performed with stereotactic localizers attached to the

fixation frame in exactly the same way as they were attached in the treatment planning CT scan. This defines a frame-based coordinate system independent of the patient's actual position, which is a prerequisite for any further analysis. For the first fraction, lead ball bearings (BB) were additionally put onto the laser adjustment lines for target point verification, so no further portal imaging was necessary.

When we started using the Siemens Primatom, the correct positioning of the patient could only be verified by manually highlighting representative anatomical landmarks on selected CT slices. For example, about three bony landmarks on the isocentre plane were predefined on the planning CT in the treatment planning system and then located on the control CT using the CT scanner console. The average coordinate difference between the scans then gave an estimation of the average displacement error. Although technically feasible, this procedure was quite time consuming and movements visible on only some CT slices could be missed.

We therefore developed a new workflow to both reduce the time requirements and improve the accuracy of the analysis, and integrated it into our in-house developed radiotherapy software environment. The control CT scan is transferred via a network to our treatment planning system VIRTUOS. Inside the treatment planning system, the localizers of the control CT and the planning CT are stereotactically correlated, making the coordinates in both cubes directly comparable. The region of the control CT cube containing the target volume is then automatically matched onto the planning CT. The transformation determined in this step immediately gives the current displacement error. At the moment, we use two rigid matching algorithms: Rigid correlation matching (RCM) based on bony anatomy considers only translational movements and provides the target point correction vector, and mutual information matching (MIM) for bony and soft structures considers translational and rotational movements. Both matching algorithms derive the transformation vector T between planning volume A and transformed control volume B_T by searching for maximal similarity in the region of interest Ω, measured by the correlation coefficient CC and the mutual information MI, respectively.

The correlation coefficient between A and B_T is calculated by:

$$CC(A,B_T) = \sum_{\vec{x}_i \in \Omega_{A,B}} \left(A(\vec{x}_i) - \overline{A}\right) * \left(B_T(\vec{x}_i) - \overline{B_T}\right) \quad (1)$$

whereby $\overline{A}$ is the mean value of A and $\overline{B_T}$ the mean value of B_T.

A three-dimensional Fourier transformation of A and B_T into the frequency space using a fast Fourier transformation (FFT) transforms the convolution in Equation (1) into a simple multiplication. After inverse transformation, we obtain the correlation volume that holds the CC values for all possible 3D translation vectors, and the global maximum can easily be found. Since we use discrete Fourier transformation, the precision is restricted to the voxel dimension. The RCM analysis of a typical CT dataset (512×512 points, 30 slices) by a standard PC takes less than 30 s. RCM matching was performed for the complete region around the target volume and separately for the upper und lower quarter. Significant differences between the three results indicate that the deviation is more complex than a pure translation.

The similarity between volume A and volume B_T measured by mutual information is given by:

$$MI(A,B_T) = \sum_a \sum_b p_{AB_T}(a,b) \cdot \log \frac{p_{AB_T}(a,b)}{p_A(a) \cdot p_{B_T}(b)} \quad (2)$$

where a and b are the Hounsfield units of A and B, respectively, and $p_A(a)$ the probability density of a and $p_{AB\ T}(a,b)$ the combined density of A and B_T [10, 11]. We do not use all points of A and B to determine each p, but rather a sample of approximately 200 000 values, which is about 2.5% of the complete dataset. This significantly speeds up the calculation without deterioration in the result. In an iterative optimization procedure, B_T is translated and rotated until MI reaches a maximum. Therefore an optimization of six variables (t_x, t_y, t_z, and r_x, r_y, r_z) must be performed. In our implementation, we use Powell's approach [12] to determine the transformation where MI reaches its maximum. This approach provides subvoxel precision. The MIM analysis of a typical CT dataset (512×512 points, 30 slices) is calculated by a standard PC in about 3 min.

RCM is significantly faster than MIM, always finds the global optimum and gives a transformation that can be corrected for by a simple shift of the target point. We perform RCM matching of the upper and lower quarter of the region of interest and the MIM matching only to check for deviations that cannot be corrected for by translation only. In any case, the user has to visually check that the resulting match is correct. With standard tools, such as red-green overlay and checkerboard provided by VIRTUOS, this manual check usually takes less than 1 min.

Adaptive radiotherapy

In adaptive radiotherapy, deviations of patient repositioning and anatomy from the initial planning CT scan are detected and, if necessary, corrected for. This is in contrast to conventional static radiotherapy where the plan is based on one single CT scan and delivered to the patient throughout all fractions. Different levels of adaptation can be defined:

In level 0, the treatment plan is based on several CT scans rather than a single one, and the information about statistical movements of the target and organs at risk are integrated into the treatment plan. This can be accomplished by defining patient-specific or at least site-specific safety margins [13] or by including statistical methods into the inverse optimization process [14, 15].

Level 1 corrects for errors offline, *i.e.* the correction is done after several CT scans are gathered. Systematic interfractional errors can be detected and corrected. If the main deviation is a translation, usually it is sufficient to shift the target point and leave the plan unchanged (level 1A). If the error is more complex, the contours have to be

adapted to the new geometry, and a new plan has to be generated by re-running the optimization of the inverse planning program (level 1B).

Level 2 uses the same methods as level 1, but here the correction is placed in between the CT scan and the directly-following linac irradiation. By analogy with level 1 definitions, level 2A stands for shifting the target point and 2B for generating a new plan. This way not only the systematic error, but also daily random interfractional errors can be corrected. Since the patient remains in the fixation device during the adaptation procedure, the time requirements for this step are more critical than for the lower adaptation levels.

Level 3 eventually also takes into account intrafractional errors. This task requires an imaging device operating during the irradiation itself and cannot be accomplished by a linac-CT scanner combination.

In the following discussion we will focus on our experiences with Primatom-based radiotherapy for prostate, paraspinal and head and neck cases. However, the general aspects and conclusion apply to other indications as well.

Results and discussion

Dose

The additional dose delivered to the patient by frequent CT scans should be as low as possible. Since we do not need the best possible image quality for localization, we use a low mAs product (which introduces some noise to the image) and only scan slices containing the target volume plus approximately 2 cm in cranial and caudal direction. This way, the measured CT dose *e.g.* per prostate scan was 0.003 Gy at the isocentre and 0.0053 Gy at 1 cm depth. Considering the overall benefit of higher treatment accuracy, we do not find this dose clinically relevant.

Prostate cancer

Patients with prostate cancer treated at our institution are immobilized by a wrap-around body cast and a head mask. Usually they receive weekly control CT scans during the treatment course. Figure 2 shows the displacements of the bony structures around the prostate in the control scans relative to their position in the planning CT scan for 10 prostate patients (P1–P10) as they were calculated by rigid correlation matching. The symbols (▲, ●, ■) indicate the mean displacement values for each coordinate in x, y and z direction, with the range represented by the standard deviation of all values observed. Checks with RCM for the upper and lower quarter of the target volume separately showed differences below 1 mm, and checks with mutual information matching confirmed that the rotational error was negligibly small with only around 0.5° (maximum 1°) for all three rotational axes. As can be seen in Figure 2, even without corrections of the target point the repositioning accuracy of the bony anatomy was very good, with displacements below 3 mm in almost all cases. The correct positioning of the bony anatomy alone already leads to good repositioning of the prostate itself, as is indicated by the results of Beard et al [16] who reported deviations of the prostate above 1 cm in 3% of all cases after bony matching, whereas Wong et al [7] reported deviations above 1 cm in 15% of all cases without bony matching. Manually checking the soft tissues also showed that in our data the displacements of the prostate itself were bigger than the bony variations. In a separate study, the positions of the prostate, bladder and rectum were statistically analysed and taken into account by adding a margin to the gross tumour volume (GTV) and clinical target volume (CTV) to obtain the planning target volume (PTV) (adaptation level 0) [13, 17]. To reduce these margins and further improve the accuracy of prostate treatments, we are currently working on matching algorithms that will enable the automatic correction of interfractional displacements of the prostate itself on adaptation level 2. Deformation of the shape of the prostate and seminal vesicles is reported to be small relative to organ motion [18], so simply shifting the target point (level 2A) will probably be sufficient.

Paraspinal tumours

Paraspinal tumours of different histological origins are challenging because of their close proximity to the spinal cord as a critical organ at risk. For treatment we immobilize these patients by a wrap-around body cast and a head mask and perform regular control CT scans. Since the tumours are very closely related to, or even inside the bony spine, the evaluation of bony landmarks is an exact measure of the tumour position. Figure 3 shows the accuracy and precision of repositioning for seven patients with paraspinal tumours treated at our institution. Also for the paraspinal tumours, rotational errors were negligible as we verified visually, by piecewise RCM and by MIM. The overall repositioning accuracy was good. The accuracy in ventro-dorsal (y: ●) direction was equal to or better than 5 mm. In lateral (x: ▲) and craniocaudal (z: ■) direction the typical displacement was around 3 mm. However, in these directions maximal errors above 10 mm were observed. Lateral displacements especially can become critical for these patients, as it is exemplarily shown in Figure 4 for the paraspinal case P7 (a patient with a chordoma of the lumbal spine). The left panel shows the planning CT scan, the right panel shows the stereotactically matched control CT scan of fraction 20. Note the slightly lower image quality of the control CT scan due to the low mAs product we used for scanning. The contours of target, boost and spinal cord are based on the planning CT scan and, by comparing the relation of these contours to the underlying anatomy of the control scan, one immediately sees that the lateral displacement shifts the spinal cord into the high dose area intended for the boost, and that parts of the boost volume are moving out of the high dose area.

Paraspinal targets are not significantly affected by intrafractional organ motion, *e.g.* due to breathing [19], did not show a relevant rotational component and did not change their shape during the treatment course. Therefore we could correct for setup errors by simply shifting the target point. As can be seen in Figure 3, the interfractional error had a pronounced systematic

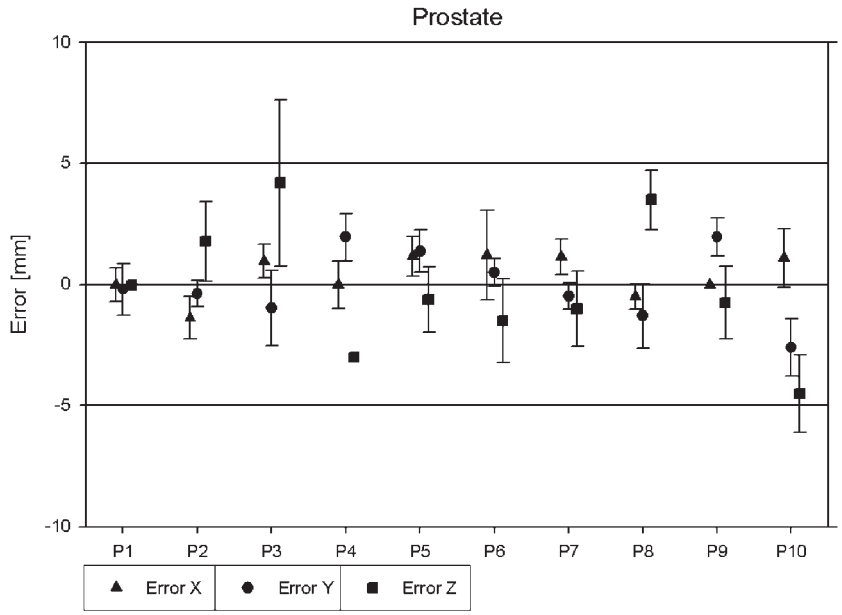

Figure 2. Interfractional setup errors in *x*, *y*, *z* direction of 10 prostate patients, based on bony anatomy calculated by the rigid correlation matcher. For each patient, the mean translational error and its standard deviation is plotted.

component. When several (3–4) CT scans revealed such a systematic error, we corrected the target point accordingly and performed further control CT scans (adaption level 1A). Two cases had a highly critical proximity of tumour to the spinal cord (*e.g.* patient 7 in Figure 4) and showed a stronger random error component, so we performed daily CT scans and corrected the target point directly prior to irradiation (level 2A).

Head and neck tumours

The target volume for head and neck tumours regularly includes the base of skull and extends to the upper thoracic aperture. The patients are fixated with a head mask and a vacuum pillow. The cranial part inside the head mask is very accurately repositioned during the whole treatment course. In contrast, the lower extracranial part shows more variations. The result is a complex deformation of the target volume that cannot be described by a translation and cannot be corrected easily by shifting the target point without changing the treatment plan.

Here we show an exemplary case of a patient who was treated for teratocarcinosarcoma of the paranasal sinuses. During the treatment course frequent control CT scans were performed, and while the intracranial part was accurately positioned throughout all fractions, the lower, extracranial part of the body was systematically shifted approximately 1.5 cm along the *y*-axis from the middle of the treatment course onwards, see Figure 5 comparing the planning CT with the control CT of fraction 20. Note that the contours in Figure 5 refer to the planning CT and do not fit to the anatomical situation at

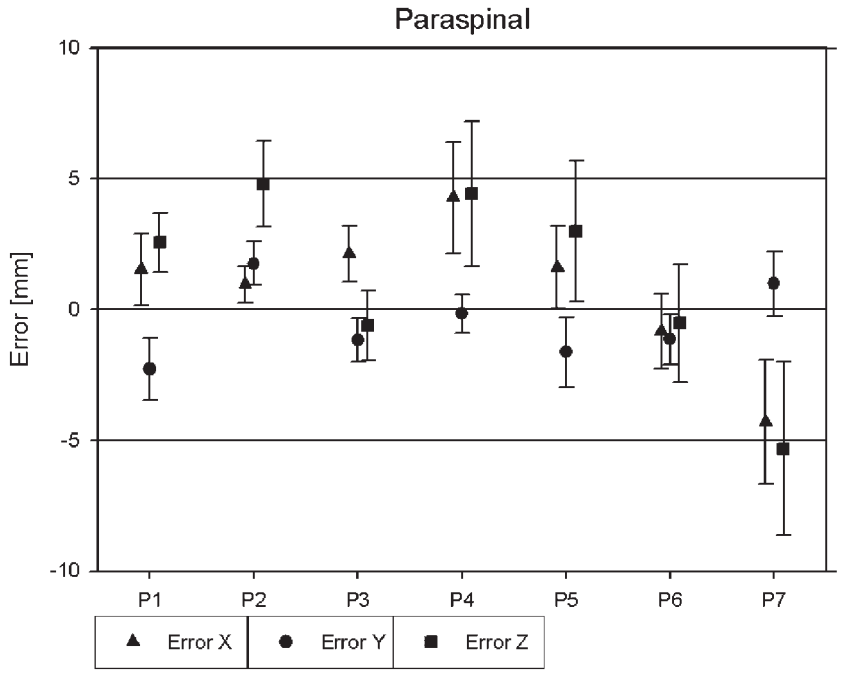

Figure 3. Interfractional setup errors in *x*, *y*, *z* direction of seven paraspinal patients, based on bony anatomy calculated by the rigid correlation matcher. For each patient, the mean translational error and its standard deviation is plotted.

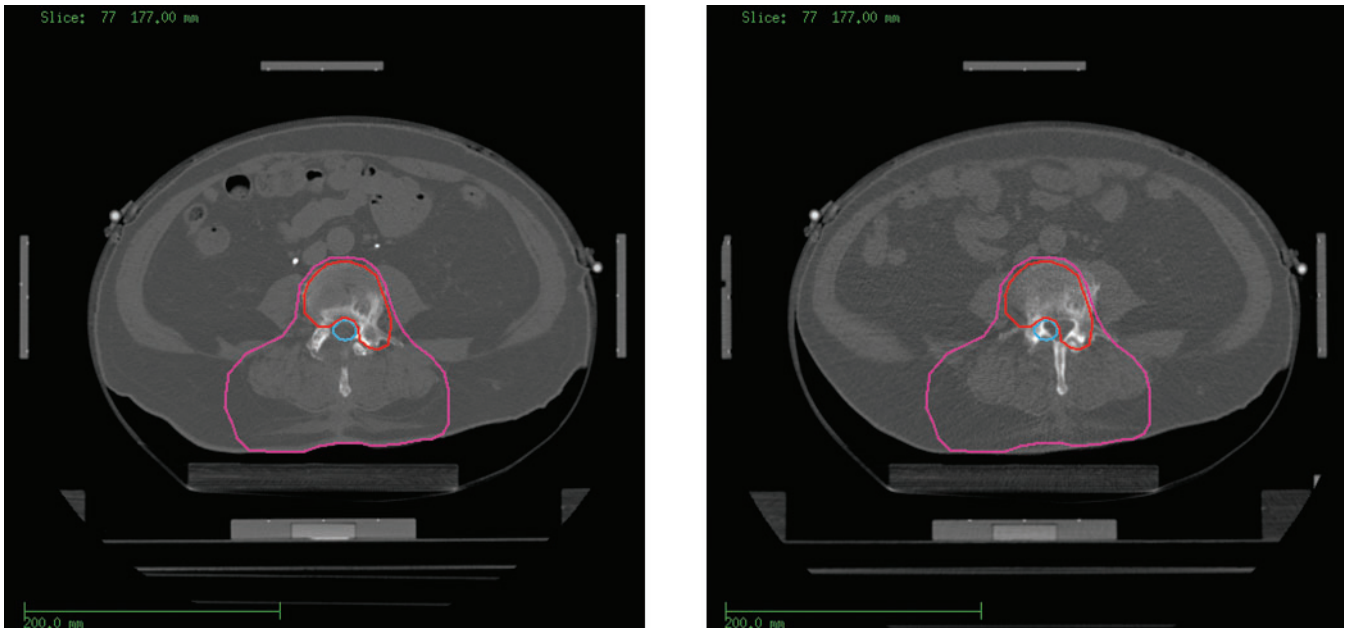

Figure 4. Planning CT scan and control CT scan at fraction 20 of the paraspinal case #7. The contours of the target volume, the boost volume and the spinal cord are also shown.

fraction 20. We therefore re-drew the organ contours for fraction 20 and re-calculated the dose of the original plan on the CT of fraction 20. The results are shown in the form of dose–volume histograms (DVHs) in Figure 6. Figure 6a is the original plan based on the planning CT scan and Figure 6b is the same plan applied to the situation at fraction 20 with updated organ contours. One can see that especially the coverage of the lower target volume has significantly deteriorated. The shift of the extracranial part of the body was systematically seen on three successive control CTs, so we decided to adapt the plan to the new geometry by re-running the optimization in our inverse planning program (KonRad by Siemens OCS) for the control CT scan with the new contours, but without changing the original setting of dose constraints and weighting factors. The new plan was calculated in approximately 2 min, and as shown in Figure 6c the adapted plan resembles the original plan much better than the uncorrected one. Because the contours had to be re-drawn manually, at the moment this procedure takes too much time to fit in between the CT scan and the directly-following irradiation to correct for random interfractional setup errors. However, it allows for a very good adaptation to complex systematic variations occurring during the treatment course (adaptation level 1B).

General aspects

The Siemens Primatom is a combination of a linear accelerator and a CT scanner in one room, sharing the same couch. It is built upon standard components which are clinically proven and which work reliably. The patient remains immobilized between the CT scan and the following irradiation. At the moment, we use the Primatom regularly for all patients with extracranial targets. Currently, correction of detected errors in clinical practice is by target point correction either after several CT scans or for each fraction separately (level 1A and 2A) and plan re-optimization for systematic, complex setup errors (level 1B). Real time plan re-optimization (level 2B) is not practical at the moment because of the time constraints.

Patients with paraspinal tumours can greatly benefit from the higher accuracy of the treatment. Target point correction seems sufficient; elastic deformation or plan re-optimization was not necessary for the patients we treated. For prostate patients, the bony anatomy is already quite precisely repositioned due to our rigid immobilization device. Here we expect further improvements by elastic matching algorithms that automatically detect the position of the prostate itself (based on Primatom CT scans) and adapt the plan either by target point correction or re-optimization. Also, for patients with head and neck tumours the quality of the radiotherapy could be significantly improved. For these cases, plan re-optimization appeared to be more important than for other tumour sites due to the complex nature of the interfractional deformations.

The linac-CT scanner combination already meets all hardware requirements to completely eliminate interfractional setup errors from the treatment course. However, a fast and robust workflow is necessary for widespread use in clinical practice, and to accomplish this further development of algorithms and software tools (*e.g.* automatic elastic matching) is needed. Real-time plan adaptation to elastic deformations in particular is under current investigation [20] and not in clinical practice yet.

Concerning the documentation of an adapted radiation treatment course, the most desirable final record would be a treatment plan where the doses to each volume element delivered throughout the course are superimposed, resulting in concise dose statistics for each structure and a single DVH for the complete

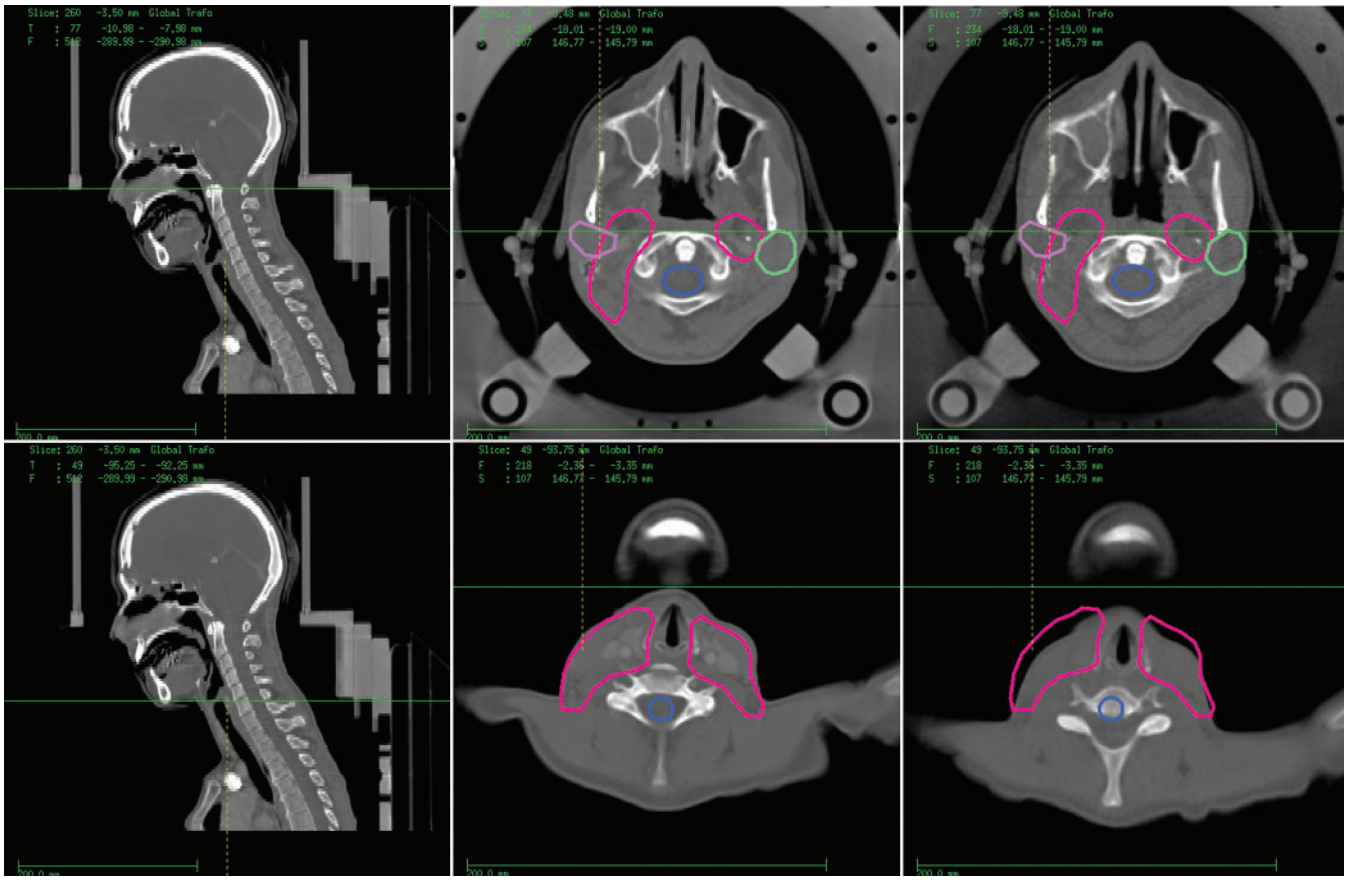

Figure 5. Exemplary head and neck case – comparison of planning CT and control CT at fraction 20. In the first row the good repositioning in the upper part of the target can be seen, and the second row shows the error of approximately 1.5 cm along the *y*-axis in the lower part of the target volume.

treatment. However, this requires the tracking of each voxel throughout all CT scans. Simply averaging the DVHs of the single fractions to obtain a final DVH would lead to erroneous results since, in a DVH, the spatial information is lost. Techniques for tracking the voxels are under current development; at the moment, each modified (adapted) treatment plan is documented separately (as in Figure 6a,c).

Our patient immobilization device with customized wrap-around body casts alone leads to quite high repositioning accuracy, but is also quite labour and time intensive to build. When using adaptive radiotherapy strategies, the fixation can probably be made less sophisticated, lowering the overall workload and further strengthening the role of a combined imaging/treatment device such as the linac-CT scanner combination.

Conclusions

The linac-CT scanner combination is a device for adaptive radiotherapy that delivers all information necessary to eliminate interfractional setup errors from a fractionated treatment course. Currently available matching algorithms

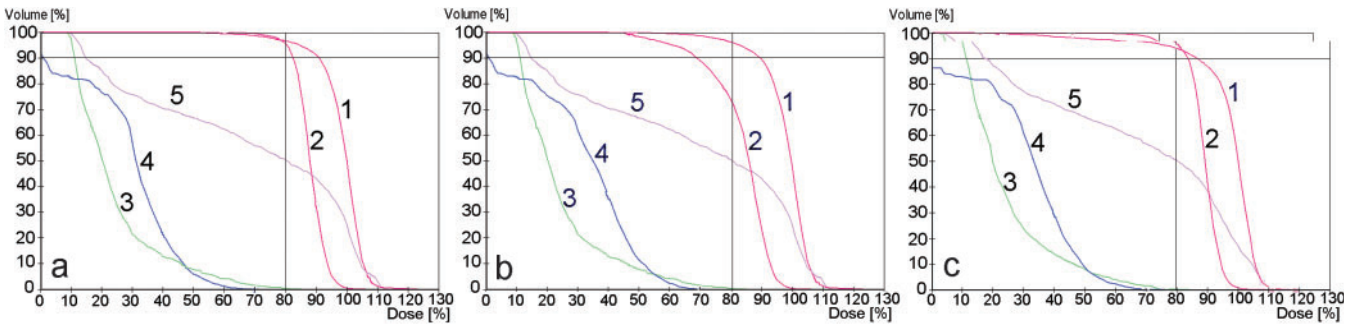

Figure 6. Same case as in Figure 5. Dose–volume histograms of (a) original plan, applied to planning CT, (b) original plan, applied to fraction 20 with updated contours and (c) re-optimized plan. For better comparison, the 80% dose/90% volume point is highlighted. The structures are 1-upper target volume, 2-lower target volume, 3-left parotid gland, 4-spinal cord, 5-right parotid gland.

and software components make it well suited for real-time and off-line target point corrections, and for off-line re-optimization. Further investigation needs to be carried out until it can be used clinically for real-time re-optimization. In principle the device is not suited for adaptation to intrafractional variations.

References

1. Lohr F, et al. Noninvasive patient fixation for extracranial stereotactic radiotherapy. Int J Radiat Oncol Biol Phys 1999;45:521–7.
2. Herfarth KK, et al. Extracranial stereotactic radiation therapy: set-up accuracy of patients treated for liver metastases. Int J Radiat Oncol Biol Phys 2000;46:329–35.
3. Groh BA, Siewerdsen JH, Drake DG, Wong JW, Jaffray DA. A performance comparison of flat-panel imager-based MV and kV cone-beam CT. Med Phys 2002;29:967–75.
4. Jaffray DA, Siewerdsen JH, Wong JW, Martinez AA. Flat-panel cone-beam computed tomography for image-guided radiation therapy. Int J Radiat Oncol Biol Phys 2002;53:1337–49.
5. Uematsu M, et al. A dual computed tomography linear accelerator unit for stereotactic radiation therapy: a new approach without cranially fixated stereotactic frames. Int J Radiat Oncol Biol Phys 1996;35:587–92.
6. Kuriyama K, et al. A new irradiation unit constructed of self-moving gantry-CT and linac. Int J Radiat Oncol Biol Phys 2003;55:428–35.
7. Wong JR, et al. Image-guided radiotherapy for prostate cancer by CT-linear accelerator combination: prostate movements and dosimetric considerations. Int J Radiat Oncol Biol Phys 2005;61:561–9.
8. Cheng CW, et al. Commissioning and clinical implementation of a sliding gantry CT scanner installed in an existing treatment room and early clinical experience for precise tumor localization. Am J Clin Oncol 2003;26:e28–e36.
9. Karger CP, Jakel O, Debus J, Kuhn S, Hartmann GH. Three-dimensional accuracy and interfractional reproducibility of patient fixation and positioning using a stereotactic head mask system. Int J Radiat Oncol Biol Phys 2001;49:1493–504.
10. Collignon A, et al. Automated multi-modality image registration based on information theory. Information Processing in Medical Imaging 1995;262–74.
11. Viola P, Wells W, III. Alignment by maximization of mutual information. Int J Computer Vision 1997;137–54.
12. Press WH, Teukolsky SA, Vetterling WT, Flannery BP. Numerical recipes in C. Cambridge University Press, 1995.
13. Didinger B, Schulz-Ertner D, Wannenmacher M, Debus J. [Modern techniques in the radiotherapy of prostate cancer. Non-surgical treatment options for localized stages]. Radiologe 2003;43:448–54.
14. Unkelbach J, Oelfke U. Incorporating organ movements in inverse planning: assessing dose uncertainties by Bayesian inference. Phys Med Biol 2005;50:121–39.
15. Birkner M, Yan D, Alber M, Liang J, Nusslin F. Adapting inverse planning to patient and organ geometrical variation: algorithm and implementation. Med Phys 2003;30:2822–31.
16. Beard CJ, et al. Analysis of prostate and seminal vesicle motion: implications for treatment planning. Int J Radiat Oncol Biol Phys 1996;34:451–8.
17. Didinger B. Berücksichtigung von interfraktionellen Bewegungen bei der Präzisionsbestrahlung des Prostatakarzinoms - Konsequenzen für Zielvolumina und Dosis-Volumen-Histogramm. 2003. M.D. Thesis, University of Heidelberg, Germany.
18. Deurloo KE, et al. Quantification of shape variation of prostate and seminal vesicles during external beam radiotherapy. Int J Radiat Oncol Biol Phys 2005;61:228–38.
19. Shiu AS, et al. Near simultaneous computed tomography image-guided stereotactic spinal radiotherapy: an emerging paradigm for achieving true stereotaxy. Int J Radiat Oncol Biol Phys 2003;57:605–13.
20. Mohan R, et al. Use of deformed intensity distributions for on-line modification of image-guided IMRT to account for interfractional anatomic changes. Int J Radiat Oncol Biol Phys 2005;61:1258–66.

Int. J. Radiation Oncology Biol. Phys., Vol. 75, No. 3, pp. 933–940, 2009

0360-3016/09/$–see front matter

ELSEVIER

doi:10.1016/j.ijrobp.2009.04.010

PHYSICS CONTRIBUTION

QUANTITATIVE ASSESSMENT OF IMAGE-GUIDED RADIOTHERAPY FOR PARASPINAL TUMORS

Eva M. Stoiber, M.D.,* Gerhard Lechsel, Ph.D.,† Kristina Giske, M.Sc.,† Marc W. Muenter, M.D.,* Angelika Hoess, M.S.,† Rolf Bendl, Ph.D.,†‡ Juergen Debus, M.D., Ph.D.,* Peter E. Huber, M.D., Ph.D.,* and Christian Thieke, M.D., Ph.D.*

*Department of Radiation Oncology, German Cancer Research Center and University Clinic Heidelberg, Heidelberg, Germany; †Division of Medical Physics in Radiation Oncology, German Cancer Research Center, Heidelberg, Germany; and ‡Department of Medical Informatics, Heilbronn University, Heilbronn, Germany

Purpose: To evaluate stereotactic positioning uncertainties of patients with paraspinal tumors treated with fractionated intensity-modulated radiotherapy; and to determine whether target-point correction via rigid registration is sufficient for daily patient positioning.

Patients and Methods: Forty-five patients with tumors at the cervical, thoracic, and lumbar spine received regular control computed-tomography (CT) scans using an in-room CT scanner. All patients were immobilized with the combination of Scotch cast torso and head masks. The positioning was evaluated regarding translational and rotational errors by applying a rigid registration algorithm based on mutual information. The registration box was fitted to the target volume for optimal registration in the high-dose area. To evaluate the suitability of the rigid registration result for correcting the target volume position we subsequently registered three small subsections of the upper, middle, and lower target volume. The resulting residual deviations reflect the extent of the elastic deformations, which cannot be covered by the rigid-body registration procedure.

Results: A total of 321 control CT scans were evaluated. The rotational errors were negligible. Translational errors were smallest for cervical tumors (-0.1 ± 1.1, 0.3 ± 0.8, and 0.1 ± 0.9 mm along left–right, anterior–posterior, and superior–inferior axes), followed by thoracic (0.8 ± 1.1, 0.3 ± 0.8, and 1.1 ± 1.3 mm) and lumbar tumors (-0.7 ± 1.3, 0.0 ± 0.9, and 0.5 ± 1.6 mm). The residual deviations of the three subsections were <1 mm.

Conclusions: The applied stereotactic patient setup resulted in small rotational errors. However, considerable translational positioning errors may occur; thus, on the basis of these data daily control CT scans are recommended. Rigid transformation is adequate for correcting the target volume position.

Paraspinal tumors, Rigid registration, IMRT, IGRT.

INTRODUCTION

Both primary and metastatic paraspinal tumors pose a critical challenge for radiotherapy. Overdosage to the spinal cord as the most important critical structure might result in sensitive and/or motoric deficiencies up to para-/tetraplegia. On the other hand, sufficient dose must be brought to the tumor because failure in local control can have similar adverse consequences. The requirements of applying a high dose to the tumor while sparing an adjacent critical structure make paraspinal tumors a prototypic example in which ultra-precise dose application must be achieved. The importance of extracranial stereotaxy (1–3) and intensity modulation (4–6) especially for radiotherapy of paraspinal tumors is widely accepted. What is not as clear is the best procedure for patient fixation and image guidance. Different approaches and protocols are used, depending on in-house standards and existing equipment. The main sources of errors to address in this context are inter- and intrafractional variations. For few patient fixation devices the minor importance of intrafractional motion was already shown in studies with pre- and posttreatment computed tomography (CT) scans (7, 8).

To compensate for patient motion during fractionated radiotherapy several strategies are possible. The most expensive would be regular replanning based on continuously acquired control CT scans. However, frequent replanning is considered too time-consuming to be performed in a daily clinical routine. Easier adaptation strategies can be selected if the observed patient and internal structure motions are homogenous and uniformly directed. One of these strategies is a simple target-point correction realized by movements of the treatment table. It has to be considered, however, that the vertebral column *per se* is a flexible structure, and therefore

Reprint requests to: Eva M. Stoiber, M.D., Department of Radiation Oncology, German Cancer Research Center, INF 280, 69120 Heidelberg, Germany. Tel: (+49) 6221-42-2587; Fax: (+49) 6221-42-2514; E-mail: e.stoiber@dkfz.de

P.E.H. and C.T. are co-senior authors.

Conflict of interest: none.

Received Feb 16, 2009, and in revised form March 4, 2009. Accepted for publication April 3, 2009.

elastic deformations of the spine and target volume are possible. To avoid those deformations we use customized torso-mask fixation at the German *Cancer* Research Center, but even with rigid fixation patient and organ motions might occur.

The aim of this study was to justify the suitability of the target-point correction when treating paraspinal tumors with appropriate patient fixation. We present the method we have used to ensure that for our patient fixation internal structure motions are small and uniformly directed. We additionally describe the treatment procedure and the stereotactic setup accuracy achieved.

PATIENTS AND METHODS

Patient characteristics

In total, 82 patients with paraspinal tumors were treated with image-guided intensity-modulated radiotherapy at the German *Cancer* Research Center between 2002 and 2006. Thirty-seven of these patients were excluded from the positioning analysis because they did not receive full-course radiotherapy or showed major artefacts due to metal implants on the kilovoltage CTs. The remaining 45 patients were analyzed in this study; of these, 22 also underwent surgery with orthopedic implants for stabilization but showed only minor artefacts on the images. With respect to tumor localization, 11 patients had cervical, 21 thoracic, and 13 lumbar paraspinal tumors. Thirty-seven patients were treated for primary neoplasms, predominantly chordomas. The remaining 8 patients were treated for spinal metastases; 3 of them had prior radiation to the same treatment site.

Treatment device

The patients were treated with a 6-MV linear accelerator combined with an in-room CT scanner sharing the same couch (Primatom; Siemens OCS, Malvern, PA). The CT scanner is a diagnostic single-slice spiral scanner on rails arranged perpendicular to the linear accelerator gantry axis. After receiving a CT scan, the patient can be brought into treatment position without getting up, by rotating the couch around 90°.

Patient fixation

Every patient was immobilized with an individually customized fixation device. It consists of a wrap-around body cast made of Scotch cast around the upper or lower trunk (depending on tumor localization) complemented by an individual Scotch cast head mask to eliminate head rotations, which otherwise might lead to movements of the spine (9). The fabrication process takes a total of 3 days. Examples of patient fixation are shown in Fig. 1.

Treatment planning and delivery

Treatment was carried out using intensity-modulated radiotherapy for optimal sparing of the organs at risk, most importantly the spinal cord. The target volume surrounded the spinal cord or cauda equina completely or at least partially in all patients. For better delineation of the spinal cord, magnetic resonance scans were used in addition to the planning CT scan. Treatment plans were generated using the in-house treatment planning system VIRTUOS (10) and the inverse planning tool KonRad (Siemens OCS).

The patients were positioned using a stereotactic body frame for exact target-point localization. The stereotactic body frame was attached for image acquisition on the first day of treatment and for all following control CT scans. With these localizers it is possible to automatically correlate each control CT with the corresponding planning CT in our treatment planning system. Treatment was carried out using a step-and-shoot technique with a multileaf collimator with 10-mm leaf width in the isocenter plane. The total dose was delivered in 15–33 fractions per patient (median, 30 fractions per patient). The prescribed doses reached from 30.6 Gy to 68.2 Gy; the lower doses were prescribed for patients with relevant prior irradiation.

Control CT scan procedure

During the fractionated treatment course, every patient received a control CT scan directly before the irradiation on the first treatment day and at least once per week. In critical cases (e.g., patients with larger repositioning variability or for re-irradiations) the frequency of the CT scans was increased up to daily CT scans for every fraction. The control CT scans were performed with the stereotactic localizers attached to the fixation frame the same way as during the acquisition of the planning CT scan. The scanned volume included the whole target volume plus margins of at least 1 cm above and below; the reconstructed slice thickness was 3 mm. Altogether, a total of 321 CT studies from the 45 patients were obtained. The median number of CT scans was 7 per patient, ranging from 3 to 29 scans. For paraspinal tumors near the cervical spine, in total 90 CT studies were obtained (range, 3–28 per patient; mean, 8 per patient), in the thoracic spine 153 CT studies (range, 3–29 per patient; mean, 7 per patient), and in the lumbar spine 78 CT studies (range, 4–13 per patient; mean, 6 per patient).

Image registration

For each patient, the control CT scans were stereotactically correlated with the respective planning CT scan, making the coordinates in both CT cubes directly comparable. The bounding box for rigid registration surrounded the target volume completely plus 1 cm margin in the left–right (LR) and anterior–posterior (AP) axes (Fig. 2). In the superior–inferior (SI) axis no additional margin was used. The planning isocenter, which was located in the center of the target volume in all cases, was defined as the correction reference point. In consequence, the calculated translational and rotational errors referred to this point. The control CT cube was matched onto the planning CT by applying a widely accepted mutual-information–based rigid-body registration procedure considering both translational and rotational movements. This method was evaluated in phantom studies and achieved subvoxel accuracy (11).

Quantification of positioning accuracy

Analysis of positioning errors per patient. To assess the quality and reproducibility of the patient positioning over the treatment course, the translational and rotational errors of the control CTs of all patients were evaluated with respect to the planning CT. For each patient $p \in \{1, \ldots, N\}$ each control CT $f_p \in \{1, \ldots, n_p\}$ was registered to the original planning CT using a rigid registration algorithm. The mismatch is expressed in the form of three translational and three rotational errors $\mathbf{TR}_{p,f} = (tx_{p,f}, ty_{p,f}, tz_{p,f}, rx_{p,f}, ry_{p,f}, rz_{p,f})$ along the LR axis, the AP axis, and the SI axis. The mean value $\langle \mathbf{TR}_{p,f} \rangle_f$ of each deviation component expresses the systematic positioning shift for every patient during the treatment course. Here $\langle x_{a,b} \rangle_a$ denotes the average of the field $x_{a,b}$ over index a. The random positioning error is described by the standard deviation (SD):

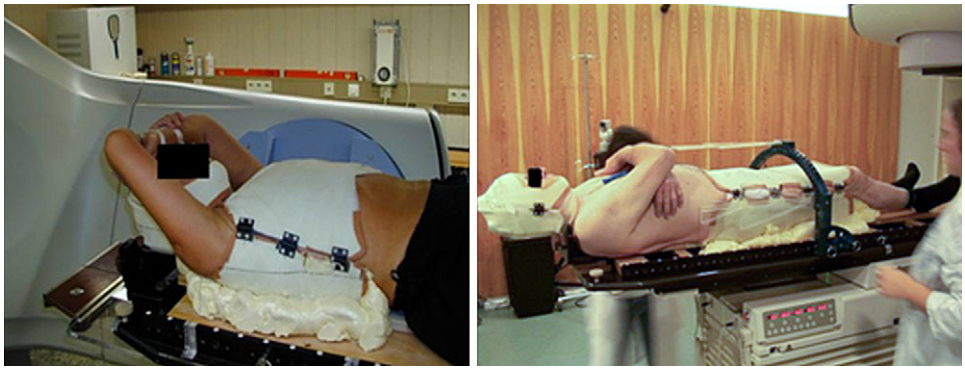

Fig. 1. Patient fixation with body cast and head mask. Left: Fixation for cervical and thoracic paraspinal tumors. Right: Fixation for lumbar tumors (with stereotactic localizers attached).

$$\boldsymbol{\sigma}\left(\mathbf{TR}_{p,f}\right)_f = \sqrt{\left\langle \left[\mathbf{TR}_{p,f} - \left\langle \mathbf{TR}_{p,f} \right\rangle_f\right]^2 \right\rangle_f}. \quad (1)$$

However, this SD was determined from a relatively small sample size, with a median of five to six setup measurements per patient. To indicate the whole extent of the positioning errors the length of the three-dimensional (3D) displacement vector $t_{p,f}$ is calculated as:

$$\|\mathbf{t}_{p,f}\| = \sqrt{tx_{p,f}^2 + ty_{p,f}^2 + tz_{p,f}^2}. \quad (2)$$

The respective mean values for each patient including the SDs are presented and discussed in this study.

Translational and rotational errors dependent on tumor site. The analyzed patient cohort was divided by tumor location into three groups: cervical, thoracic, and lumbar. To assess patient positioning according to the three treatment sites, the mean value $\langle\langle \mathbf{TR}_{p,f}\rangle_f\rangle_p$ and the respective SD of the translational and rotational errors were obtained. To not overweigh the errors of the few patients who were found to have large repositioning errors and therefore received a lot of control CT scans (i.e., 25–29 control CT scans per patient), first averaging over all control CT scans of every patient was performed and afterward averaging over the number of patients belonging to each group. The same procedure was applied to obtain the mean group-specific absolute deviation length using Eq. 2.

Evaluation of target point correction. All control CTs were registered to the corresponding planning CT using the standard registration box (Fig. 2). To evaluate whether rigid registration of the control CT scans is sufficient for correcting the spinal cord position during the treatment course, the registration boxes ROI 1, ROI 2, and ROI 3 (Fig. 3) were introduced and subsequently registered separately with respect to the planning CT using the same rigid registration algorithm. The differences between both registration results define the differential shifts $\Delta TR_{p,f}^{ROI}$. These residual deviations reflect the extent of the elastic deformations, which as a matter of principle cannot be covered by the rigid-body registration procedure, thus presenting a tool to illustrate the amount of deficiencies of the target-point correction in $\Delta TR_{p,f}^{ROI}$ fractionated radiotherapy. The absolute values of the obtained differential shifts were first averaged for each region of interest (ROI 1–3) of every patient and then over each study group.

RESULTS

The mean length of the target volume along the body SI axis was 8.0 cm for the cervical (range, 3.9–14.4 cm), 9.7 cm for the thoracic (3.0–19.5 cm), and 12.4 cm for the lumbar group (3.0–24.9 cm).

On average, 7 CT scans were performed for each patient (range, 3–29). Patients who showed larger setup errors during the treatment course received more CT scans compared with patients with smaller setup errors. The process for the online correction of the setup errors added approximately 10 min to the treatment time. Translational and rotational errors were documented, but only the translational error could be corrected by a shift of the treatment table.

Quantification of positioning accuracy

Translational errors for the whole patient population. For the analysis of the translational shifts per patient, the setup shifts as determined by the registration process were obtained. No obvious time trends were seen in any of the patients.

Figures 4a–c show the mean translational errors of all patients along the three axes. The overall mean translational setup error in the LR axis was 0.28 mm, in the AP axis 0.15 mm, and in SI axis 0.57 mm. Figure 4d shows the histogram of the mean 3D translational shift per patient for the entire population. The mean (± SD) absolute 3D displacement error was 3.55 ± 1.3 mm.

Translational and rotational errors dependent on tumor site. The cervical, thoracic, and lumbar parts of the spine and the respective fixations might result in different mobility and consequently different repositioning accuracies. Therefore we evaluated the translational and rotational errors separately for the three tumor localizations.

The results of the analysis are summarized in Table 1. Overall, the 3D displacement error (± SD) was 2.6 ± 1.0 mm for a patient treated at the cervical spine, 3.8 ± 1.3 mm for a thoracic patient, and 4.0 ± 1.5 mm for a lumbar patient. The mean systematic translational errors were between −0.7 and 1.1 mm in all three directions. The smallest translational systematic and random errors in all three axes were seen for patients with tumors located in the cervical spine. Mean systematic and random rotational errors were <1° for all treatment locations in all three directions.

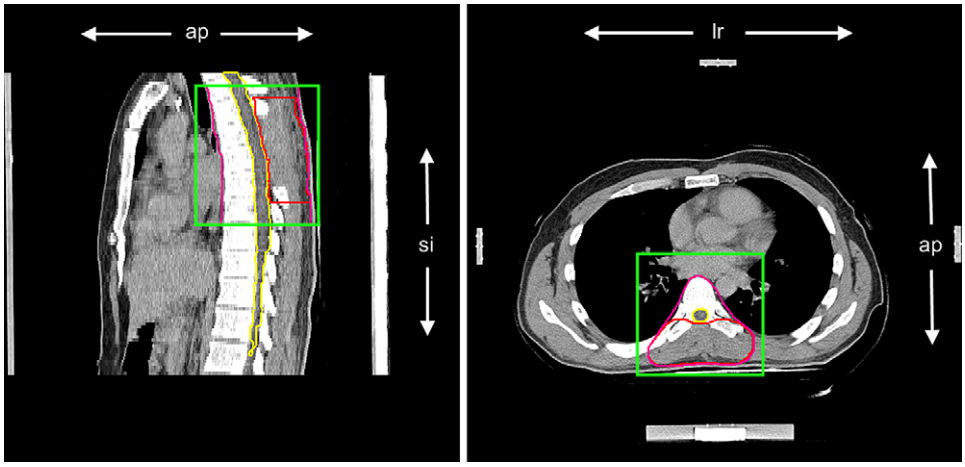

Fig. 2. Exemplary case with a thoracic paraspinal tumor. Outlined are the target and boost volume (magenta), the spinal cord (yellow), and the registration box (green) in sagittal view (left) and axial view (right). lr = left–right axis; ap = anterior–posterior axis; si = superior–inferior axis.

Detailed analysis of positioning errors of cervical treatments. The translational deviations from the planned isocenter for the patients treated at the cervical spine (Fig. 5a) ranged from −5.4 to +4.4 mm in the LR direction, from −5.9 to +3.5 mm in the AP direction, and from −2.7 to +2.0 mm in the SI direction. Mean deviations (± SD) were −0.1 ± 1.1 mm in the LR axis, 0.3 ± 0.8 mm in the AP axis, and 0.1 ± 0.9 mm in the SI axis.

In total, 90 CT scans of 11 patients were evaluated, resulting in 270 translational values. In 119 (44%) of 270 measurements the translational errors were less than ±1 mm, in 224 (83%) less than ±2 mm. In only 17% (46) of all measurements were the translational errors at least 2 mm. The maximum translational error was −5.9 mm in AP direction for Patient 5.

In 208 (77%) of 270 measurements the rotational errors were <1° (Fig. 5b). In only 10 measurements (0.037%) was the rotational error >2°, with 6 of those belonging to a single patient (Patient 8), all along the LR axis. The maximal rotational error was also recorded for Patient 8 at 3.5° around the x-axis. Overall, random rotational and translational errors were ≤0.6° and ≤1.1 mm, respectively.

Detailed analysis of positioning errors of thoracic treatments. A total of 153 CT scans of 21 patients treated for tumors at the thoracic spine were evaluated, resulting in 459 translational and rotational values each (Fig. 5c). Overall, systematic translational errors were highest in the SI direction and lowest in the AP direction. The mean deviations were 0.8 ± 1.1 mm in the LR axis, 0.3 ± 0.8 mm in the AP axis, and 1.1 ± 1.3 mm in the SI axis. The translational errors were at least 2 mm in 188 (41%) of 459 measurement for all three axes. Of the 43 measurements (9%) with translational errors of at least 5 mm, 34 (7%) occurred in only 2 patients. For Patient 7 a total of 29 CT scans were obtained; 20 of these CT scans showed a translational error in the LR dimension of >5 mm, with a maximum of 10.9 mm once. However, maximum translational errors in the AP and SI axes in this patient were <3 and <4 mm, respectively. In Patient 12, seven measurements in LR axis and SI axis each were >5 mm; this patient was scanned 25 times. Therefore, in the remaining 19 patients treated for lesions at the thoracic spine only nine translational errors >5 mm were recorded.

In 332 (72%) of 459 measurements the rotational error was <1°, in 436 measurements (95%) <2° (Fig. 5d). The maximum rotational errors, exceeding 3° around the SI axis, occurred four times in Patient 9.

Detailed analysis of positioning errors of lumbar treatments. In total, 78 CT scans of 13 patients were evaluated,

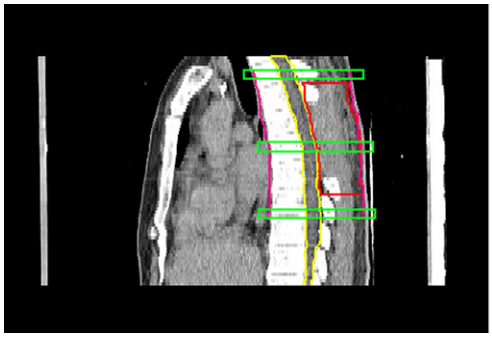

ROI 1	The 3 top CT slices of the target volume
ROI 2	The 3 or 4 middle CT slices of the target volume (3 for an uneven number of CT slices containing target volume, 4 for an even number)
ROI 3	The 3 inferior CT slices of the target volume

Fig. 3. Same case as in Fig. 2. The registration boxes ROI 1–3 (green), target and boost volume (magenta), and spinal cord (yellow) are outlined.

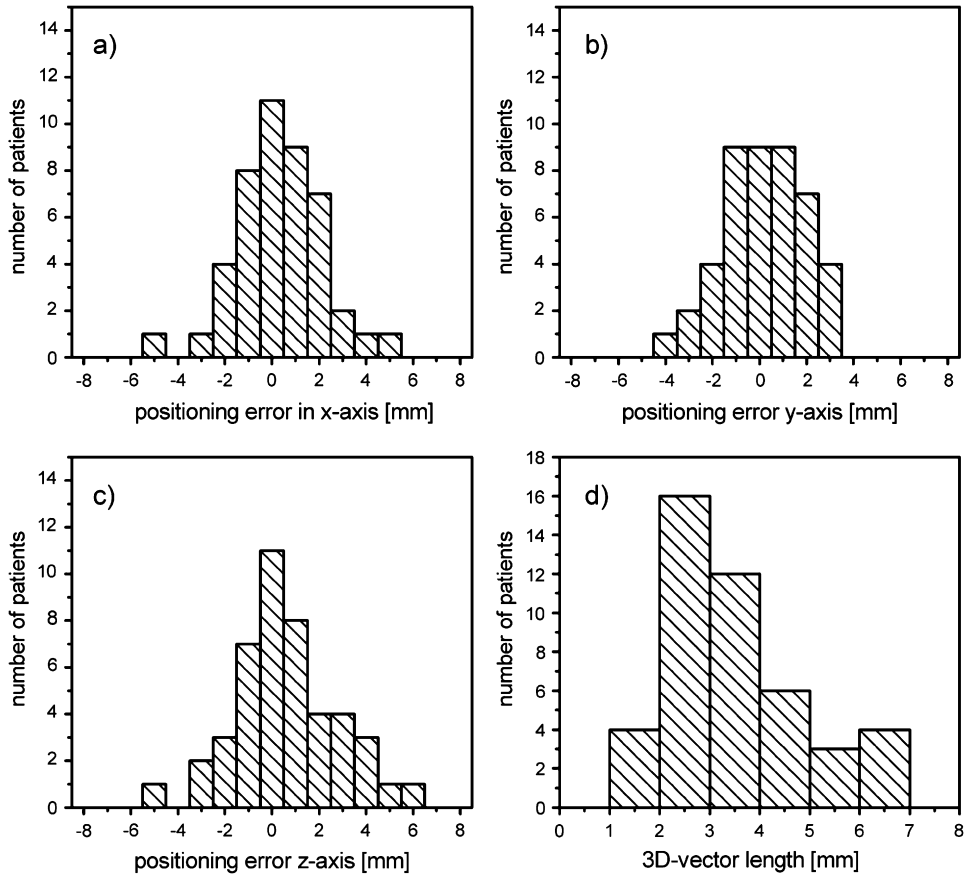

Fig. 4. (a–c) Average translational error per patient along x (left–right), y (anterior–posterior), and z (superior–inferior) axes. (d) Average three-dimensional displacement vector of all patients.

resulting in 234 translational and rotational values each. For all patients treated at the lumbar spine (Fig. 5e) the mean systematic translational deviations were −0.7 ± 1.3 mm in the LR axis, 0.0 ± 0.9 mm in the AP axis, and 0.5 ± 1.6 mm in the SI axis. In 94 (40%) of 234 measurements the translational errors were at least 2 mm in any of the directions. Eighteen translational measurements (8%) were >5 mm, with 10 of these values belonging to only 1 patient (Patient 7), mostly concerning the LR axis.

In 192 (82%) of 234 measurements the rotational errors were <1°, in 229 measurements (98%) <2° (Fig. 5f). The maximal rotational error was recorded for Patient 6 at 2.4° around the SI axis.

Evaluation of target-point correction. Table 2 shows the residual translational deviations of the top, middle, and bottom part after whole-target volume registration. These deviations show the magnitude of the elastic deformations, which can only be corrected using an elastic transformation to result in a perfect anatomic structure alignment. The observed remaining errors were <1 mm for all three tumor sites and axes.

DISCUSSION

The individual patient fixation used in our institution clearly is quite labor-intensive to build. The fabrication process takes 3 days in total, which can be prohibitive for routine use in clinics with heavier patient loads. However, once fabricated, the daily setup is rapid, and all patients tolerated the immobilization well. From the evaluation of the subvolume registration we conclude that rigid registration resulting in a single translation and rotation vector adequately describes

Table 1. Systematic and random positioning errors for paraspinal tumors located in the cervical, thoracic, and lumbar spine

		Translational error (mm)			Rotational error (°)		
Location	3D displacement (mm)	LR axis	AP axis	SI axis	LR axis	AP axis	SI axis
Cervical (n = 11)	2.6 ± 1.0	−0.1 ± 1.1	0.3 ± 0.8	0.1 ± 0.9	−0.3 ± 0.5	0.0 ± 0.4	0.1 ± 0.6
Thoracic (n = 21)	3.8 ± 1.3	0.8 ± 1.1	0.3 ± 0.8	1.1 ± 1.3	−0.1 ± 0.6	0.1 ± 0.4	0.2 ± 0.4
Lumbar (n = 13)	4.0 ± 1.5	−0.7 ± 1.3	0.0 ± 0.9	0.5 ± 1.6	−0.2 ± 0.3	0.0 ± 0.4	0.0 ± 0.4

Abbreviations: 3D = three-dimensional; LR = left–right; AP = anterior–posterior; SI = superior–inferior.
Values are mean (systematic) ± standard deviation (random). Three-dimensional displacement per patient is also given.

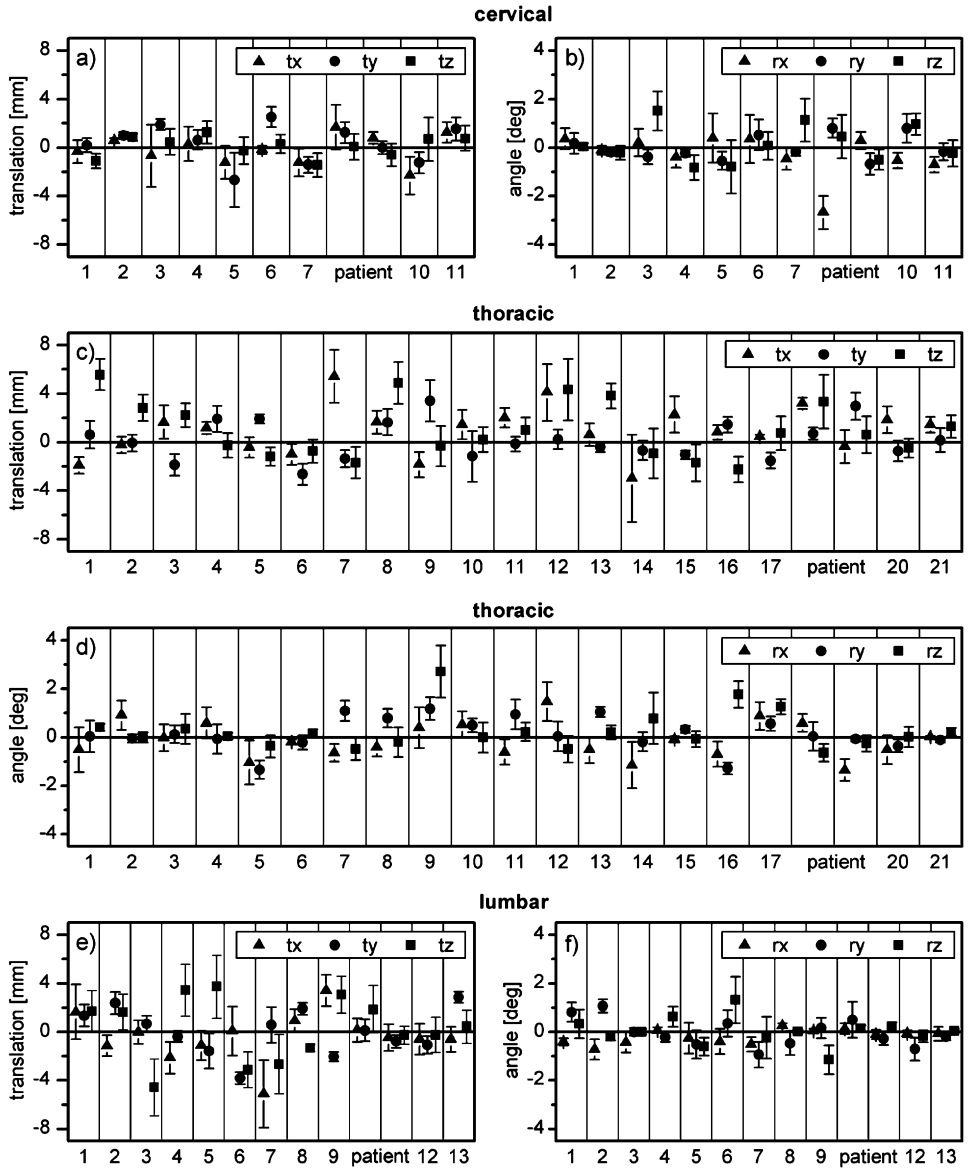

Fig. 5. Mean values and standard deviations of translational (t) (a, c, e) and rotational (r) errors (b, d, f) in x, y, and z axes separately for each of the 45 patients, grouped according to treatment site: cervical (a, b), thoracic (c, d), and lumbar (e, f).

the setup error, and deformable registration is not needed in these cases. It should be noted that the registration box was tightly fitted to the high-dose area, so that the stereotactic verrors reported here are the most relevant for correct dose deposition. When registering complete CT data sets, the resulting total displacement error does not necessarily adequately describe the actual position of the target volume. Because the vertebral column *per se* is a quite flexible

Table 2. Absolute residual translational errors of ROI 1–3 after whole-target volume registration

	Absolute residual translational errors ± standard deviation (mm)								
	ROI 1 (top)			ROI 2 (middle)			ROI 3 (bottom)		
Location	LR axis	AP axis	SI axis	LR axis	AP axis	SI axis	LR axis	AP axis	SI axis
Cervical	0.4 ± 0.4	0.4 ± 0.3	0.8 ± 0.4	0.3 ± 0.2	0.3 ± 0.2	0.4 ± 0.5	0.4 ± 0.4	0.4 ± 0.2	0.8 ± 0.3
Thoracic	0.3 ± 0.2	0.4 ± 0.2	0.7 ± 0.5	0.3 ± 0.2	0.4 ± 0.3	0.7 ± 0.4	0.3 ± 0.2	0.3 ± 0.2	0.3 ± 0.5
Lumbar	0.4 ± 0.3	0.5 ± 0.5	0.8 ± 0.4	0.3 ± 0.1	0.4 ± 0.1	0.5 ± 0.5	0.3 ± 0.2	0.4 ± 0.3	0.8 ± 0.7

Abbreviation: RIO = region of interest. Other abbreviations as in Table 1.

structure, our findings can at least partly be accredited to the rigid fixation we used. Less rigid fixation methods might allow more complex elastic deformations.

Rotational errors

To date few data on the magnitude and relevance of rotational errors in paraspinal patients is available in the literature. Different approaches to measure rotational errors have been described, among them invasive approaches (12). The patient fixation used plays a critical role in the magnitude of observed rotations. For example, Guckenberger *et al.* (13) evaluated rotational setup errors for 6 patients with thoracic tumors and found large differences between patients immobilized with an Elekta Bodyframe or an individualized vacuum mold. The Bodyframe resulted in much smaller systematic and random rotational errors of <1°, whereas the vacuum mold allowed rotations of up to 8°. Most rotational errors in our study were <1°; for example, a typical rotational error we observed around the LR and AP axes was 0.7°. For this error to result in a translational displacement of 1 mm in the periphery of the target volume, the tumor length along the SI axis must be approximately 160 mm. In most cases we treated the target volume length was well below that. So we conclude that for our patient fixation the correction of rotational errors is in general not necessary. In cases in which rotational errors should be corrected, treatment tables with 6 degrees of freedom, such as the HexaPOD (14) or a treatment couch mounted onto a robotic arm (15), are available. Other investigators account for rotational errors in the design of the target volume (16, 17).

Translational errors

In a previous study with 5 paraspinal patients using the same patient fixation and stereotactic setup as described in this article, a mean two-dimensional vectorial setup error of 2.3 ± 1.3 mm for thoracic and 1.8 ± 1.2 mm for lumbar spine tumors in the axial plane was observed (9). Our study confirmed this accuracy but also revealed that despite the stereotactic setup in some cases the error can be considerably higher. We generally correct translational errors of the LR and AP axes greater than 2 mm, but this threshold may vary depending on the prescribed dose and individual case. In critical cases we performed the target-point correction immediately after the control CT scan before irradiation, which added approximately 10 min to the treatment time for registration and visual verification. This time span was feasible in daily practice and was well tolerated by the patients.

The measured setup uncertainties are in good agreement with the findings of other institutions. Yenice *et al.* (18) reported translational errors using a noninvasive stereotactic body frame and found average systematic and random errors to be 2 mm and 1.5 mm, respectively; the resulting 3D positioning error was 3.3 mm. Guckenberger *et al.* (19) calculated a slightly larger 3D positioning error of 5.2 ± 2.2 mm for paraspinal tumors on the basis of a cone-beam CT study. Patients in this study were immobilized in thermoplastic head–shoulder masks for tumor localization in the cervical spine and with a customized total-body vacuum cushion for thoracic and lumbar tumor localizations. The authors of this study came to the conclusion that correction of the translational component of setup errors, especially translational errors in the axial plane, is of primary importance regarding the spinal cord dose (19, 13). After correcting for translational errors, the residual errors can be assumed to be 1 mm (20).

Further considerations

The magnitude of the presented stereotactic positioning errors is comparable to those of previously described stereotactic patient positioning devices. However, even in our stereotactic setup in some cases large positioning deviations did occur. This can be for various reasons; for example, weight loss under therapy or reduced patient's body perception when entering the fixation device. So even with a rigid setup, image guidance throughout the whole treatment course is necessary.

The deformations of the target volume using the described patient fixation with the torso were shown to be negligible. For higher patient comfort it might be possible to lighten the fixation without compromising the rigidity of the spinal column (*e.g.,* by removing the frontal half of the head mask). However, it must be noted that any changes to the patient fixation require a thorough re-evaluation of the whole adaptive procedure.

Even in the era of image guidance, where setup errors can be corrected on a daily basis, rigid patient fixation for paraspinal treatments seems to be necessary because it minimizes the flexibility of the spinal cord (especially for longer target volumes that include multiple vertebral bodies), so that no elastic deformations occur and a simple target-point correction is sufficient. After target-point correction the main source of remaining errors may be intrafractional motion. The issue of intrafractional motion was not addressed in our study. Ideally, such a study should be based on linear accelerator–mounted imaging that is capable of monitoring the position of the spinal cord (or at least the bony vertebral column) throughout the dose delivery process.

Because of the very good alignment of the actual treatment with the planning situation by simple target-point correction, we did not calculate the dosimetric effect of the remaining geometric uncertainties. For other treatment sites, however, it is highly desirable not only to report on the geometric but also on the dosimetric consequences of different patient fixations and adaptive regiments. For example, head-and-neck treatments with higher anatomic variability between fractions necessitate strategies for dealing with larger residual errors when registering different subvolumes or even require deformable registration and replanning (21, 22).

The additional dose delivered to the patient by the control CT scan itself was <1 cGy Computed Tomography Dose Index (range, 0.25–0.85 cGy) and can be neglected compared with the benefit it can provide for the patient. Because the in-room CT scanner meets diagnostic standards, the image quality is excellent, with even lower doses compared with both kilovoltage and megavoltage cone-beam CT (23). On

the other hand, because the bony vertebrae provide clear anatomic landmarks even in images with lower quality, both kilovoltage and megavoltage linear accelerator–attached cone-beam CT also seem to be suitable for ultra-precise paraspinal treatments (24, 25).

CONCLUSION

We analyzed the stereotactic setup accuracy of patients treated for paraspinal tumors. On the basis of the presented data we have shown that relying on the stereotactic positioning might be insufficient for some cases. To ensure accurate patient positioning for these cases, daily image guidance is recommended in all patients treated for paraspinal lesions with high doses.

Furthermore, it is important to ensure the suitability of the applied patient fixation for the chosen setup correction strategy. Target-point correction via rigid registration as an adaptive strategy is found to be adequate for precise paraspinal radiotherapy for the described patient fixation.

REFERENCES

1. Avanzo M, Romanelli P. Spinal radiosurgery: Technology and clinical outcome. *Neurosurg Rev* 2009;32:1–13.
2. Finn MA, Vrionis FD, Schmidt MH. Spinal radiosurgery for metastatic disease of the spine. *Cancer Control* 2007;14: 405–411.
3. Niranjan A, Maitz AH, Lunsford A. Radiosurgery techniques and current devices. *Prog Neurol Surg* 2007;20:50–67.
4. Gong Y, Wang J, Bai S. Conventionally-fractionated image-guided intensity modulated radiotherapy (IG-IMRT): A safe and effective treatment for cancer spinal metastasis. *Radiat Oncol* 2008;3:11.
5. Yamada Y, Lovelock DM, Bilsky MH. A review of image-guided intensity-modulated radiotherapy for spinal tumors. *Neurosurgery* 2007;61:226–235.
6. Pai Panandiker A, Ning H, Likhacheva A. Craniospinal irradiation with spinal IMRT to improve target homogeneity. *Int J Radiat Oncol Biol Phys* 2007;1(68):1402–1409.
7. Shiu AS, Chang EL, Ye JS, *et al*. Near simultaneous computed tomography image-guided stereotactic spinal radiotherapy: An emerging paradigm for achieving true stereotaxy. *Int J Radiat Oncol Biol Phys* 2003;57:605–613.
8. Kriminski SA, Lovelock DM, Seshan VE. Comparison of kilovoltage cone-beam computed tomography with megavoltage projection pairs for paraspinal radiosurgery patient alignment and position verification. *Int J Radiat Oncol Biol Phys* 2008; 1(71):1572–1580.
9. Lohr F, Debus J, Frank C, *et al*. Noninvasive patient fixation for extracranial stereotactic radiotherapy. *Int J Radiat Oncol Biol Phys* 1999;45:521–527.
10. Bendl R, Hoess A, Schlegel W. Virtual simulation in radiotherapy planning. *Lect Notes Comput Sci* 1995;905:287–292.
11. Kim J, Fessler JA, Lam KL, *et al*. A feasibility study of mutual information based setup error estimation for radiotherapy. *Med Phys* 2001;28:2507–2517.
12. Onimaru R, Shirato H, Aoyama H. Calculation of rotational setup error using the real-time tracking radiation therapy (RTRT) system and its application to the treatment of spinal schwannoma. *Int J Radiat Oncol Biol Phys* 2002;54:939–947.
13. Guckenberger M, Meyer J, Vordermark D, *et al*. Magnitude and clinical relevance of translational and rotational patient setup errors: A cone-beam CT Study. *Int J Radiat Oncol Biol Phys* 2006;65:934–942.
14. Meyer J, Wilbert J, Beyer K. Position accuracy of cone-beam computed tomography in combination with a hexapod robot treatment table. *Int J Radiat Oncol Biol Phys* 2007;67: 1220–1228.
15. D'Souza WD, Naqvi SA, Yu CX. Real-time intra-fraction-motion tracking using the treatment couch: A feasibility study. *Phys Med Biol* 2005;50:4021–4033.
16. Langer MP, Papiez L, Spirydovich S, *et al*. The need for rotational margins in intensity-modulated radiotherapy and a new method for planning target volume design. *Int J Radiat Oncol Biol Phys* 2005;63:1592–1603.
17. Stroom JC, de Boer HC, Huizenga H. Inclusion of geometric uncertainties in the radiotherapy treatment planning by means of coverage probability. *Int J Radiat Oncol Biol Phys* 1999; 43:905–919.
18. Yenice KM, Lovelock DM, Hunt MA, *et al*. CT image-guided intensity-modulated therapy for paraspinal tumors using stereotactic immobilization. *Int J Radiat Oncol Biol Phys* 2003;55: 583–593.
19. Guckenberger M, Meyer J, Wilbert J, *et al*. Precision required for dose-escalated treatment of spinal metastases and implications for image-guided radiation therapy (IGRT). *Radiother Oncol* 2007;84:56–63.
20. Guckenberger M, Meyer J, Wilbert J. Precision of image-guided radiotherapy (IGRT) in six degrees of freedom and limitations in clinical practice. *Strahlenther Oncol* 2007;183: 307–313.
21. Thieke C, Malsch U, Seeber A, *et al*. Adaptive radiotherapy of head and neck cancer using automatic elastic matching of CT images (Abstr.). *Radiother Oncol* 2006;81(Suppl. 1):S27.
22. Thieke C, Malsch U, Schlegel W. Kilovoltage CT using a linac-CT scanner combination. *Br J Radiol* 2006;79:79–86.
23. Stützel J, Oelfke U, Nill S. A quantitative image quality comparison of four different image guided radiotherapy devices. *Radiother Oncol* 2008;86:20–24.
24. Pouliot J, Bani-Hashemi A, Chen J. Low-dose megavoltage cone-beam CT for radiation therapy. *Int J Radiat Oncol Biol Phys* 2005;61:552–560.
25. Hansen EK, Larson DA, Aubin M. Image-guided radiotherapy using megavoltage cone-beam computed tomography for treatment of paraspinous tumors in the presence of orthopedic hardware. *Int J Radiat Oncol Biol Phys* 2006;66:323–326.

Thieke et al. Radiation Oncology (2015) 10:267
DOI 10.1186/s13014-015-0575-5

Radiation Oncology

RESEARCH Open Access

Long-term results in malignant pleural mesothelioma treated with neoadjuvant chemotherapy, extrapleural pneumonectomy and intensity-modulated radiotherapy

Christian Thieke[1,2,5*], Nils H. Nicolay[1,2,4], Florian Sterzing[1,2], Hans Hoffmann[3], Falk Roeder[1,2,4,5], Seyer Safi[3], Juergen Debus[1,2] and Peter E. Huber[1,2,4*]

Abstract

Introduction: We investigated the clinical outcome and the toxicity of trimodal therapy of malignant pleural mesothelioma (MPM) treated with neoadjuvant chemotherapy, extrapleural pneumonectomy (EPP) and adjuvant intensity-modulated radiotherapy (IMRT).

Methods: Chemotherapy regimens included Cisplatin/Pemetrexed, Carboplatin/Pemetrexed and Cisplatin/Gemcitabine, followed by EPP. 62 patients completed the adjuvant radiotherapy. IMRT was carried out in two techniques, either step&shoot or helical tomotherapy. Median target dose was 48 Gy to 54 Gy. Toxicity was scored with the Common Terminology Criteria (CTC) for Adverse Events. We used Kaplan-Meier method to estimate actuarial rate of locoregional control (LRC), distant control (DC) and overall survival (OS), measured from the date of surgery. Rates were compared using the logrank test. For multivariate analysis the Cox proportional hazard model was used.

Results: The median OS, LRC and DC times were 20.4, 31.4 and 21.4 months. The 1-, 2-, 3-year OS rates were 63, 42, 28 %, the LRC rates were 81, 60, 40 %, and the DC rates were 62, 48, 41 %. We observed no CTC grade 4 or grade 5 toxicity. Step&shoot and helical tomotherapy were equivalent both in dosimetric characteristics and clinical outcome. Biphasic tumor histology was associated with worse clinical outcome compared to epitheloid histology.

Conclusions: Mature clinical results of trimodal treatment for MPM were presented. They indicate that hemithoracic radiotherapy after EPP can be safely administered by either step&shoot IMRT and tomotherapy. However, the optimal prospective patient selection for this aggressive trimodal therapy approach remains unclear. This study can serve as a benchmark for current and future therapy concepts for MPM.

Keywords: Malignant pleural mesothelioma, Trimodal therapy, Intensity modulated radiation therapy, Extrapleural pneumonectomy, Chemotherapy

* Correspondence: christian.thieke@med.uni-muenchen.de; p.huber@dkfz.de
[1]Department of Radiation Oncology, Heidelberg University Hospital, Heidelberg, Germany
Full list of author information is available at the end of the article

Introduction

Malignant pleural mesothelioma (MPM) is an aggressive disease with a poor prognosis, currently treated with different combinations of chemotherapy, surgery and radiotherapy. For each single treatment modality, significant improvements have been achieved over the last years. With respect to chemotherapy regimens, Pemetrexed combined with Cisplatin has been established [1]; in surgery approaches, extrapleural pneumonectomy (EPP) and pleurectomy/decortication (P/D) have been technically advanced resulting in tolerable toxicity [2]; moreover the introduction of intensity-modulated radiotherapy (IMRT) allows to conform the high dose area tightly to the target volume and spare adjacent organs at risk [3].

However, despite these individual advancements the optimal combination and treatment strategy for each individual patient still remains unclear. Randomized clinical trials have been difficult to organize due to the rareness of the disease, patients presenting very differently at the time of diagnosis in terms of tumor spread, histology and general performance status, and different technical possibilities and experiences at different clinical centers. Therefore, evaluations of the clinical outcome of cohorts treated systematically by a certain regimen are relevant to assess its potential and also the associated risks for the patients.

In this work, we assessed and analyzed the clinical outcome of consecutive MPM patients treated in Heidelberg, Germany, by hemithoracic intensity-modulated radiotherapy in a trimodal setting after neoadjuvant chemotherapy and EPP.

Methods

Inclusion criteria

All MPM patients that completed adjuvant radiotherapy at the Heidelberg University Hospital after chemotherapy and EPP between 2003 and 2010 were included in this study. This required adequate recovery from surgery. To be eligible for EPP, the patients were required to have localized disease (maximum cT4N2M0), epitheloid or biphasic tumor histology, and a sufficient general performance status. This study was approved by the independent ethics committee of the medical faculty of the University of Heidelberg.

Chemotherapy

All patients received neoadjuvant chemotherapy prior to surgery, consisting of either Cisplatin/Pemetrexed, Carboplatin/Pemetrexed or Cisplatin/Gemcitabine.

Extrapleural pneumonectomy (EPP)

EPP included the removal of the complete afflicted lung together with the parietal pleura, pericardium and diaphragm. It was performed via an extended S-shaped anterolateral thoracotomy incision in the sixth intercostal space. Sites of prior open biopsy, thoracoscopy incisions, or chest tube tracks were excised separately. After resection, the diaphragm was replaced by a Monofilament Polypropylene mesh (Bard Mesh; Davol, Inc, Cranston, RI), and the pericardium was reconstructed with a xenopericard patch (Supple Peri-Guard; Synovis Surgical Innovations, St Paul, MN). In all patients undergoing EPP, a systematic mediastinal lymph node dissection was performed.

Radiotherapy

Immobilization

During the acquisition of the contrast-enhanced computed tomography (CT) scan for treatment planning (and also later for irradiation), patients were immobilized by a vacuum body mattress and a Scotch-cast head mask, with the arms above the head on a resting plate. The surgical incisions were marked by thin metal wires during the planning CT scan.

Segmentation

As planning target volume (PTV), the complete ipsilateral thoracic cavity was segmented from lung apex to insertion of the diaphragm, including the ribs, the reconstructed pericardium and diaphragm, and extending up to the skin surface along the surgical incisions, with a safety margin of 5 mm which could be reduced at directly adjacent organs at risk. It was also made sure that all internal metal clips from surgery were included in the target volume. The contralateral lung, heart, liver, esophagus, spinal cord, and kidneys were segmented as organs at risk.

IMRT planning

The treatment was performed either as step&shoot IMRT or helical tomotherapy IMRT. For step&shoot IMRT, treatment planning was performed using Konrad (Siemens, Erlangen, Germany). We placed 9–12 coplanar, non-equidistant beams in order to achieve optimal target coverage and sparing of the contralateral lung. For helical tomotherapy, we used the Tomotherapy planning system (Accuray, Sunnyvale, CA, USA). A field width of 2.5 cm was chosen. An example plan used for step-and-shoot IMRT treatment showing both segmentation and the resulting dose distribution is shown in Fig. 1.

IMRT delivery

Step&shoot IMRT was delivered by Siemens Primus and Siemens Artiste linear accelerators (Siemens, Erlangen, Germany) at 6 MV with regular image guidance (at least once per week) by an in-room CT scanner (Siemens Primatom, Erlangen, Germany). Helical tomotherapy was delivered by a Tomotherapy Hi-Art system (Accuray, Sunnyvale, CA, USA) at 6 MV, using built-in image

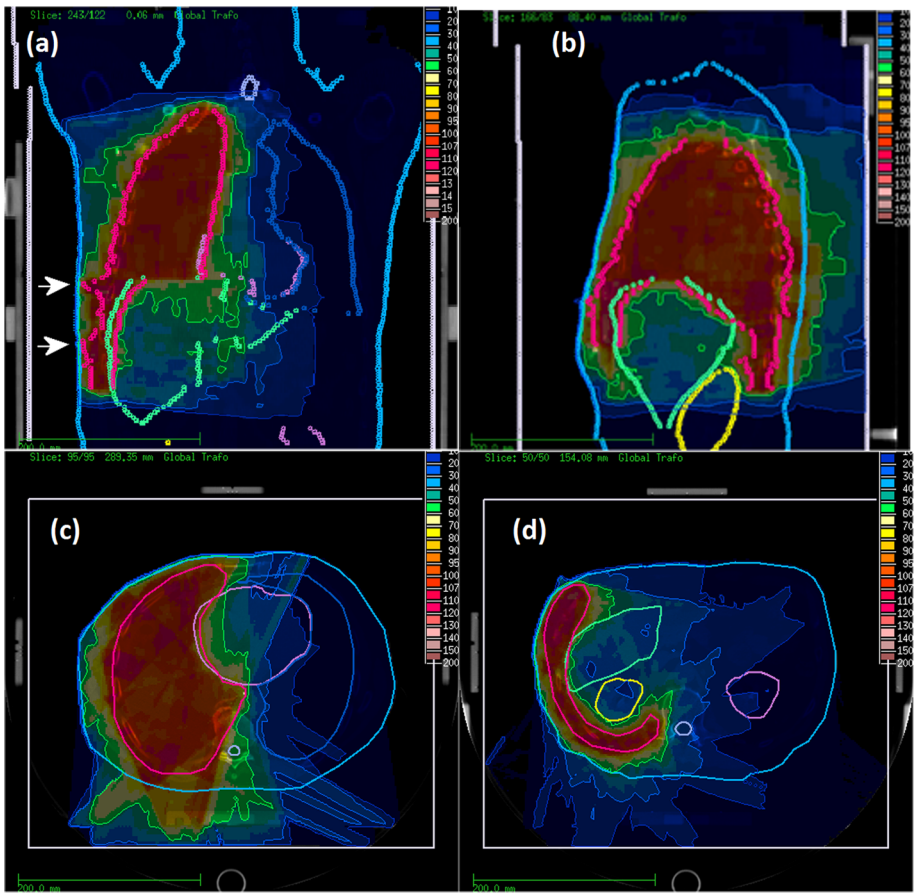

Fig. 1 Structure definition and dose distribution for one MPM patient (Step & Shoot IMRT). In the coronar projection (**a**), the inclusion of the EPP incisions into the target volume are marked by white arrows. The sagittal projection (**b**) shows the caudal extension of the target volume with sparing of the liver and the kidney. In the two transverse slices the sparing of the heart (**c**) and again liver and kidney (**d**) can be seen

guidance acquired at 3 MV. Median target dose was 48 to 54 Gy in 2 Gy fractions.

Follow-up

Regular follow up visits were performed at our institution or the referring center. At our institution, patients were scheduled for follow up visits 6 weeks after end of radiotherapy and then every 3 months for the first 2 years, every 6 months for the three following years and annually thereafter. Each follow-up visit included a patient interview, clinical examination and computed tomography (CT) of the chest. In case of evidence for locoregional recurrence or distant spread, additional tests or imaging studies were performed to confirm or exclude disease progression at the discretion of the treating physician. Missing data were completed by calling the patient and/or the treating physician.

Toxicity was scored with the Common Terminology Criteria (CTC) for Adverse Events version 4.0. Locoregional failure was defined as tumor relapse within the treated ipsilateral hemithorax. Distant control was defined as absence of tumor relapse outside the treated ipsilateral hemithorax. In patients without assessment of locoregional control/distant spread at the time of death, the timepoint of the last locoregional control/distant spread status was used for calculation.

Statistical analysis

The Kaplan-Meier method was used to estimate actuarial rates of locoregional control (LRC), distant control (DC), and overall survival (OS). Subgroups were compared using the logrank test. The Cox proportional hazard model was used for multivariate analysis. A p-value of ≤ 0.05 was considered significant. Survival times were calculated from the date of EPP surgery. Data were analysed using Statistica 6.0 (Statsoft, Tulsa, OK, USA).

Results

Patient characteristics

Between 2003 and 2010, 62 patients (pts) completed postoperative radiotherapy after EPP in a trimodal treatment setting in our institution. The patient characteristics are

outlined in Table 1. The most common postoperative tumor staging was ypT3N0M0 (with 41 pts T3 and 43 pts N0), but also T2 (7 pts), T4 (4 pts), N1 (7 pts) and N2 (6 pts) stages occurred.

Treatment characteristics

All patients received neoadjuvant chemotherapy. Regimens used were Cisplatin/Pemetrexed (30 pts, 48.4 %), Carboplatin/Pemetrexed (23 pts, 37.1 %) and Cisplatin/Gemcitabine (9 pts, 14.5 %). Mostly 3 or 4 cycles of chemotherapy were given; 5 patients received 6 cycles and 1 patient received 7 cycles. The EPP surgery was carried out mainly at the Thoracic Hospital at the University Clinic Heidelberg (58 pts, 82.9 %), but also in other hospitals (12 pts, 17.1 %). The median interval between the date of diagnosis and date of EPP surgery was 4.4 months. The median interval between surgery and start of radiotherapy was 8.4 weeks (range, 1.3–46.1 weeks).

We started intensity-modulated radiotherapy for MPM in 2003 with step & shoot technique. From 2006 on, helical tomotherapy was used as an additional IMRT technique. The first patients received median doses of 48Gy (2 pts, 3.2 %) and 50Gy (16 pts, 25.8 %) to the target volume in 2 Gy fractions. Later, the median target dose was increased to 54Gy (44 pts, 71.0 %). In total, 41 pts (66.1 %) were treated with step&shoot and 21 pts (33.9 %) with helical tomotherapy IMRT.

Dosimetric comparison of step&shoot and helical tomotherapy IMRT

Several key dosimetric parameters were extracted from the treatment planning systems to characterize the treatment. They are listed in Table 2, including the standard deviation (SD). The parameters are listed separately for step&shoot-IMRT and helical tomotherapy as well as combined for all patients. The mean target dose is a little lower for step&shoot, since some of these patients were planned to a median target dose of 48–50Gy, whereas all tomotherapy patients were planned to a median target dose of 54Gy. The target dose coverage and homogeneity is slightly better for helical tomotherapy, with doses to some organs at risk (liver for right-sided MPM, heart) also slightly higher. Especially the contralateral lung could be spared very effectively with a mean lung dose (MLD) of (7.6 ± 2.2) Gy, a V5Gy of (66.2 ± 23.0) % and a V20Gy of (1.7 ± 1.9) % for step&shoot-IMRT and a MLD of (7.0 ± 1.2) Gy, a V5Gy of (71.5 ± 18.6) % and a V20Gy of (0.7 ± 1.3) % for helical tomotherapy, respectively.

Table 1 Patient characteristics

Total number of patients	62
Age at diagnosis	
Median	57.9 years
Range	[34.5–70.4 years]
Gender	
Male	52 (83.9 %)
Female	10 (16.1 %)
Tumor location	
Left	27 (43.5 %)
Right	35 (56.5 %)
Histology	
Epitheloid	44 (70.9 %)
Biphasic	18 (29.1 %)

Table 2 Dosimetric parameters of the treatment plans

	Step & Shoot	Helical Tomotherapy	All Patients
	41 patients	21 patients	62 patients
	Mean value ± SD	Mean value ± SD	Mean value ± SD
Target volume (PTV)			
Mean Dose [Gy]	52.1 ± 2.3	53.5 ± 0.5	52.6 ± 2.0
Standard Deviation [Gy]	3.5 ± 1.5	2.4 ± 1.2	3.1 ± 1.5
V95% [%]	85.3 ± 5.3	92.3 ± 5.2	87.6 ± 6.2
V90% [%]	93.3 ± 3.8	94.2 ± 3.9	94.2 ± 3.9
Contralateral Lung			
Mean Lung Dose [Gy]	7.6 ± 2.2	7.0 ± 1.2	7.4 ± 2.0
V5Gy [%]	66.2 ± 23.0	71.5 ± 18.6	67.9 ± 21.6
V20Gy [%]	1.7 ± 1.9	0.7 ± 1.3	1.4 ± 1.8
Liver (right-sided MPM)			
Mean Dose [Gy]	21.9 ± 3.9	26.4 ± 3.8	23.4 ± 4.4
V30Gy [%]	24.7 ± 8.3	33.5 ± 7.8	27.5 ± 9.0
Liver (left-sided MPM)			
Mean Dose [Gy]	9.1 ± 2.3	10.4 ± 1.5	9.6 ± 2.1
V30Gy [%]	2.0 ± 2.5	2.5 ± 2.7	2.2 ± 2.5
Heart			
V45Gy [%]	7.3 ± 7.5	12.4 ± 6.1	9.0 ± 7.4
Ipsilateral kidney			
Mean Dose [Gy]	9.9 ± 5.1	9.3 ± 2.5	9.7 ± 4.4
V15Gy [%]	23.4 ± 23.2	16.5 ± 13.0	21.0 ± 20.4
Contralateral kidney			
Mean Dose [Gy]	3.1 ± 1.6	4.5 ± 1.5	3.6 ± 1.7
V15Gy [%]	0.1 ± 0.2	0.3 ± 0.6	0.2 ± 0.4
Spinal Cord			
Maximum Dose [Gy]	36.0 ± 5.7	37.3 ± 5.3	36.4 ± 5.5
Esophagus			
V55Gy [%]	0.9 ± 1.7	2.2 ± 2.4	1.4 ± 2.1

SD standard deviation, *PTV* planning target volume

Toxicity of radiotherapy

Most common side effects were mild nausea and skin erythema CTC grade 1–2. Many patients reported fatigue during radiation treatment which improved after completion of treatment. One patient developed symptomatic anaemia during therapy, requiring the transfusion of erythrocyte concentrates, but recovered well. One patient showed radiological signs of pneumonitis in the CT scan after radiotherapy, but was clinically asymptomatic and needed no intervention (pneumonitis CTC grade 1). One patient (treated with step&shoot IMRT, MLD 10.7 Gy, V5Gy 92 %, V20Gy 5 %) developed clinically symptomatic radiation pneumonitis, which resolved completely after treatment with prednisolone (CTC grade 3). We observed no CTC grade 4 or grade 5 adverse effects of the irradiation.

Overall survival, locoregional control, distant control

The median follow-up time was 17.0 months (range, 2.4–111.9 months). Only 6 patients were still alive at the time of analysis, with a median follow-up time of 60.6 months (range, 8.9–111.9 months). The data point at 8.9 months was censored because the patient was lost to follow-up, the other patients alive at the time of analysis had a follow-up time of at least 40 months.

The median overall survival (OS) for all 62 pts was 20.4 months. The OS after 1 year, 2 years and 3 years was 63 % (SD 6 %), 42 % (SD 6 %) and 28 % (SD 6 %), respectively. Median locoregional control (LRC) was 31.4 months. LRC after 1 year, 2 years and 3 years was 81 % (SD 6 %), 60 % (SD 9 %) and 40 % (SD 11 %), respectively. Median distant control (DC) was 21.4 months. DC after 1 year, 2 years and 3 years was 62 % (SD 7 %), 48 % (SD 8 %) and 41 % (SD 10 %), respectively.

The Kaplan-Meier curves for OS, LRC and DC are shown in Fig. 2.

Factors associated with survival

Multivariate analysis showed that with respect to OS among all the variables tested, the male gender tended to result in worse prognosis although not reaching significance (Hazard Ratio (HR) 1.7; 95 % Confidence Interval (CI95) 0.7–4.9; $p = 0.2$). The only two significant variables were the postoperative

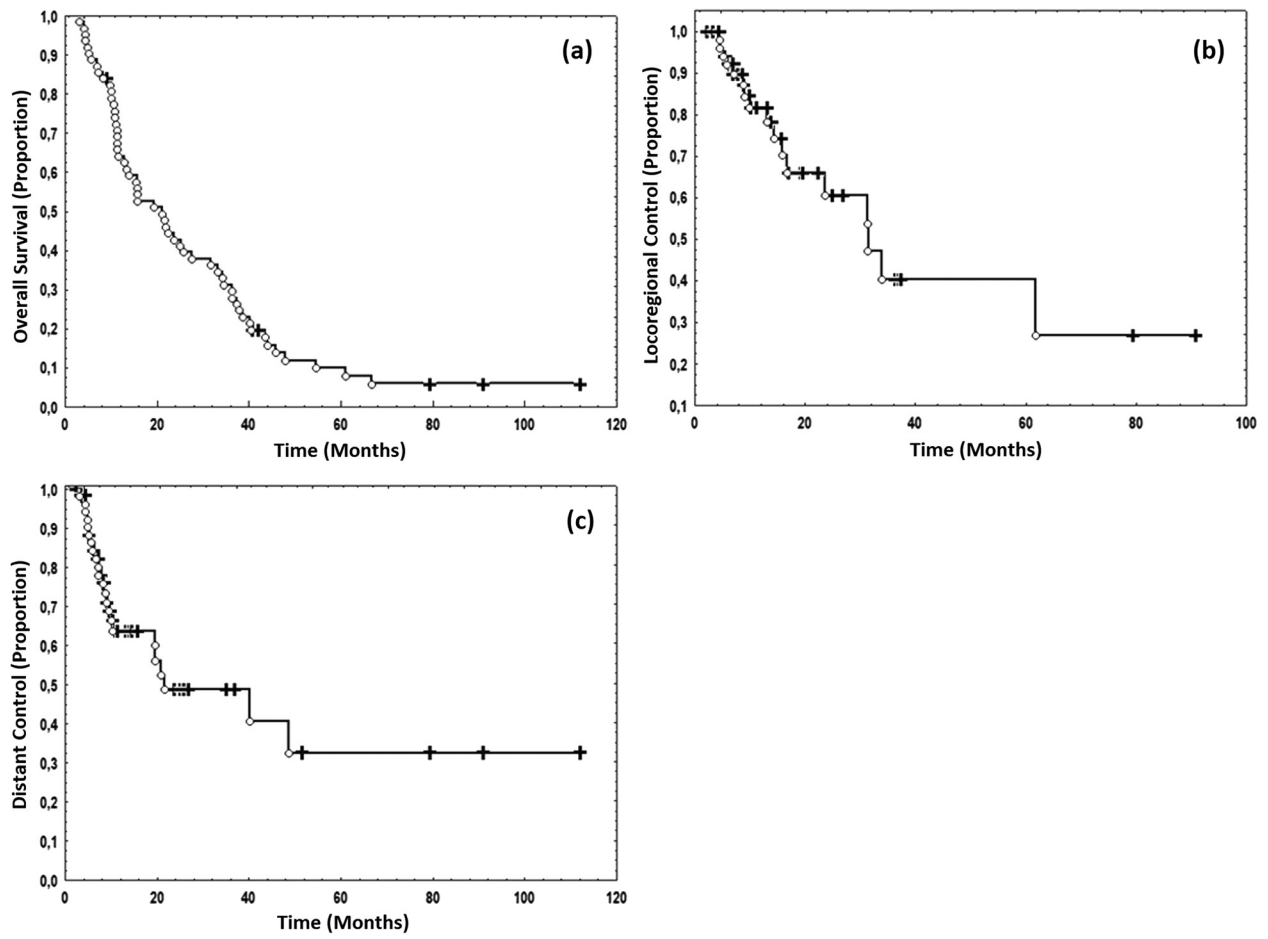

Fig. 2 Kaplan-Meier curves for all patients. **a** Overall survival, **b** locoregional control and **c** distant control

resection status R (per higher status HR 3.9; CI95 1.3–12.2; $p = 0.01$ and biphasic histology (HR 2.2; CI95 1.2–5. 4; $p = 0.03$). With respect to locoregional control, no variable tested reached significance in multivariate analysis. However higher R status (HR 3.2; CI95 0.45–23.5; $p = 0.2$) and biphasic histology (HR = 3.4; CI95 0.77–14. 9; $p = 0.1$) tended to result in reduced local control. With respect to distant control, both higher R Status (HR 10.9; CI95 1.3–76. 2; $p = 0.02$) and biphasic histology (HR 7.4; CI95 2.2–25.4; $p = 0.003$) were significantly associated with worse outcome. Other variables including the IMRT technique (step&shoot vs. helical tomotherapy), dose distributions such as target mean dose, target coverage, lung dose, clinical factors such as lymph node involvement (N status), and patient factors such as age had no influence on OS, LRC and DC. Kaplan-Meier curves illustrating the equivalence of irradiation techniques are depicted in Fig. 3 and the influence of the histology is depicted in Fig. 4.

Discussion

In this work we present the long-term clinical outcome of trimodal therapy of MPM consisting of neoadjuvant chemotherapy, EPP and adjuvant hemithoracic IMRT from a single institution. To our knowledge, our cohort of 62 consecutive patients is one of the largest with the longest follow-up times reported in the literature. The median OS, LRC and DC were 20.4, 31.4 and 21.4 months. The actuarial 1-, 2-, and 3-year OS was 63, 42, 28 %, the LRC 81, 60, 40 %, and the DC was 62, 48, 41 %. No CTC grade 4 or grade 5 toxicity was observed.

A cohort of 86 MPM patients treated with IMRT after EPP (57/86 without chemotherapy) were recently analyzed by Gomez et al. [4], who reported excellent locoregional control rates. Compared to these results, we observed longer median OS (20.4 vs. 14.7 months) with slightly better OS rates after 1 and 2 years (63 % vs. 55 % and 42 % vs. 32 %). Our locoregional control rates after 1 and 2 years were slightly worse (81 % vs. 88 % and 60 % vs. 71 %), but distant control rates after 1 and

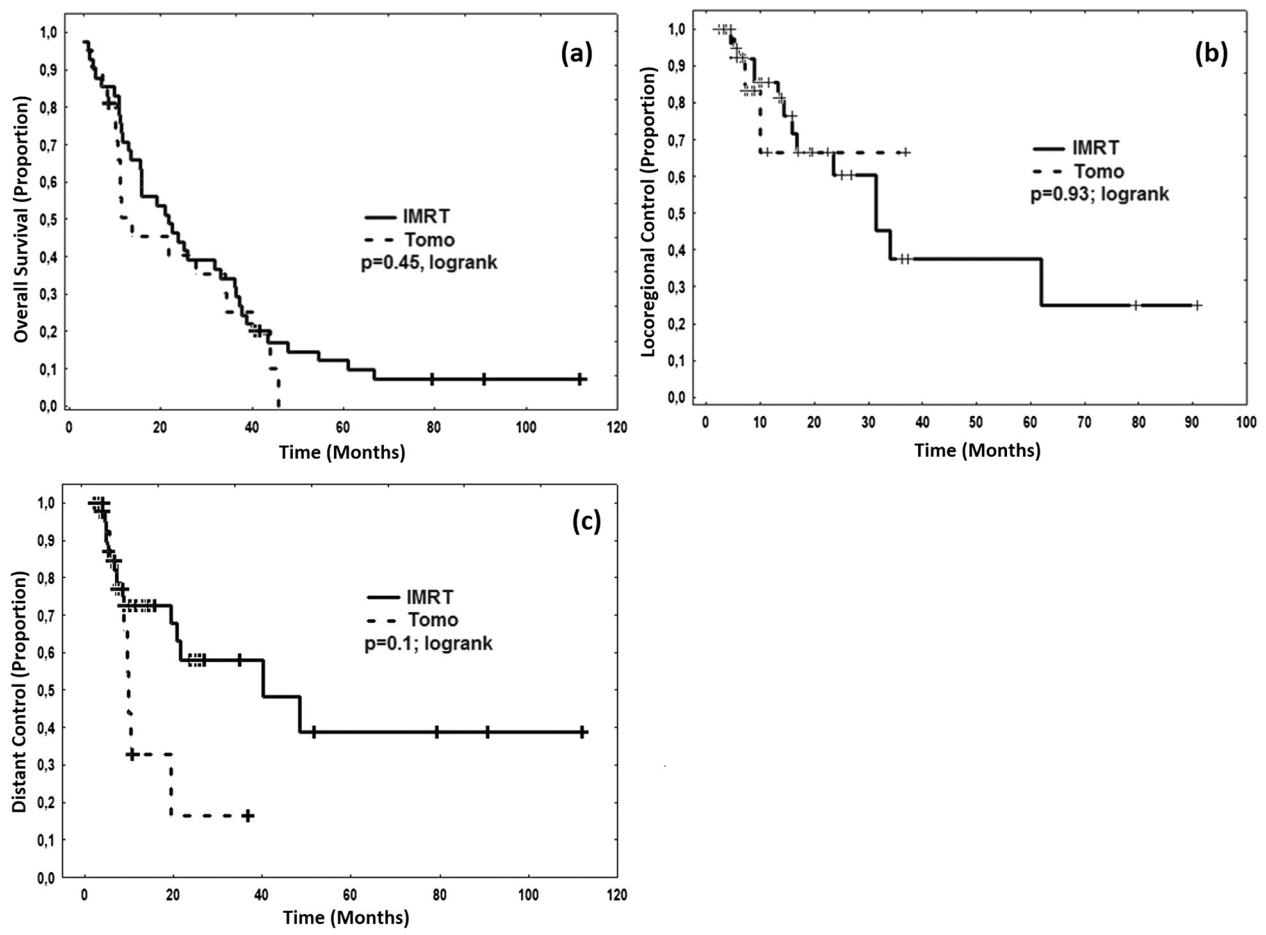

Fig. 3 Kaplan-Meier curves separated for type of radiation treatment. Step&shoot-IMRT ("IMRT") vs. helical tomotherapy-IMRT ("Tomo") shows no significant difference regarding **a** overall survival, **b** locoregional control and **c** distant control

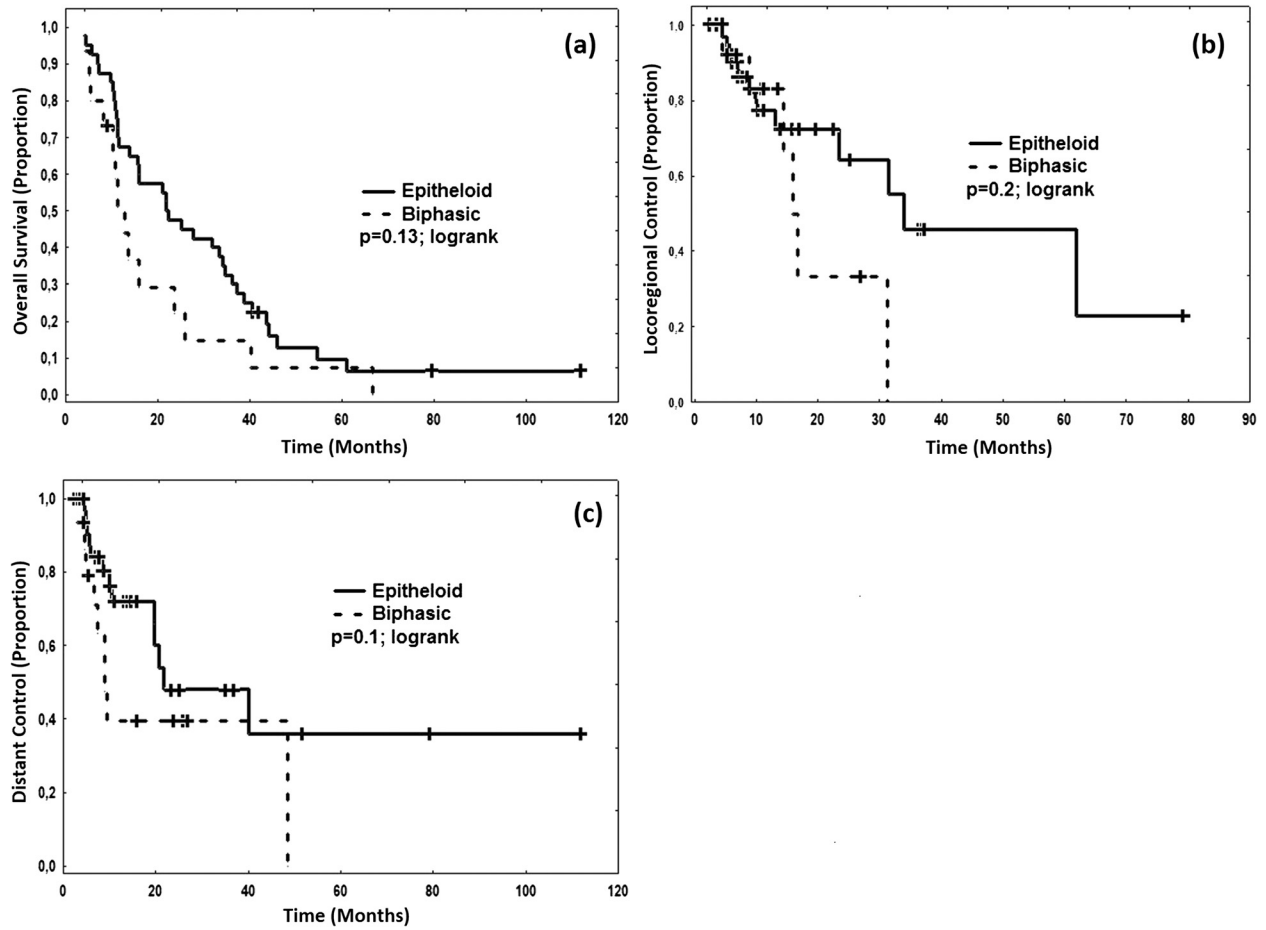

Fig. 4 Kaplan-Meier curves separated for histology. Biphasic histology tended to be associated with worse prognosis compared to epitheloid histology with respect to **a** overall survival, **b** locoregional control and **c** distant control

2 years slightly better (62 % vs. 55 % and 48 % vs. 40 %). The dosimetric parameters of the radiotherapy were roughly equivalent. The chemotherapy might have caused the differences in DC and OS. This is consistent with other reports where trimodal treatment of MPM led to survival times of 20 months or more [5, 6]. We have summarized the treatment characteristics, survival times and acute lung toxicity of several reports in a table that is accompanying this paper as an additional file (see "Additional file 1").

As reference time point from which the survival times were measured, we chose the date of surgery, as in [4, 7, 8]. This has to be considered when comparing the results with other reference time points such as the date of diagnosis [9–11], start of chemotherapy [12] or date of study enrolment [13] to avoid a lead time bias of up to several months (in our case, a median of 4.4 months between diagnosis and the day of EPP surgery). The survival times we observed were among the best reported in the recent medical literature [4, 7–17].

One main organ system to be considered regarding the toxicity of radiotherapy is the remaining contralateral lung. The radiotherapy, even delivered up to median target doses of 54 Gy, was well tolerated with no higher (4 or 5) grade toxicity to the contralateral lung. The mean lung dose (MLD) to the contralateral lung was (7.4 ± 2.0) Gy in all patients. Considering the rate of fatal pneumonitis reported several years ago (6 out of 13 patients experiencing grade 5 pneumonitis, with a median MLD of 15.2 Gy in the group of patients developing pneumonitis [18]) and the improvements made over the last years regarding better lung sparing, resulting in lower lung toxicity [7], there seems to be a dose-effect relationship for fatal pneumonitis, and an MLD around 7 Gy seems to be associated with an acceptable low risk of higher grade lung toxicity [8]. Because of the severe and fatal adverse effects of radiotherapy reported in other cohorts, we think that even though we did not observe high grade toxicity, the radiotherapy protocol should not be intensified further, neither by enlargening the target volume nor by escalating the dose beyond

54 Gy, unless new radiotherapy techniques will become available that would allow such intensification without increasing the dose to the organs at risk. Since all patients received IMRT with image guidance, using inverse planning and collimators with narrow leafs, the radiotherapy the patients received can be considered as state-of-the-art even for today's standards.

Comparing the two IMRT techniques step&shoot and helical tomotherapy, we found no significant difference, neither in dosimetric terms (see also [19]) nor in clinical outcome. This notion is also supported by the finding that none of the dosimetric variables that were statistically analyzed, including the median target dose, affected clinical outcome such as OS, LRC and DC. The results indicate that both techniques nowadays allow for safe conformal hemithoracic radiotherapy with effective sparing of organs at risk, especially the contralateral lung. Major physical parameters for step&shoot IMRT and helical tomotherapy were similar, explaining the equivalence in dosimetric terms and clinical outcome: The leaf width of the multileaf colimator (MLC) in the isocenter plane was 5 mm for step&shoot and 6.25 mm for helical tomotherapy, both accelerators operated at 6 MV, and both techniques included image guidance (in-room CT for step&shoot, integrated MV-CT for tomotherapy).

Further improvements in radiotherapy might be achieved in the future in particular with respect to side effect reduction, e.g., through volumetric rotational irradiation (e.g., [20]) or through the use of particles. These techniques will require also higher standards regarding plan robustness, image guidance and plan adaptation.

One major point of discussion and controversy in clinical treatment of MPM is the radicality and aggressiveness, respectively, of the therapy concept, mainly determined by the surgical procedure. It has been argued that EPP can do more harm than good because of its peri- and postoperative morbidity and mortality [21], and that even chemotherapy alone can result in similar survival times [22]. However the maturity of the clinical data or the patient numbers are often limited, or other factors make comparisons difficult, so that there are no definite conclusions possible yet. E.g., the MARS study [21] was a feasibility trial in which only 19 patients actually received EPP. In [22] the median OS of the whole cohort was 13 months while only a subgroup of 51 out of 173 patients reached 22 months, and the authors state that comparisons with other studies are difficult because surgery for MPM in Scandinavia, where the study was conducted, is performed only for very early stages with the best performance status.

In recent years, the less radical pleurectomy/decortication (P/D) surgery procedure has frequently been proposed and carried out as an alternative to EPP surgery. In a systematic review and meta-analysis [2], it was stated that P/D might be performed with lower morbidity and mortality than EPP while resulting in comparable long-term survival, however the authors also noted that the comparison of both procedures has several limitations and the choice for a specific therapy is still highly individual based on the extension of the disease, the patient comorbidities and the center's experience. The dose-shaping potential of IMRT allows high-dose (50 Gy) adjuvant radiotherapy even after P/D where the ipsilateral lung has to be spared as an additional organ at risk. First reports indicate promising clinical results: A median OS of 24 months (from date of diagnosis, 76 pts [23]), 33 months (from date of surgery, 20 pts [24]) and 28.4 months (from date of surgery, 24 pts [25]). The follow-up times however are still somewhat limited.

We carried out a retrospective study on a group of MPM patients selected in the sense that they were able to receive adjuvant radiotherapy after chemotherapy and EPP. The decision for radiotherapy was made after EPP individually for each patient depending on the postoperative development, so there was no strict intention-to-treat for trimodal therapy from the beginning. EPPs were performed in several different hospitals with some patients being referred to our institution for radiotherapy only. Therefore, an analysis that included also the patients having received EPP without adjuvant radiotherapy was not possible. Given these limitations, and the fact that the disease is relatively rare and no uniform treatment technique and algorithm has been established, our results, similar to published results by other groups, can only be compared with historical data.

Clearly, randomized clinical trials would be ideal for investigating the optimal therapy regimen for each individual patient, but as described, they are hard to conduct. Therefore the main findings of the presented study are 1) the conclusions regarding the safety of the adjuvant radiotherapy after EPP in general, 2) the shown equivalence of step&shoot IMRT and helical tomotherapy and 3) the mature clinical outcome data for trimodal therapy. We believe that the data may contribute to some guidance what can be optimally expected from this complicated, aggressive and technically sophisticated regimen. Furthermore, the data can serve as a benchmark to be compared to in future reports on the clinical outcome of other treatment strategies.

MPM remains a therapeutic challenge. Despite the radical strategy, the overall survival times presented here still show the poor prognosis of MPM patients. Both the rate of distant metastases and local treatments need further improvements by systemic and local options. While surgery, radiotherapy and conventional chemotherapy will probably remain the stage dependent mainstay of MPM

therapy, it is likely that future concepts might integrate novel strategies such as targeted drugs or immunological approaches based on personalized molecular medicine data.

Conclusions

Mature clinical results of trimodal treatment for MPM were presented. They indicate that hemithoracic radiotherapy after EPP can be safely administered by either step&shoot IMRT and tomotherapy. However, the optimal prospective patient selection for this aggressive trimodal therapy approach remains unclear. This study can serve as a benchmark for current and future therapy concepts for MPM.

Additional file

Additional file 1: Literature overview of recent studies evaluating radiotherapy (RT) after extrapleural pneumonectomy (EPP).
(PDF 77 kb)

Competing interests

The authors declare that they have no competing interests.

Authors' contributions

CT and PH acquired the clinical data, performed the statistical analysis, interpreted the data and drafted the initial manuscript. NN, FS, HH, FR and SS participated in the design of the study, acquired clinical data, and critically revised the manuscript. JD and PH conceived of the study, participated in its design and coordination and helped to draft the manuscript. All authors read and approved the final manuscript.

Acknowledgments

We would like to thank Dr. Thomas Muley from the Thoraxklinik at Heidelberg University Hospital for his help in retrieving clinical data.

Author details

[1]Department of Radiation Oncology, Heidelberg University Hospital, Heidelberg, Germany. [2]CCU Radiation Oncology, German Cancer Research Center, Heidelberg, Germany. [3]Department of Thoracic Surgery, Thoraxklinik, Heidelberg University Hospital, Heidelberg, Germany. [4]CCU Molecular Radiation Oncology, German Cancer Research Center, Heidelberg, Germany. [5]Present address: Department of Radiation Oncology, University of Munich (LMU), Marchioninistr. 15, 81377 Munich, Germany.

Received: 26 October 2015 Accepted: 18 December 2015
Published online: 30 December 2015

References

1. Vogelzang NJ, Rusthoven JJ, Symanowski J, Denham C, Kaukel E, Ruffie P, et al. Phase III study of pemetrexed in combination with cisplatin versus cisplatin alone in patients with malignant pleural mesothelioma. J Clin Oncol. 2003;21:2636–44.
2. Cao C, Tian D, Park J, Allan J, Pataky KA, Yan TD. A systematic review and meta-analysis of surgical treatments for malignant pleural mesothelioma. Lung Cancer. 2014;83:240–5.
3. Ahamad A, Stevens CW, Smythe WR, Vaporciyan AA, Komaki R, Kelly JF, et al. Intensity-modulated radiation therapy: a novel approach to the management of malignant pleural mesothelioma. Int J Radiat Oncol Biol Phys. 2003;55:768–75.
4. Gomez DR, Hong DS, Allen PK, Welsh JS, Mehran RJ, Tsao AS, et al. Patterns of failure, toxicity, and survival after extrapleural pneumonectomy and hemithoracic intensity-modulated radiation therapy for malignant pleural mesothelioma. J Thorac Oncol. 2013;8:238–45.
5. Chi A, Liao Z, Nguyen NP, Howe C, Gomez D, Jang SY, et al. Intensity-modulated radiotherapy after extrapleural pneumonectomy in the combined-modality treatment of malignant pleural mesothelioma. J Thorac Oncol. 2011;6:1132–41.
6. Cao C, Tian D, Manganas C, Matthews P, Yan TD. Systematic review of trimodality therapy for patients with malignant pleural mesothelioma. Ann Cardiothorac Surg. 2012;1:428–37.
7. Patel PR, Yoo S, Broadwater G, Marks LB, Miles EF, D'Amico TA, et al. Effect of increasing experience on dosimetric and clinical outcomes in the management of malignant pleural mesothelioma with intensity-modulated radiation therapy. Int J Radiat Oncol Biol Phys. 2012;83:362–8.
8. Tonoli S, Vitali P, Scotti V, Bertoni F, Spiazzi L, Ghedi B, et al. Adjuvant radiotherapy after extrapleural pneumonectomy for mesothelioma. Prospective analysis of a multi-institutional series. Radiother Oncol. 2011;101:311–5.
9. Sylvestre A, Mahé MA, Lisbona A, Zefkili S, Savignoni A, Bonnette P, et al. Mesothelioma at era of helical tomotherapy: results of two institutions in combining chemotherapy, surgery and radiotherapy. Lung Cancer. 2011;74:486–91.
10. Helou J, Clément-Colmou K, Sylvestre A, Campion L, Amessis M, Zefkili S, et al. Helical tomotherapy in the treatment of malignant pleural mesothelioma: The impact of low doses on pulmonary and oesophageal toxicity. Cancer Radiother. 2013;17:755–62.
11. Fahrner R, Ochsenbein A, Schmid RA, Carboni GL. Long term survival after trimodal therapy in malignant pleural mesothelioma. Swiss Med Wkly. 2012;25:142.
12. Krayenbuehl J, Dimmerling P, Ciernik IF, Riesterer O. Clinical outcome of postoperative highly conformal versus 3D conformal radiotherapy in patients with malignant pleural mesothelioma. Radiat Oncol. 2014;9:32.
13. Federico R, Adolfo F, Giuseppe M, Lorenzo S, Martino DT, Anna C, et al. Phase II trial of neoadjuvant pemetrexed plus cisplatin followed by surgery and radiation in the treatment of pleural mesothelioma. BMC Cancer. 2013;13:22.
14. Rice DC, Stevens CW, Correa AM, Vaporciyn AA, Tsao A, Forster KM, et al. Outcomes after extrapleural pneumonectomy and intensity-modulated radiation therapy for malignant pleural mesothelioma. Ann Thorac Surg. 2007;84:1685–92.
15. Stahel RA, Weder W, Riesterer O, Xyrafas A, Opitz I, Beyeler M, et al. Neoadjuvant chemotherapy and extrapleural pneumonectomy of malignant pleural mesothelioma (MPM) with or without hemithoracic radiotherapy: final results of the randomized multicenter phase II trial SAKK17/04. European Society for Medical Oncology (ESMO), ESMO 2014 Congress, Madrid, Spain, LBA37 (late breaking abstract).
16. Kristensen CA, Nøttrup TJ, Berthelsen AK, Kjaer-Kristoffersen F, Rayn J, Sørensen JB, et al. Pulmonary toxicity following IMRT after extrapleural pneumonectomy for malignant pleural mesothelioma. Radiother Oncol. 2009;92:96–9.
17. Van Schil PE, Baas P, Gaafar R, Maat AP, Van de Pol M, Hasan B, et al. Trimodality therapy for malignant pleural mesothelioma: results from an EORTC phase II multicentre trial. Eur Respir J. 2010;36:1362–9.
18. Allen AM, Czerminska M, Jänne PA, Sugarbaker DJ, Bueno R, Harris JR, et al. Fatal pneumonitis associated with intensity-modulated radiation therapy for mesothelioma. Int J Radiat Oncol Biol Phys. 2006;65:640–5.
19. Sterzing F, Sroka-Perez G, Schubert K, Münter MW, Thieke C, Huber P, et al. Evaluating target coverage and normal tissue sparing in the adjuvant radiotherapy of malignant pleural mesothelioma: helical tomotherapy compared with step-and-shoot IMRT. Radiother Oncol. 2008;86:251–7.
20. Krayenbuehl J, Riesterer O, Graydon S, Dimmerling P, Kloeck S, Ciernik IF. Intensity-modulated radiotherapy and volumetric-modulated arc therapy for malignant pleural mesothelioma after extrapleural pleuropneumonectomy. J Appl Clin Med Phys. 2013;14:4130.
21. Treasure T, Lang-Lazdunski L, Waller D, Bliss JM, Tan C, Entwisle J, et al. Extra-pleural pneumonectomy versus no extra-pleural pneumonectomy for patients with malignant pleural mesothelioma: clinical outcomes of the Mesothelioma and Radical Surgery (MARS) randomised feasibility study. Lancet Oncol. 2011;12(8):763–72.
22. Hillerdal G, Sorensen JB, Sundström S, Riska H, Vikström A, Hjerpe A. Treatment of malignant pleural mesothelioma with carboplatin, liposomized doxorubicin, and gemcitabine: a phase II study. J Thorac Oncol. 2008;3(11):1325–31.
23. Rimner A, Spratt DE, Zauderer MG, Rosenzweig KE, Wu AJ, Foster A, et al. Failure patterns after hemithoracic pleural intensity modulated radiation

therapy for malignant pleural mesothelioma. Int J Radiat Oncol Biol Phys. 2014;90:394–401.
24. Minatel E, Trovo M, Polesel J, Baresic T, Bearz A, Franchin G, et al. Radical pleurectomy/decortication followed by high dose of radiation therapy for malignant pleural mesothelioma. Final results with long-term follow-up. Lung Cancer. 2014;83:78–82.
25. Chance WW, Rice DC, Allen PK, Taso AS, Fontanilla HP, Liao Z, et al. Hemithoracic intensity modulated radiation therapy after pleurectomy/decortication for malignant pleural mesothelioma: Toxicity, patterns of failure, and a matched survival analysis. Int J Radiat Oncol Biol Phys. 2014;91:149–56.